

AN EXPERIMENTAL STUDY OF TURBULENT NATURAL  
CONVECTION IN WATER AND MERCURY

by

ASHOK JAIN

B. Tech., Indian Institute of Technology (Bombay), 1973

---

A MASTER'S THESIS

submitted in partial fulfillment of the  
requirements for the degree

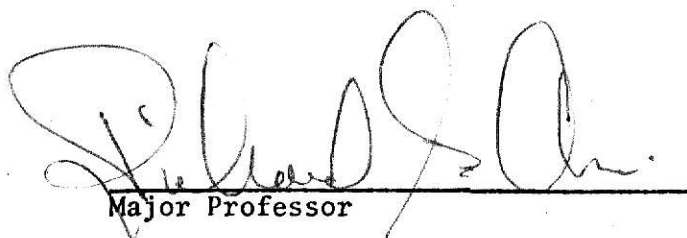
MASTER OF SCIENCE

Department of Chemical Engineering

KANSAS STATE UNIVERSITY  
Manhattan, Kansas

1975

Approved by:



Major Professor

**THIS BOOK  
CONTAINS  
NUMEROUS PAGES  
THAT WERE  
BOUND WITHOUT  
PAGE NUMBERS.**

**THIS IS AS  
RECEIVED FROM  
CUSTOMER.**

2668  
T4  
1975  
J33  
C.2  
Document

LIST OF FIGURES

TABLE OF CONTENTS

LIST OF TABLES

I. INTRODUCTION	1
APPLICATIONS	1
SIGNIFICANCE OF THE PRESENT STUDY	2
II. LITERATURE REVIEW	4
LAMINAR FREE CONVECTION	4
Isothermal Case	4
Nonisothermal Case	7
TURBULENT FREE CONVECTION	7
Transition	8
Theoretical Analyses	8
Experimental Work	12
III. STATISTICAL ANALYSIS OF SCALAR TURBULENT FIELDS	15
INTRODUCTION	15
STATISTICAL QUANTITIES AND THEIR SIGNIFICANCE	16
THEORETICAL ANALYSIS OF TEMPERATURE POWER SPECTRUM	18
Stratification and Incipient Boiling	22
COMPUTATIONAL TECHNIQUES	23
The Fast Fourier Transform (FFT)	24
Decimation in Frequency	24
Autocorrelation by FFT	25
Pruning	25
Overlapped Periodograms	25
IV. EXPERIMENTAL APPARATUS	27
EQUIPMENT	27

INSTRUMENTATION	29
V. MEASURING PROCEDURE, DATA ANALYSIS, AND RESULTS	34
SYSTEM STARTUP AND CHECKS	34
TEMPERATURE PROFILES	36
TEMPERATURE FLUCTUATION MEASUREMENTS	37
DIGITIZATION	41
STATISTICAL ANALYSIS	42
Water	42
Mercury	51
HEAT TRANSFER RELATION	55
VI. DISCUSSION OF RESULTS	63
TEMPERATURE PROFILES	63
TEMPERATURE FLUCTUATIONS, INTENSITY DISTRIBUTIONS, AND INTERMITTENCY	63
TEMPERATURE SPECTRA	65
AUTOCORRELATION AND PERIODICITY	69
ERRORS	70
VII. CONCLUSIONS AND RECOMMENDATIONS FOR FURTHER STUDY	72
REFERENCES AND BIBLIOGRAPHY	75
APPENDIXES	
A. GLOSSARY	i
B. NOMENCLATURE	iv
C. NOISE ANALYSIS	vii
D. REPRESENTATIVE RUNS	ix
E. SAMPLE CALCULATIONS	xvi
F. COMPUTER PROGRAMS	xxi



## LIST OF TABLES

### Table

1	Summary of Work on Laminar Natural Convection	5
2	Critical Grashof Number for Onset of Instability	9
3	Summary of the Work on Turbulent Free Convection	11

## LIST OF FIGURES

### Figure

1	8-Point Decimation in Frequency FFT	26
2	A Butterfly	26
3	Vertical Plate and Thermocouple Probe	28
4	Probe Positioning Mechanism	30
5	Sheathed Thermocouple	31
6	Probe Positioning Mechanism in Constant Temperature Bath	32
7	Dimensionless Temperature Distribution for Water	38
8	Dimensionless Temperature Distribution for Mercury	39
9	Block Diagram for Data Acquisition and Processing	43
10	Power Spectrum as Calculated by FFT and Through Autocorrelation	45
11	Variation of Temperature Power Spectra in the Vertical Direction	46
12	Variation of Temperature Power Spectra in the Vertical Direction (near-boiling conditions at the Plate)--Water	47
13	Variation of Temperature Power Spectra in the Horizontal Direction--Water	48
14	Variation of Temperature Power Spectra in the Horizontal Direction (near-boiling conditions at the Plate)--Water	49
15	Autocorrelation of Turbulent Temperature Fluctuations	50
16	Variation of Intensity in Water	52
17	Variation of Integral Time Scale	53
18	Power Spectrum Showing the Severe Aliasing Problem in Mercury	54
19	Variation of Power Spectra in the Vertical Direction--Mercury	56
20	Variation of Power Spectra in the Vertical Direction--Mercury	57

## Figure

21	Variation of Power Spectra in the Horizontal Direction-- Mercury	58
22	Variation of Power Spectra in the Horizontal Direction-- Mercury	59
23	Power Spectra Above the Plate	60
24	Variation of Intensity in Mercury	61
25	Nusselt Number vs. Rayleigh Number	62
26-27	Noise Analysis	vii
28-34	Representative Runs	ix

## CHAPTER I

## INTRODUCTION

A fundamental understanding of natural convection flows is of importance to an engineer, a mathematician, a scientist, a geophysicist, a meteorologist, and a host of other professionals who encounter such flows in a variety of situations. These flows arise as a result of a difference in density caused by a temperature difference (in the case of heat transfer) between two points in an otherwise stationary fluid. 'Natural' or 'free' appended to 'convection' signifies motion induced without any external work on the fluid. Interest in this field is at a high level and is demonstrated by the fact that it has been attracting more than one hundred publications per year during the last few years.

## APPLICATIONS

Natural convection flows are observed to occur in many natural, industrial, and domestic systems. Apart from the traditional applications such as the heat transfer from walls, radiators, refrigerator-condenser coils, etc., there has been a surge of activity in a number of new fields arising out of the need to find technological solutions to some of our most pressing problems, most notably, energy. In this category fall applications such as solar energy collectors, nuclear reactors, and studies concerning fluid flow in the earth's interior, atmosphere, and oceans. In a nuclear reactor natural convection effects may be significant in the core at the fuel rods and also in the cooling system during pump failure or startup and shutdown. A knowledge of natural convection is also important in the design of industrial and domestic equipment, and in environmental chambers such as underwater and space habitats.

There has been a growing interest in the use of liquid metals as heat transfer media especially for high temperature, high heat flux applications such as the cooling of nuclear reactors. Liquid metals have also been used extensively in cooling aircraft engine valves. The retorting of liquid metals is accomplished by means of natural convection heating. Also of importance are flows in the earth's core which is made up of low Prandtl number fluids.

From a theoretical point of view, the natural convection phenomenon has been of interest as it constitutes a system of coupled differential equations. This coupling results from the fluid flow being caused by the temperature gradient in the boundary layer. The solutions to these equations for the turbulent case involves various assumptions, but experimental verifications of these have been limited in number.

#### SIGNIFICANCE OF THE PRESENT STUDY

Although turbulent natural convection occurs frequently in nature and elsewhere, it is perhaps the least understood and studied among all natural convection phenomena. The convective motions occurring in nature are invariably turbulent because of the large dimensions in which they occur. In other applications there is a practical reason for using turbulent natural convection. Mixing of two equal density fluids is accomplished most efficiently by turbulent natural convection. The use of natural convection for transfer of heat eliminates the necessity of a circulation system and, therefore, reduces initial and operating costs. But heat transfer rates in the laminar zone are small and natural convection equipment, as a result, tends to be large and sometimes inefficient. Thus, to enhance heat transfer rates, operation in the turbulent region

is necessary. This study also merits importance, first, because of a lack of experimental data permitting an understanding of the structure of turbulent natural convection boundary layer flow and, secondly, to the best of the author's knowledge publications on experimental measurements of statistical quantities on turbulent natural convection have been extremely limited even for a simple geometry like a vertical flat plate and for commonly used fluids like water and mercury.

This work was initiated, therefore, to understand the structure of turbulent natural convection flow by measuring various statistical quantities, such as temperature 'power' spectra and turbulent intensities, in a steady, two-dimensional free convection heat transfer from a vertical flat plate with uniform heat-flux, immersed in a stationary bath of fluid. It is expected that an understanding of the structure will aid future improvements in phenomenological descriptions. Mean temperature profiles were also measured with that end in view. Mention may also be made of the fact that measurements of power spectra would provide additional experimental support for the development of the statistical theory of turbulent scalar fields. In the course of the experimental investigation the available methods for fast and efficient digital harmonic analysis were examined for applicability to turbulent natural convection data. The major factors governing the shape of the estimated spectra with change in turbulence level were determined. Our experiences should prove useful to a variety of future investigations in turbulent flows. Finally, to demonstrate further the applicability of the data taken, a method of predicting heat-transfer rates based on surface-renewal theory is also discussed.

## CHAPTER II

### LITERATURE REVIEW

Contrary to ordinary misconception, natural convection, both laminar and turbulent, is potentially as large a subject as forced convection. Its importance has increased in the recent years due to an increase in its applications (Chapter I). The more than one hundred publications each year on this topic concern themselves with all feasible combinations of geometry, media, surface, and environmental conditions. This survey recognizes the problems associated with reviewing all pertinent literature (especially foreign publications and theoretical analyses) and confines itself mainly published literature on a vertical flat plate at high and moderately high Grashof numbers. Literature of a fundamental nature on laminar natural convection or for other geometries has been included only as an aid to understanding and to expose the reader to important developments in this area. Readers interested in a more general survey are referred to an excellent study by Ede [26] or some of the more recent ones [119, 52, 16].

#### LAMINAR FREE CONVECTION

Isothermal Case. The first meaningful attempt at the solution of mass, momentum, and energy balances for steady-state natural convection from a vertical, isothermal, flat plate was given by Lorenz [64] in 1881\*. Lorenz made certain sweeping assumptions, but arrived at a result astonishingly close to experimental data.

The next jump forward came directly as a result of Prandtl's

---

\*See Tables 1 and 3 for summary of work on laminar and turbulent natural convection.

**THIS BOOK  
CONTAINS  
NUMEROUS PAGES  
WITH DIAGRAMS  
THAT ARE CROOKED  
COMPARED TO THE  
REST OF THE  
INFORMATION ON  
THE PAGE.**

**THIS IS AS  
RECEIVED FROM  
CUSTOMER.**



Case	Author	Result	Assumptions and Conditions	Remarks
1. Steady state, isothermal, analytical	Lorenz (1881)	$Nu_L = 0.548(Gr_L \cdot Pr)^{\frac{1}{4}}$	(a) No flow perpendicular to plate (b) $T_{fluid} = f(y)$ (c) $T_{\infty} = \text{constant}$	(1) Result in good agreement with experiment (2) $h_x$ becomes independent of $x$ , contrary to experience
2. "	Schmidt & Beckmann (1939)	$Nu_x = 0.39(Gr_x \cdot Pr)^{\frac{1}{4}}$ $Nu_L = 0.52(Gr_L \cdot Pr)^{\frac{1}{4}}$	(a) Boundary-layer assumptions (b) $Pr = 0.733(\text{air})$ (c) $x < 2'$	Introduced similarity transformation method to Natural Convection
3. "	Squire (1938)	$Nu_x = 0.51Pr^{\frac{1}{2}}(Pr+20/21)^{-\frac{1}{4}}$ $Nu_L = 0.68Pr^{\frac{1}{2}}(Pr=20/21)^{-\frac{1}{4}}$ $(Gr_L \cdot Pr)^{\frac{1}{4}}$	Boundary-layer thickness same for velocity and temperature fields	Use of Integral Equation Method. Results approximate.
4. Steady state, constant heat-flux; analytical	Sparrow & Gregg (1956)	$Nu_x = mx^{\frac{1}{4}}(0.735/\sqrt{2}) \cdot Gr_x^{\frac{1}{4}}$ $m$ is a constant	$Pr = 0.7$	Use of similarity transformation.
5. Steady state, isothermal, theoretical	Yang & Jerger (1964)	Temperature profile depends on $Gr$ and $x$	(a) Moderate $Gr$ (b) $Pr = 0.72, 10$	Numerical solution using the perturbation method
6. Steady state, constant heat-flux; theoretical	Chang, Akins & Bankoff (1966)	"	(a) Moderate $Gr_x$ (b) $Pr = 0.01, 0.03, 0.1$	"

TABLE 1. Summary of Work on Laminar Natural Convection

boundary-layer theory. Pohlhausen [78] solved the boundary layer equations by a similarity transformation and found that the temperature and velocity distributions could be expressed in terms of  $y/x^{1/4}$ . This compared favorably with the experimental measurements made by Schmidt and Beckmann [89] in 1939. Extension of this work to incorporate different conditions and Prandtl numbers has been made by various authors [89, 99, 62].

In addition to the similarity transformation method used by the authors above, the integral equation method was first used in natural convection by Squire [98]. In this method the boundary layer equations were integrated across a boundary layer which were assumed to be the same for both velocity and temperature. Improvements have been proposed by various authors. Sparrow and Gregg [94] included temperature dependence of physical properties in their solution. Gebhart [35] found that the viscous dissipation in the boundary layer was small for all Prandtl numbers when the only body force was gravity. Scherberg [87] found that for uniform wall temperatures, the leading edge configuration only altered the relative starting location of the boundary layer and did not affect the velocity and temperature profiles far from the leading edge. A theoretical and experimental study by Schechter and Isbin [86] indicated that fluid motion occurs both upward and downward simultaneously.

Analytical solutions based on Prandtl's boundary-layer theory are bound to be erroneous for low Grashof numbers because boundary layer assumptions are valid only for large Grashof numbers. Yang and Jerger [117] and Chang et al. [17], therefore, used a perturbation analysis which was expected to be more accurate for moderate Grashof numbers.

In addition to some of the work discussed, a large number of experimental observations are available for testing analytical solutions. Due to

non-idealized conditions the discrepancies between experimental and theoretical work are sometimes significant. The data obtained by Sparrow and Gregg [94] indicated that the experimental heat-transfer coefficients are greater than the theoretical ones. That the velocity in the outer regions of the boundary layer is higher than expected has also been observed by Eichhorn [27]. These results are understandable if one realizes that most of the data were taken in air where uncontrolled air currents were significant.

Nonisothermal Case. The nonuniform surface temperature case is encountered very often in practical situations. Finston [30] extended Pohlhausen's transformation and found that the similarity variable takes the form  $y/x^{1/5}$  in the uniform heat-flux case. In 1956, Sparrow and Gregg [94] solved the differential equations for the laminar, constant heat-flux case by similarity transformation. Later [95] they found more exact solutions and discussed the relation between average Nusselt number and Grashof number.

The integral method was applied to the nonuniform heat-flux case by Sparrow [93]. Results for the constant heat-flux case were in good agreement with the more exact solutions by the differential method. Attempts at generalizing the method have been made [106, 3]. Sugawara's et al. [99] experimental results agree with these analyses.

## TURBULENT FREE CONVECTION

In his survey, Ede [26] points out the lack of adequate analytical and experimental work on turbulent flow even for a simple geometry like the vertical flat plate. This is no doubt because turbulence is less tractable than laminar flow. In the last few years, however, research has been increasing with a fair amount of work appearing both in the analytical

and experimental areas.

Transition. The existence of turbulence in natural convection was first observed by Griffiths and Davis [66] while observing temperature and velocity profiles and the variation of heat-transfer coefficients with distance along the plate. The critical Rayleigh number has been suggested to lie between  $7 \times 10^8$  to  $2 \times 10^9$  by various authors [28, 24, 45], but ambiguity about unique critical values still persists. An attempt to theoretically determine the critical Rayleigh number was made by Klyachko [57]. Szewczyk [100] tackled the same problem experimentally using a dye as a tracer and arrived at a critical Grashof number of  $1.4 \times 10^9$ . Tritton [107] studied the instability problem using a quartz fiber anemometer and found that a breakdown of vortices into turbulence occurred at a Grashof number of  $9 \times 10^6$ --a figure much lower than that given by any other worker. Sparrow et al. [97] used a perturbation analysis and obtained theoretical values of the critical Grashof numbers for seven values of Prandtl number. Their results are given in Table 2. In a recent study, Godaux and Gebhart [41] indicated that the amount of convected thermal energy, and not Grashof number, was a better correlator of the features of transition. A detailed description of the development of turbulence has been given by Eckert and Soehngen [25]. In addition to observations on the development of a vortex street, Fujii [32, 33] also observed an increase in local coefficients at the point of transition by a factor of 1.6; similar, and sometimes more significant, increases can be expected at higher Grashof numbers. This is, in fact, a major reason for using turbulence as a means of enhancing efficiency. An excellent discussion on this, and other aspects of turbulence, is given by Bradshaw [15].

Theoretical Analyses. The main trend in the theoretical analysis of

Table 2  
Critical Grashof Number for Onset of Instability  
(Sparrow et al. [97])

Pr	Gr <sub>x</sub>
0.733	$1.93 \times 10^6$
1.0	$3.08 \times 10^6$
1.5	$6.55 \times 10^6$
2.0	$1.21 \times 10^7$
3.5	$5.15 \times 10^7$
5.0	$1.39 \times 10^8$
7.0	$3.90 \times 10^8$

turbulent free convection has been toward the use of the integral equation method introduced by Eckert and Jackson [24]. One-seventh power law velocity and temperature profiles based on experimental data [44] and forced convection profiles were used in von Karman's momentum integral equations for boundary layer flow. These were solved using shear stress and heat flux relations derived from forced convection and Reynold's analogy. The resulting relation for Nusselt number (Table 3) seems to be in fair agreement with experimental results for  $Pr \sim 1$ . Equations for boundary-layer thickness and maximum velocity were also obtained.

Modifications of this basic technique have been made by various authors [7, 33, 61, 54, 91]. Baley [7] extended the analysis to low Prandtl number fluids by using a laminar sublayer and a turbulent outer layer. The Nusselt number was found to be proportional to  $Gr_L^{1/4}$  instead of  $Gr_L^{2/5}$  as calculated by Eckert and Jackson. Fujii [33] closely followed Eckert and Jackson's procedure and obtained a similar solution. Kato et al. [54] derived profiles of velocity and temperature by assuming eddy diffusivity distribution in addition to shear stress and heat flux. The predicted velocity profile was similar to that of Eckert and Jackson, but the temperature profile showed significant differences. Instead of using the integral method, Mason and Seban [67] attempted a numerical solution of the boundary layer equations. The predicted profiles compared favorably with experimental results and with Kato's work. Siegel [91] obtained an analytical solution for the constant heat-flux case.

The theoretical works discussed above do provide an overall view of the phenomenon, but fail to give an insight into the physical structure of turbulent free convection boundary layer. Yang and Nee [117] attempted a solution by the use of a differential field method in which eddy

Case	Author	Result	Assumptions and Conditions	Remarks
1. Isothermal plate; theoretical	Eckert and Jackson (1951)	$Nu_L = 0.0211(Gr_L Pr)^{\frac{2}{5}}$	(a) $Pr \sim 1$ (air) (b) $10^{10} < Gr_L < 10^{12}$	(1) Empirical relations from forced convection used. (2) Integer equation method.
2. Constant heat flux; theoretical	Siegel (1954)	$Nu_x = 0.0804 Pr^{\frac{1}{3}} \left( \frac{Gr_x}{1 + 0.444 Pr^{\frac{2}{3}}} \right)^{\frac{2}{7}}$		"
3. Constant heat flux; experimental	Vliet and Liu (1969)	$Nu_x = 0.59(Gr_x^* Pr)^{0.22}$	(a) $Gr_x^* \leq 10^{16}$ (b) Data taken in water.	
4. Experimental analysis for structure	Lock and Trotter (1968)	Boundary layer structure different from that of a forced layer.	Water used as an experimental fluid.	Analysis debatable and qualitative rather than quantitative.
5. Theoretical structure analysis	Yang and Nee (1969)	Boundary layer consists of three distinct layers (i) viscous sub-layer (ii) inner layer (iii) outer layer.	Total viscosity governed by a parabolic rate equation.	
6. "	Papaillon and Lykoudis (1974)	(i) Boundary layer resembles forced convection layer. (ii) 'Convection' sub-range detected in 'power' spectra.	Mercury used as experimental fluid in a cell.	Temperature 'power' spectra etc. measured.

Table 3. Summary of Work of Turbulent Free Convection

viscosity and eddy conductivity were considered unknowns. The total viscosity (molecular plus eddy) was taken to be governed by a parabolic rate equation which took into account turbulent convection, diffusion, generation, and decay. The eddy thermal diffusivity, however, was based on a constant Prandtl number. Based on their analysis the authors concluded that:

- a) The turbulent free convection boundary layer on a vertical flat plate consists essentially of three distinct regions, namely, a viscous sublayer, an inner layer, and an outer layer.
- b) Turbulent generation and decay dominate the inner layer, whereas convection and diffusion dominate the outer layer.
- c) The generation of turbulence is shear induced, and buoyancy influences only the mean velocity and temperature profiles.

Experimental Work. Experimental data on turbulent free convection is meager, and this explains the lack of understanding of the phenomenon. Even the data for overall heat-transfer correlations are confined mainly to a vertical flat plate in air or water. It is observed that a great deal of scatter exists in the available data. This prevents the formulation of a single correlation for the turbulent region. Fishenden and Saunders [31] suggested, however, that the data may be correlated by means of  $Gr \cdot Pr^n$ , where  $n$  lies between 1.3 and 1.5. The hypothetical region of negligible viscosity, where  $n$  equals 2, may thus be expected to be considerably above a Rayleigh number of  $10^{13}$ , which was the upper limit of the data examined.

A considerable disagreement exists when the experimental temperature and velocity profiles of Griffiths and Davis [44] and Cheesewright [18] are compared with the semi-empirical result of Eckert and Jackson [24]. This is attributed to the use of experimental values for boundary-layer thickness



and maximum velocity by Eckert and Jackson. The agreement between the experimental data of Griffiths and David and Cheesewright contradicts Ede's contention that the early experimental work was imperfect. In general, theoretical and semi-empirical analyses have been found to be inadequate, and this gives an impetus to experimental investigations like the present one.

A substantial amount of the experimental work has been devoted to measuring mean temperature profiles and correlating heat transfer data in a variety of situations [112, 114, 48, 77], but experimental work permitting an understanding of the structure of free convection flows have been very limited. The first reported work was by Lock and Trotter [63]. They made certain conclusions regarding the scale, intensity, and intermittency of turbulence and the concept of a laminar sublayer. Based on the maximum, minimum, and mean values for temperature fluctuations, they conclude that (for  $Ra < 1.6 \times 10^{10}$ ) the structure of a turbulent free convection boundary layer was different from that of a forced-convection layer. This contention is debatable because, as discussed in [117], root-mean-square (rms) values, instead of absolute values, should be used for comparison. Recent measurements of rms values by Papailiou and Lykoudis [76] indicate that temperature fluctuations are much smaller than the temperature drop across the boundary layer. The fluctuations observed in the wall region by Lock and Trotter, however, seem to be due to instability. Similar observations have been reported by many workers in forced convection (see references listed in [104]), but the mechanism responsible for this phenomena is not yet fully understood. The concept of a constant thickness laminar sublayer is a model of the actual phenomenon. Another model, which tries to account for the periodic fluctuations in this sublayer, is the surface renewal-

penetration model [104, 103, 81].

The work done by Papailiou [75] is of particular interest as far as an understanding of the free convection structure is concerned. Temperature profiles, intensity distributions, and 'power' spectra in mercury were measured. Their findings support a model which would take into account the existence of a laminar sublayer, a wall turbulence layer, and a free turbulent layer, thus replacing the existing theoretical models based on the integral methods. In the measured power spectra a 'dissipation subrange' having a slope of -3 in accordance with Gibson's model [38, 39] was observed. A progressive development of the 'convection subrange,' characterized by a slope of  $-5/3$ , was also observed with increasing distances from the leading edge. This subrange moved toward higher wave numbers with increasing distance along the plate as might be expected due to an intensification of the dissipation process. The existence of a convection subrange indicated that an 'inertial subrange' should exist in the velocity spectra. Instantaneous turbulent velocity data for liquid metal heat transfer was taken by Humphreys and Welty [48], but no measurements of velocity spectra were made. The results in [75] also indicate that the effect of buoyancy is restricted to low wave numbers and a Kolmogoroff 'equilibrium range' exists at high Rayleigh numbers.

A recent experimental study of the temperature and velocity fields at a vertical plate by Kirdyashkin et al. [55] also supports the view that a natural convection boundary layer is made up of three distinct regions: (a) a wall region, (b) a transition region, and (c) an outer region. The structure was thus found to be similar to that of a forced convection boundary layer by these authors.

## CHAPTER III

## STATISTICAL ANALYSIS OF SCALAR TURBULENT FIELDS

## INTRODUCTION

Analysis of turbulence leans heavily on models, experiment, and intuition because numerical solutions of the indeterminate transport equations encountered are beyond the capacity of the present-day computers. Most of the available mathematical models and methods used to characterize turbulent flow fields are based on the idea that a vector (velocity) or scalar (temperature, pressure, etc.) quantity characterizing the field can be solved into a randomly fluctuating component superimposed on a 'mean' quantity. Theoretical attempts to attribute these fluctuations to the random motion of discrete independent masses of fluid (commonly known as 'eddies') were made principally by Prandtl and Taylor. The work of the former, in the form of the well-known 'mixing-length' theory, is now mainly of historical interest [66]. The modern treatment of turbulence developed by Taylor [102] emphasizes its continuous nature as opposed to the discontinuous action implied by Prandtl. Taylor's treatment, commonly referred to as the 'Statistical Theory of Turbulence,' is similar in approach to the time-series analysis in statistics and communication engineering. However, representations are slightly modified in order to provide a physical interpretation to the measured quantities.

Most analytical descriptions of the statistics of random phenomena assume that the data are Gaussian, stationary, and ergodic.\* These assumptions are not necessary; however, they are highly desirable and

---

\*These and other terms, not defined in the text, are defined in Appendix A.

generally invoked to make a practical analysis. In this context it must be noted that:

- (i) For most flow fields (except those with high intensity, non-homogeneous, or nonisotropic turbulence, e.g., jets, shear flows, etc.) the deviations from the above-mentioned conditions are minor.
- (ii) Meaningful conclusions about the flow-field can be made by assuming the above, even though they may not be strictly valid.

In the definitions which follow, only time varying characteristics are considered.

#### STATISTICAL QUANTITIES AND THEIR SIGNIFICANCE

An essential characteristic of turbulence is its randomness. Thus, its steady mean component may be extracted leaving only the fluctuations on which to perform statistical calculations. Letting the random continuous signal be  $X(t)$ , where  $X$  may represent temperature or velocity and  $t$  the time, the temporal mean central moments for a stationary process over a finite interval  $\Theta$  are given by

$$\overline{X'^n} \approx \frac{1}{\Theta} \int_0^\Theta X'^n(t) dt, \quad (1)$$

where

$$X'(t) = X(t) - \bar{X} \text{ and, } \bar{X} = \frac{1}{\Theta} \int_0^\Theta X(t) dt \quad (2)$$

The physical interpretations of these quantities are:

- (i)  $n = 1$ ; gives  $\bar{X}'$ , the central moment mean.
- (ii)  $n = 2$ ; gives  $\overline{X'^2}$ , the variance, which is a measure of the turbulent kinetic energy of temperature fluctuation.
- (iii)  $n = 3, 4$  and  $>4$ ; give skewness, flatness, and other higher order

order moments which, when suitably normalized, can be used to determine departure from normal distributions:

The intensity of turbulence, given by  $\sqrt{\overline{X'^2}/\bar{X}}$ , specifies the mixing quality of the flow. The variance may also be considered as a deficiency in entropy of the fluid compared to a state where it has uniform temperature equal to the mean. However, its importance lies not in its physical interpretation, but in that it gives an insight into the structure of the flow. However, variance alone is insufficient to describe the flow as the same value may arise from quite different variations in temperature.

The autocovariance for finite sample length,  $\Theta$ , is defined as

$$Q(\tau) \approx \frac{1}{\Theta} \int_0^\Theta X'(t) X'(t + \tau) dt \quad (3)$$

This, when normalized with variance, is called autocorrelation.

$$R(\tau) = Q(\tau) / \overline{X'^2} \quad (4)$$

Autocorrelation is the correlation between the same quantity measured at two different times. It is useful in determining the 'integral time scale.'

Autocorrelation and power spectral density are related by the well-known Fourier transform. By noting that these are even functions, and that negative frequencies are impossible, the Fourier transformation is reduced to a cosine transformation

$$F(f) = 4 \int_0^\infty R(\tau) \cos 2\pi f\tau \, d\tau \quad (5)$$

and

$$R(\tau) = \int_0^\infty F(f) \cos 2\pi f\tau \, df \quad (6)$$

The autocorrelation and the power spectral density contain exactly the same information; however, the latter is often used because of convenience. Its wide usage has led to its acquiring a wide array of names--power spectrum, energy spectrum, spectral density, frequency spectrum, etc. These

refer to the same quantity, but numerous scaling factors are used in its presentation.

The maximum values of the lag time,  $\tau_{\max}$ , and the frequency,  $f_{\max}$ , are sufficiently large such that  $R(\tau)$  and  $F(f)$  are practically zero for larger values of  $\tau$  and  $f$ , respectively. Thus, the upper limits of the integrals in equations (3), (5), and (6) become  $\tau_{\max}$  and  $f_{\max}$ . The choice of these values is strongly dependent on the characteristics of the system. Differences of two or three orders of magnitude are common.

The spectrum represents the contribution to total variance by frequencies between  $f$  and  $f + df$ . It is the most important single quantity used in turbulence mainly because: (i) it brings out the idea of a continuous range of eddy sizes and provides a means of identifying eddies which are most significant as regards kinetic energy, and (ii) its characteristics give an insight into the microscopic structure of the flow.

An important quantity directly obtainable from the spectrum is the integral time scale mentioned earlier. It is defined as

$$\Gamma = \int_0^{\infty} R(\tau) d\tau \quad (7)$$

which is equivalent to

$$\Gamma = \frac{F(0)}{4} \quad (8)$$

It is representative of the average characteristic dimension of strongly correlated regions of fluid. Taylor considers this as the average time period of the eddies.

The above definitions, though not exhaustive, contain some of the more commonly used ones to study turbulence data. A complete list may be found in any standard reference on turbulence or random data [8, 10, 15, 36, 47, 74].

#### THEORETICAL ANALYSIS OF TEMPERATURE POWER SPECTRUM

Basic theoretical work on scalar turbulence is directed toward

predicting the behavior of power spectra and with transfer of energy from low to high frequencies where molecular effects are predominant. The developments closely follow those in the turbulent velocity field. Obukhoff [71], Yaglom [115], and Corrsin [21, 20] appear to be the first workers in this field. For an incompressible fluid the equation for  $\overline{T'^2}$  can be obtained from the energy equation [20].

$$\frac{\overline{D}}{\overline{Dt}} \overline{T'^2} = -2\overline{T'u'_k} \frac{\partial \overline{T}}{\partial x_k} - \frac{\partial}{\partial x_m} (\overline{u'_m T'^2}) + \alpha \frac{\partial^2}{\partial x_j \partial x_j} \overline{T'^2} - 2 \frac{\partial \overline{T'}}{\partial x_i} \frac{\partial \overline{T'}}{\partial x_i} \quad (9)$$

where

$$\overline{D}/\overline{Dt} \text{ is } [\partial/\partial t + \overline{U}_i (\partial/\partial x_i)]$$

In this equation the rate of change of temperature fluctuation 'power' is equal to (a) rate of production plus (b) rate of convection of 'power' plus (c) the last two terms describing molecular conduction and rate of destruction of 'power.' If the temperature and velocity fields are isotropic and independent--as they are when temperature fluctuations are small enough, the important mechanisms determining the distribution of  $T'$  are convection and diffusion. Under these conditions the mixing of  $T'$  is described by the conservative equation

$$\frac{\partial T'}{\partial t} + u'_i \nabla T' = \alpha \nabla^2 T' \quad (10)$$

which is linear permitting an estimation of the form of the spectrum at high frequencies. The interaction between velocity and temperature can be considered as an interaction between their Fourier modes which results in new modes of higher frequencies (or wave numbers). This mechanism, being similar to that in a velocity field, allows arguments similar to Kolmogoroff's hypotheses to be used in a temperature field. Kolmogoroff's postulate of local isotropy in non-isotropic turbulence may, thus, be assumed to be valid in this case also. At high Reynolds number, a 'Universal Equilibrium range' with statistical characteristics independent of the energy containing

eddies, exists at high wave numbers. The fundamental parameters governing turbulent mixing in this region are: (i) rate of viscous dissipation of turbulent kinetic energy per unit volume,  $\epsilon$ , (ii) thermal diffusivity,  $\alpha$ , (iii) momentum diffusivity,  $\nu$ , and (iv) local rate of strain parameter,  $\chi$ . If the wave numbers where molecular effects are predominant are very high compared to the energy containing wave numbers, conditions for isotropy would be satisfied for a region at the lower wave number end of the equilibrium subrange. In this region called the 'convection subrange,' the spectrum is dependent only on  $\epsilon$  and  $k$ , the wave-number magnitude. It is similar to the 'inertial subrange' in the velocity spectrum. By different arguments Obukhoff [71] and Corrsin [20, 21] independently predicted the form of the power spectrum to be

$$F(k) \propto \epsilon^{2/3} k^{-5/3} \quad (11)$$

A similar dependence was found by Gibson [38, 39] and Batchelor [4]. All these authors, however, did not take into account the fluctuations in  $\epsilon$ . When these are taken into account Van Atta [110, 111] showed a  $k^{-1.39}$  to  $k^{-1.72}$  (where  $k$  is the wave number) dependence, a variation which is clearly within the scatter of experimental data.

Beyond a certain wave number in the equilibrium range, known as the conduction cut-off, conductive effects become important. Obukhoff and Corrsin both placed its value at a magnitude of  $(\epsilon/\alpha^3)^{1/4}$ . A  $k^{-7}$  form in this region was predicted by Corrsin.

Batchelor [4, 5] was the first to point out the importance of  $\nu/\alpha$ , the ratio of momentum to thermal diffusivity, determining the spectral form and cut-off wave number. Depending on Prandtl number, three different categories were identified: (i)  $\nu \ll \alpha$  ( $Pr \rightarrow 0$ ); (ii)  $\nu \gg \alpha$  ( $Pr \rightarrow \infty$ ); and (iii)  $\nu \sim \alpha$  ( $Pr \sim 1$ ). In the first case, conduction cut-off takes place near the Obukhoff-Corrsin length scale,  $L_c = (\alpha^3/\epsilon)^{1/4}$ ; the



convection subrange, therefore, is not as extensive as the velocity inertial subrange in which the cut-off occurs near the Kolmogoroff length scale,  $L_k = (\nu^3/\epsilon)^{1/4}$ . For this case, the results agree with those of Obukhoff and Corrsin. It was concluded that the perturbations of the scalar distribution for scales smaller than  $L_k$  are due to direct interaction of the velocity fluctuations of  $k$ , such that  $1/L_c \ll k \ll 1/L_k$ , on regions of uniform temperature gradient. The assumption led Batchelor to a  $F(k) \propto k^{-17/3}$  form for the spectrum.

In the second case, cut-off is near  $(\epsilon/\nu\alpha^2)^{1/4}$ , and convection processes dominate beyond the inertial subrange. Thus, the argument that Equation (11) is valid for all  $k$  is incorrect as  $\nu$  cannot be neglected in the dimensional argument. A  $k^{-5/3}$  form holds only up to  $k \sim (\epsilon/\nu^3)^{1/4}$ . It is apparent that conduction effects are negligible in  $(\epsilon/\nu^3)^{1/4} \ll k \ll (\epsilon/\nu\alpha^2)^{1/4}$ . A  $k^{-1}$  form was predicted for this region. For higher wave numbers

$$F(k) \propto \exp(\alpha k^2/\gamma) \quad (12)$$

where

$$\gamma = -0.5(\epsilon/\nu)^{1/2} \quad (13)$$

Finally, for  $\nu \sim \alpha$ , inertial and convective subranges extend up to  $(\epsilon/\nu^3)^{1/4}$ . Beyond this the exact shape is unknown and may be different. As the velocity spectrum is observed to fall sharply, the temperature spectrum should also fall sharply.

Briefly one may say that (a) if  $\nu \gg \alpha$ , the mechanism responsible for small scale mixing is pure strain, and (b) if  $\nu \ll \alpha$ , direct interaction of small scale eddies is most important.

In two companion papers, Gibson [38, 39] showed that the small scale features of the turbulent scalar distribution are determined by points with zero gradient vector and surfaces of minimal gradient magnitude. According

to Gibson, by excluding these regions of fine-scale production from their model for  $\nu \ll \alpha$ , Batchelor et al. predicted a much more rapid decrease ( $\sim k^{-17/3}$ ) in the region  $1/L_c \ll k \ll 1/L_k$  than that predicted by him. Also, Corrsin's prediction of exponential decay beyond  $k \sim (\epsilon/\alpha^3)^{1/4}$  arises because he retains Batchelor's conclusion regarding the irrelevance of the mean local rate of strain parameter,  $\gamma$ , by replacing it with a macroscopic rate of strain. Gibson showed that, in general, the fine structure of scalar fields of arbitrary diffusivity reduces to a minimum size of  $(\alpha/\gamma)^{1/2}$  by local straining of zero or minimal gradient. Beyond this scale diffusion dominates.

Gibson solved the scalar spectral equation, given earlier, for different parts of the spectrum by using appropriate group of similarity parameters. Three coordinate systems of different similarity parameters were classified to permit a description of the scalar spectra, namely the Kolmogoroff, Batchelor, and Obukhoff-Corrsin scales. The results obtained for fluids of large Prandtl number were similar to Batchelor's for high wave numbers ( $k^{-1}$ ). For fluids of small Prandtl number, however, the high wave number part of the spectrum showed a  $k^{-3}$  dependence instead of  $k^{-17/3}$  predicted by Batchelor. Some of the available experimental data on low and high Prandtl number fluids seem to agree with his results [76, 83, 40, 43, 69].

Stratification and Incipient Boiling: Stratification in turbulence occurs when large temperature gradients, and subsequently large density gradients, exist in the flow. It becomes extremely important in turbulent natural convection flows because of the existence of large buoyancy forces. Stratification is accompanied by anisotropy and is described by the Richardson number--the ratio of buoyancy to turbulent forces. The most comprehensive discussions on this topic are given by Lumley and Panofsky [66] and Lumley [65]. When buoyancy forces are included in the turbulent energy equation,

the flux Richardson number appears in the term  $\overline{u_i' u_j'} \overline{U}_{i,j} (1-R_f)$ . For  $R_f = 0$ , i.e., no buoyancy forces, this term reduces to the familiar  $\overline{u_i' u_j'} \overline{U}_{i,j}$  form of the turbulent energy. The term vanishes when  $R_f = 1$ ; energy is removed by buoyancy forces as soon as it is produced by shear. According to Bolgiano [13, 14] the conversion of kinetic to potential energy can occur over a wide range of scales. The primary effect is to reduce the dissipation rate significantly below that which normally would be predicted on the basis of large scale eddies. The 'buoyancy subrange' (reflecting anisotropy induced by density gradient) located at the low wave number end of the equilibrium range is found to be proportional to  $k^{-7/5}$  ( $k^{-11/5}$  in the case of a velocity spectrum). Shur [90], however, observed a  $k^{-3}$  form for the buoyancy subrange in atmospheric velocity spectra. This was theoretically justified by him and others [65, 66, 90].

At temperatures approaching the boiling point of the liquid a reduction of power in the high wave numbers may be expected. The effect may be observed at temperatures much below boiling because of incipience. At high temperatures and gradient, both boiling and stratification may be significant. To the best of the author's knowledge, no theoretical work taking into account the combined effect of boiling and stratification in a turbulent field exists. Some experimental results were obtained in this work and the results are discussed later.

#### COMPUTATIONAL TECHNIQUES

A digital analyzing system has all the advantages of an analog system with practically none of the worries about calibration drift, overloading, and inaccuracies in the processing system equipment; moreover, refining of data and a change from one type of measurement to another can be made by changing a few program cards rather than the apparatus. Successful

application of digitizing techniques to turbulence has been demonstrated by Jones [51].

A discrete form of the Fourier Transform called the discrete Fourier Transform (DFT) is used in the Fourier analysis of discrete random data sequences. Thus, if  $X(m)$ ,  $m = 0, 1, \dots, N-1$ , denoted a sequence of  $N$  finite valued real or complex number then its DFT is defined as

$$C(k) = \frac{1}{N} \sum_{m=0}^{N-1} X(m) W^{km}; \quad k = 0, 1, \dots, N-1 \quad (14)$$

where

$$W = e^{-i(2\pi/N)}, \quad i = \sqrt{-1} \quad (15)$$

Equations (14) and (15) constitute the DFT pair.

The Fast Fourier Transform (FFT). The FFT is an algorithm used to compute the DFT with considerable saving in computational time. It has been thoroughly documented in a special issue of the IEEE Transactions [49]. The DFT requires  $N^2$  operations, whereas the FFT requires only  $N \log_2 N$ . Thus, for 1000 or more samples--a range encountered often in turbulence studies, a savings of 99% in computational time can be accomplished.

There are two main classes of FFT algorithms [42, 82]: (i) decimation in time and (ii) decimation in frequency. The basic philosophy in both the methods lies in 'factoring' the  $N$  data points into a matrix, then taking the Fourier transform of each column and combining the results thus obtained. Though not obvious, this factorization saves arithmetic in the same way as  $2(4 + 3)$  requires one less operation than  $(2 \times 4 + 2 \times 3)$ . The decimation in frequency method, requiring lesser number of computations than the decimation in time method, is discussed below.

Decimation in Frequency. In this form of the algorithm, the sequence is divided into two subsequences composed of the first and the last  $N/2$

points each. After some mathematics it is possible to show that:

$$C(2k + 1) = \sum_{m=0}^{N/2-1} \{Y_1(m) - Y_2(m)\} W^{2km} W^m \quad (17)$$

where

$$Y_1(m) = X(m)$$

$$Y_2(m) = X(m + N/2); m = 0, 1, \dots, N/2-1$$

The computational procedure for this method is shown in Figures 1 and 2.

Autocorrelation by FFT. That the autocorrelation may be computed by taking the DFT of the sequence and then its inverse is a well-known fact in communication engineering. The method becomes fast if the DFT's and IDFT's are calculated using the FFT algorithm. An algorithm for high speed autocorrelation for long sequences using some properties of the DFT was developed by Radar [80]. This technique is especially important in real-time estimation of power spectra and was used in the present work for analysis of water data.

Pruning. FFT pruning eliminates arithmetic operations that do not contribute to the output in the computation of DFT coefficients. It can be shown [82] that FFT pruning is faster than other FFT algorithms when (i) the number of nonzero input points is considerably smaller than the desired number of output points, or (ii) the desired number of transform coefficients is considerably smaller than the number of input points. It can be used effectively in the frequency or time domain.

Overlapped Periodograms. This form of the FFT algorithm reduces the number of computations and computer core storage requirements in addition to improving the estimates for the DFT coefficients. This method, first described by Welch [49], involves sectioning the record and averaging modified periodograms of the sections. The results obtained are approximate.

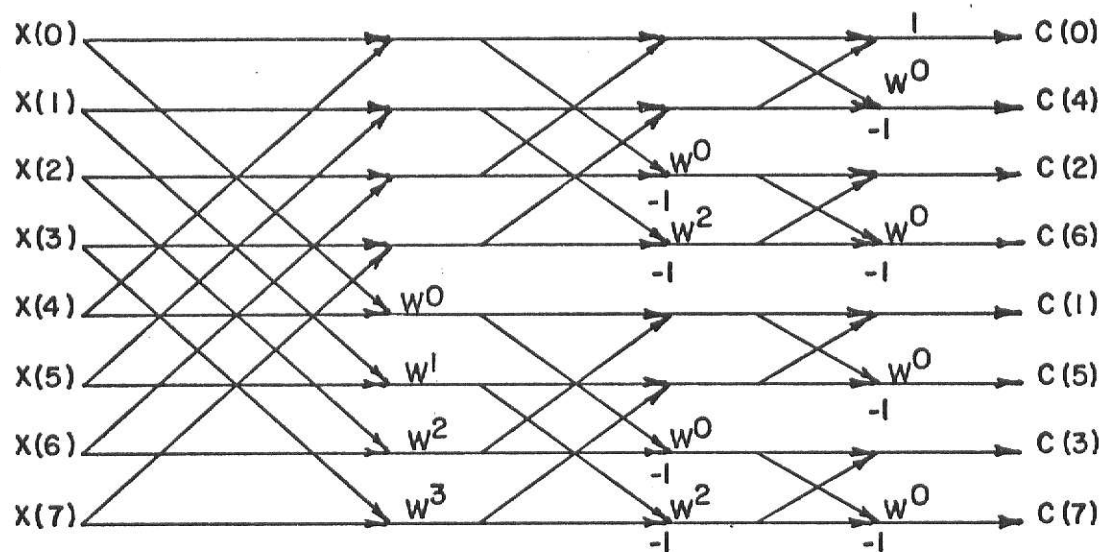


Fig. 1- 8-point decimation in frequency FFT.

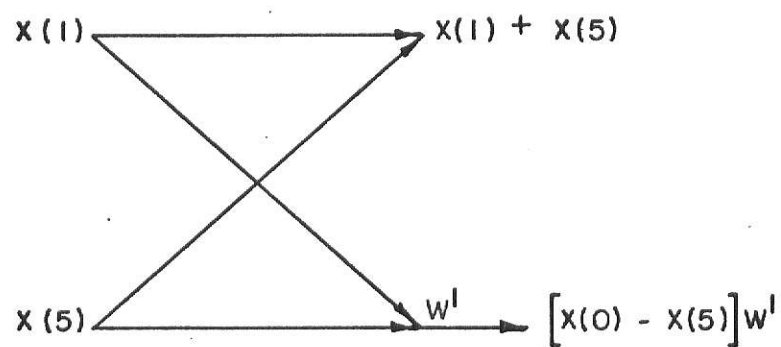


Fig. 2 - A butterfly.

## CHAPTER IV

## EXPERIMENTAL APPARATUS

The apparatus used in the present work was essentially that used by Julian [52]. The major components were a heated vertical flat plate, a container containing the liquid in which the plate was immersed, a temperature sensing device, a constant temperature bath, and instruments for recording and measuring.

## EQUIPMENT

The 4 x 2 x 0.004-in. vertical flat plate (Fig. 3) made of type-302 Stainless Steel was supported with the 2-in. edge vertical. During the initial part of the work, it was insulated from mercury by a thin coat of 'Datacoat'--a plasticized acrylic resin of high solid content. Due to frequent leakages, however, a more resilient epoxy resin paint was used later. Even this was found to be inadequate at high power levels and leakages through mercury occurred often. The plate was heated electrically by DC power from a Udyllite-Mallory standard rectoplater of 500 amps maximum capacity. The power delivered to the plate was regulated by a variac. The container, which supported the probe positioning mechanism and held the experimental fluids, had the dimensions 9 x 7 x 13 in., and was made of type-410 Stainless Steel. The probe positioning mechanism consisted of a 7/16-in. thick 8 x 13-in. plate with a slot and slide for moving the thermocouple horizontally. The slide was positioned horizontally by a 1/2-in. diameter, 32-thread per inch, precision pitch screw driven by a 2-rpm Hurst Synchronous Series DA motor. The linear speed

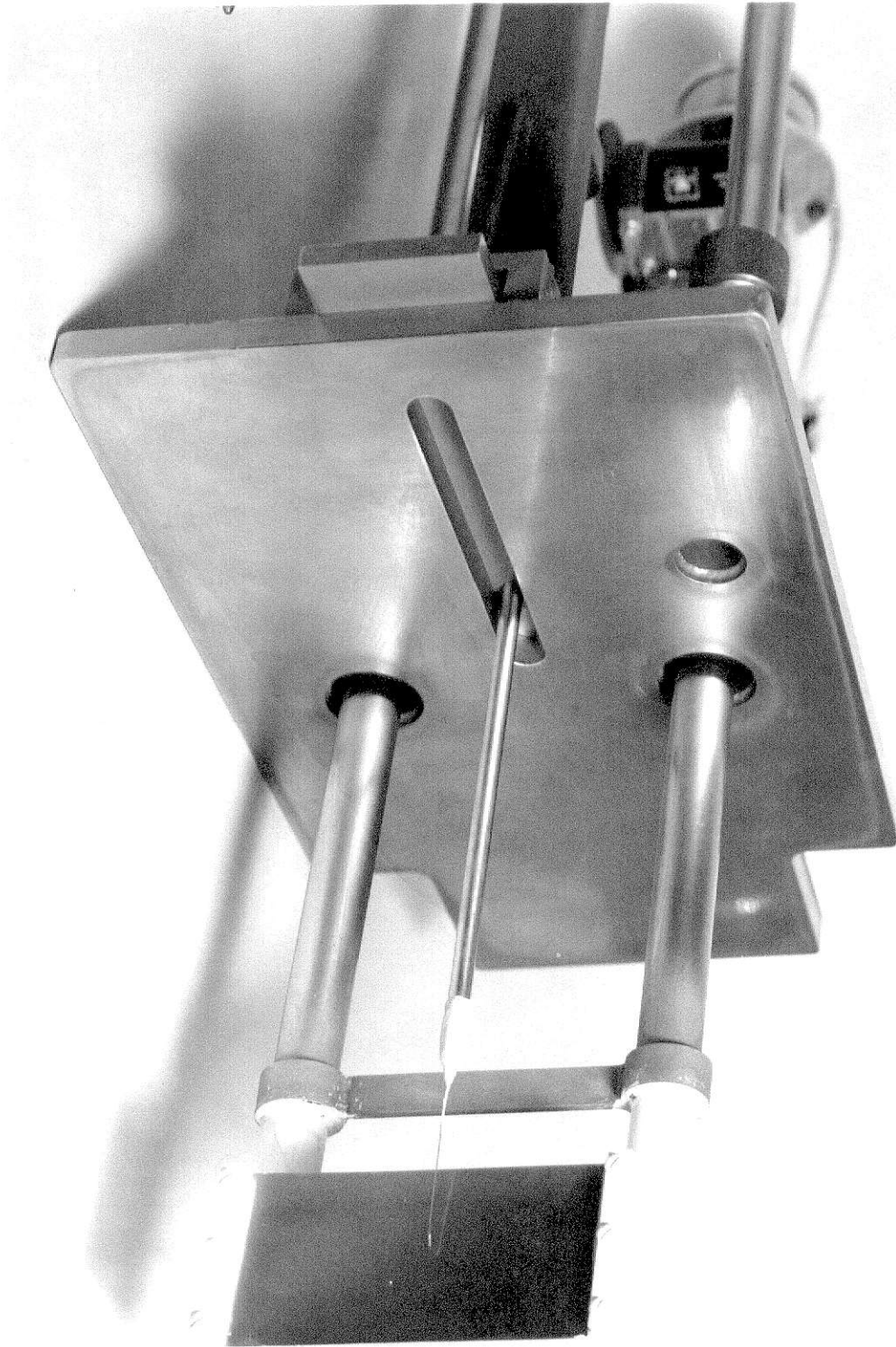


Figure 3. Vertical Plate and Thermocouple Probe



of the thermocouple was, thus, 1/16 in./min. A steel block prevented the probe being driven too far into the plate. The thermocouple could be moved vertically by another 1/2-in. diameter, 32-thread per inch, precision pitch screw. The exact position of the thermocouple from the plate was indicated by a counter connected to this screw. Fig. 4 shows a photograph of the entire mechanism. The copper bus-bars were enclosed in two 3/4-in. Stainless Steel tubes with alumina insulation. The third tube on the base plate was used for filling the container.

Temperatures were sensed by a Robinson-Halpern Model 302A-T300S-08L, sheathed, copper-constantan thermocouple. The sheath, 0.008-in. diameter, and type-302 Stainless Steel, was flattened to 0.004-in. thickness at the end. The time constant was approximately 0.02 sec. corresponding to a flat frequency response of about 8 Hz. Thus, signals up to about 10 Hz could be sensed without any significant attenuation. The probe was mounted with its axis parallel to the plate. Fig. 5 is a diagram of the probe.

The container was kept immersed in a 20-gallon Stainless Steel tank used as a constant temperature bath. Two, 750-watt, variable power, immersion heaters were used when heating was desired, and a cooling coil in conjunction with a tube-and-shell heat exchanger, both of copper, were used for cooling. The heating element was regulated by an off-on controller. Fig. 6 is a photograph of the temperature bath with the positioning mechanism and container inside it.

#### INSTRUMENTATION

The voltage generated at the thermocouple leads was recorded on a Sanborn Model 296 two-channel recorder after being passed through a



Figure 4. Probe Positioning Mechanism



Fig. 5. Sheathed Thermocouple

(Sheath diameter = 0.008"; End thickness = 0.004"; Time constant = 0.02 sec.)

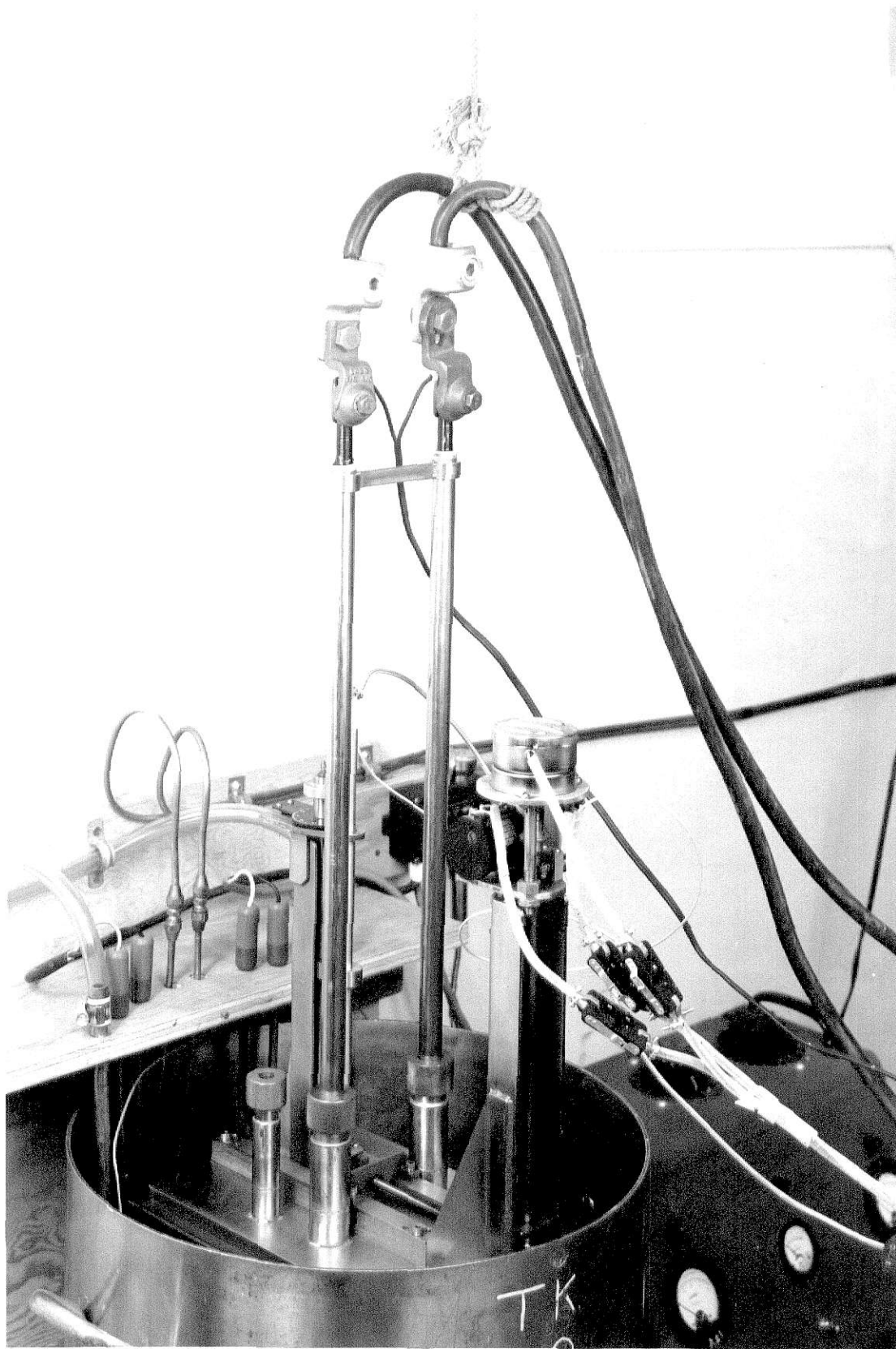


Figure 6. Probe Positioning Mechanism  
in Constant Temperature Bath

Sanborn 350-1500 low-level preamplifier. The sensitivity of this instrument was  $2 \mu\text{v/mm}$  thus allowing temperature difference measurements to within  $0.03^\circ\text{C}$ . The maximum possible error in the preamplifier was  $\pm 2\%$  and the response time was 25 milliseconds for 99.9% response to a step input. The response time of the recorder was five milliseconds to 90% of the final amplitude with less than 4% overshoot. Attenuation and chart speed could be set at one of the many available levels. Zero suppression was used to locate the zero voltage off the chart paper. When a chart speed of one mm/sec. was used, the position away from the plate could be measured to within 0.001 inch, which was equivalent to 1 mm of chart length.

The temperature fluctuations were recorded on a four-channel Hewlett-Packard (HP) 3600-series instrumentation tape recorder. The input to the HP was from the output of the Sanborn. The input level on the HP was adjusted so that the full scale reading on the HP corresponded to full scale on the Sanborn. FM record/reproduce at three tape speeds with adjustable input/output was possible. Frequency response over passband was  $\pm 1.0 \text{ dB}$  referred to 10% of the upper band-edge frequency and signal-to-noise ratio was 48 at 3-3/4 ips.

The voltage drop across, and current through, the copper rods connected to the plate was measured by a Data Precision digital multimeter (accuracy about 0.01%) and a Weston DC ammeter (accuracy about 0.8%), respectively. Currents above 250 amps were measured with a shunted General-Electric DC millivoltmeter.

## CHAPTER V

## MEASURING PROCEDURE, DATA ANALYSIS, AND RESULTS

## SYSTEM STARTUP AND CHECKS

The first step in the procedure, both for mercury and water, was equipment preparation and system startup. Equipment preparation consisted of placing the container in the constant temperature bath, adding the working liquid (water or mercury) to it and then clamping the probe positioning mechanism onto it. Additional liquid was added through the entry tube to completely fill the container. Distilled water was used and mercury was purified (by oxidation and filtering) before addition. Water, with a rust inhibitor added, was added to the constant temperature bath until the level was about two inches above the top of the slide on the probe positioning mechanism.

The power cables and all other leads were connected next. The cables were clamped as tightly as possible in order to insure good electrical contact. This precaution was necessary in order to prevent excessive heat dissipation. The output from the Sanborn recorder was fed into the Hewlett-Packard (HP) tape recorder. The equipment was grounded at various points to reduce the background noise level.\*

The power-supply, circulating pump, heaters, cooling water, Sanborn recorder, and Hewlett-Packard recorder were turned on and set to the desired conditions. For current levels of more than 240 amps a shunt

---

\*A power spectrum of the signal-plus noise for water (Fig. 25, Appendix C) analyzed to 100 Hz indicated that the level of noise was negligible compared to the signal level. In mercury, however, two sharp peaks of substantial power level were detected (Fig. 26, Appendix C). These gave rise to severe aliasing problems and therefore had to be cut off.

with voltmeter was used instead of the ammeter. For water, at least 12-13 hours were allowed for the system to come to steady state, although about two hours were normally sufficient. Due to its good conductivity, mercury did not require such a long time to come to steady state. Also at higher power levels the insulating paint on the plate and leads broke down easily so that only 3-7 hours were allowed. Heating the water for long times also ensured that most of the dissolved air was driven out. This was aided by the application of a vacuum to the entry tube.

Reproducibility of the data and a check on the steady state of the system was made by repeating the measurements after about an hour, and by shutting off and restarting the system a few times. A 1-2°C change in the mean values was observed, and this was attributed to the difficulty in exactly reproducing all the variables involved.

Most of the measurements in both the liquids were made at 1, 1/2, and 1-7/8 inches from the leading edge of the plate although some data were taken on the lower portion and above the plate. Test and initial runs were made at power levels below 100 watts in mercury and 800 watts in water. Most of the reported data, however, were taken at power levels between 100 to 400 watts for mercury and 800 to 1200 watts for water. Near-boiling temperatures at the plate were reached in some of the reported results in water. Due to the small height of the plate, the use of high power levels together with measurements confined to the upper region of the plate were necessary for significant turbulence levels to be reached. All the data were taken in the horizontal plane since the plate position could be accurately determined in this manner.

## TEMPERATURE PROFILES

The procedure for measurement and analysis of temperature profiles was essentially the one used by Julian [52]. The Sanborn recorder, on which the profiles were recorded, was calibrated before each set of experimental measurements by adjusting the response of the recorder to the known voltage of a standard cell. The zero position of the scale was set at the zero (right-hand edge) of the chart.

The thermocouple was set at the desired position up the plate by turning the micrometer dial until the desired reading on the counter was obtained. The thermocouple probe was driven in the horizontal direction by a synchronous motor at a constant rate of  $1/16''$  per minute. A mark was made on the chart after every revolution of the motor corresponding to  $1/32''$  of the probe movement. The temperature sensed by the probe, while moving toward or away from the plate, was recorded continuously on the Sanborn recorder. The position at which the probe contacted the plate was located on the strip-chart as being the point where the temperature abruptly leveled off. The temperature far from the plate, at which no change was observed, was taken as the bulk temperature. The probe was flexible enough so that it did not retain a permanent set when driven into the plate. The voltage drop across the copper rods, current in the circuit, bath temperature, position of the probe along recorder, attenuation, zero suppression, and chart speed were also recorded.

After making a few records of the profile, and a few of the temperature fluctuations (discussed later), the x-position of the probe was changed and similar data taken at the new location. The whole procedure



was repeated with different power levels.

Typical profiles for water and mercury are shown in Figs. 27 and 28 (Appendix D). Twenty to forty-five values of temperature (in terms of millimeters of chart width) and position (in terms of millimeters of chart length) were obtained from two or three different profiles. These data together with zero-suppression, attenuation, sensitivity, chart speed, voltage drop across the copper rods, current in the copper rods, the x-position of the probe, and the temperature at the plate and the bulk were processed by the IBM 370 system. The sequence of calculations performed by the computer is given in "Sample Calculations" (Appendix E). A listing of the computer program utilizing this sequence is included in Appendix F. The main quantities calculated were: (a) the temperature of each position on the profile using the thermocouple calibration chart, (b) the position of the probe from the plate, (c) the heat flux at the plate, (d) the Nusselt and modified Grashof numbers using the physical properties of the liquid\* and (b) and (c) above, and, finally, (e) the dimensionless distance and temperature.

The non-dimensional temperature distributions for different power levels and at different positions up the plate for water and mercury are presented in Figs. 7 and 8.

#### TEMPERATURE FLUCTUATION MEASUREMENTS

Temperature histories of various stations away from the plate were taken with the same thermocouple as used for the temperature profiles.

---

\*The physical properties were determined from least-square polynomial fit of these quantities versus temperature as given in Julian [52]. A reference temperature of  $(0.7 T_w + 0.3 T_\infty)$  as recommended by Sparrow [92] was used.

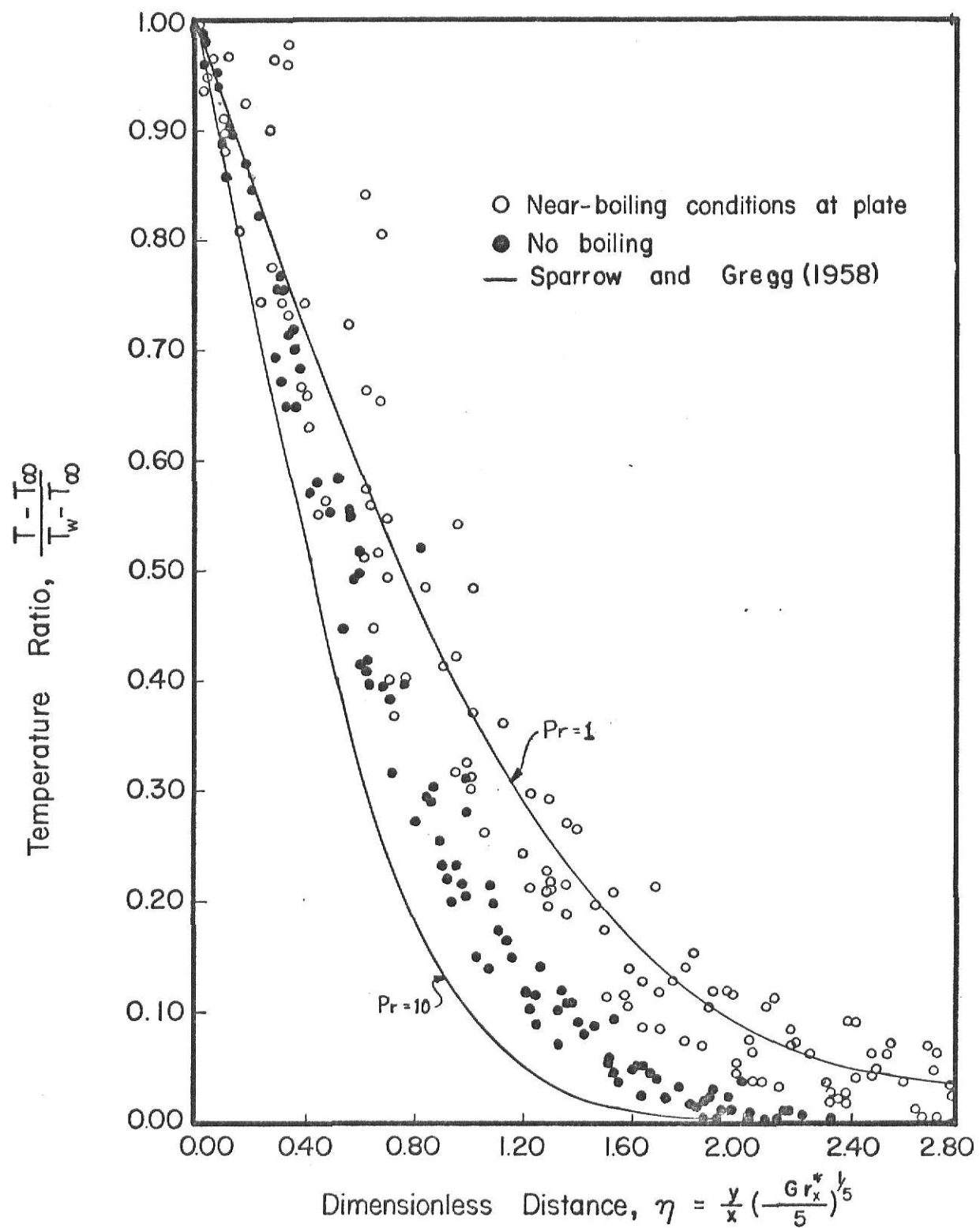


Fig. 7 Dimensionless Temperature Distribution for Water  
 $(10^9 \leq Gr_x^* \leq 10^{11})$

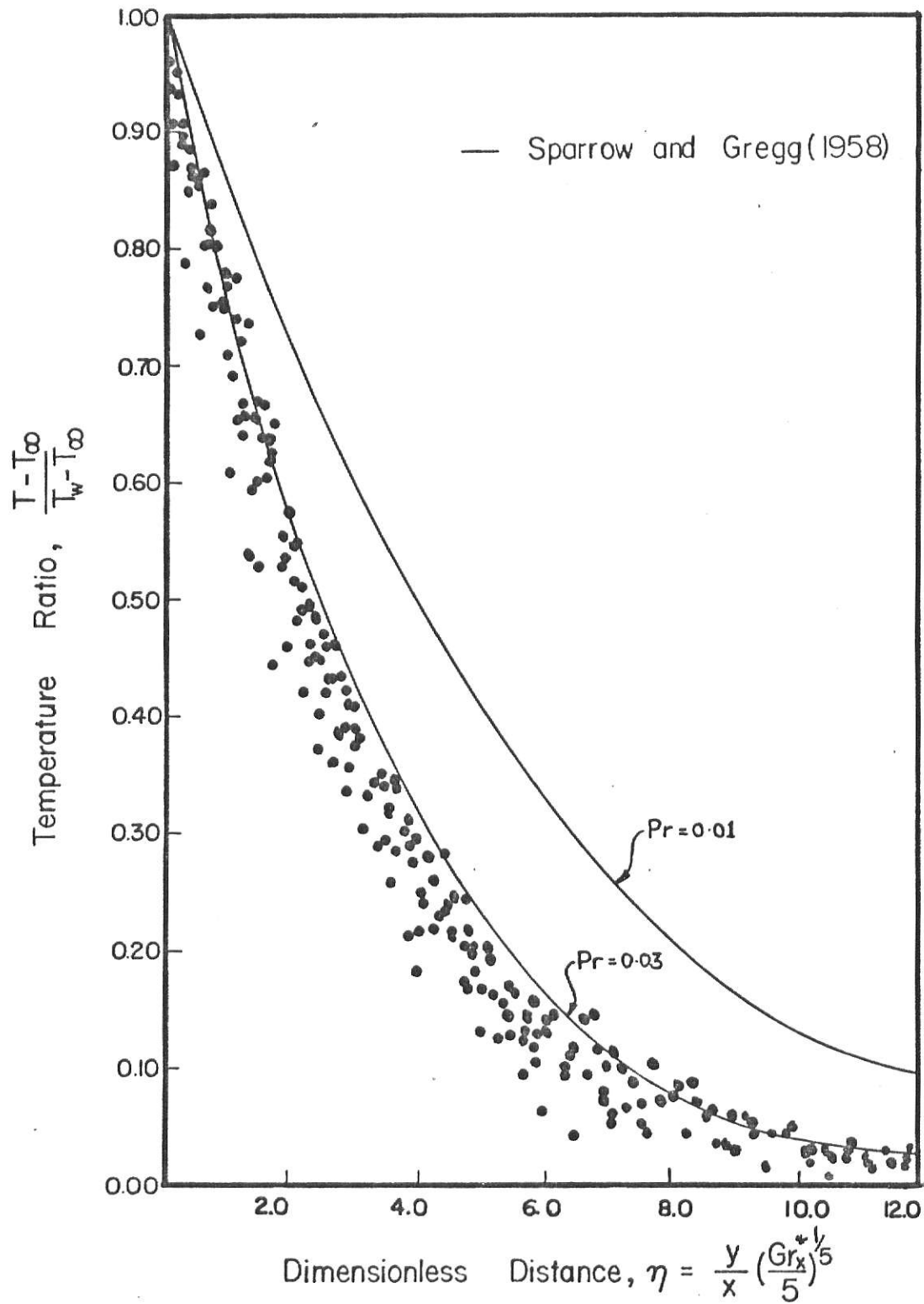


Fig. 8 Dimensionless Temperature Distribution for Mercury.  
 $(10^8 \leq Gr_x^* \leq 10^{10})$

Its frequency response was flat up to about 7 Hz. The upper limit of frequencies analyzed was thought to be adequate for the following reasons:

- (a) A previous study on natural convection from a 400-mm high plate in mercury [75] indicated the 'power' in frequencies greater than 15-20 Hz was substantially lower than that in the energy containing region. The height of the plate used in the present work was much smaller than the one used in that study so that dissipation processes, which contribute to the high frequency power, would not have developed fully in our case.
- (b) Preliminary measurements showed that this contention was correct.

Electrical noise from the 3-phase rectifier and elsewhere presented significant problems especially in mercury where the signal-to-noise ratio was very low because of the low signal power. When mercury data were analyzed, significant aliasing problems were faced. The problem was overcome by digital methods discussed later. Such methods were not necessary for water data due to the large signal-to-noise ratio there.

Temperature fluctuations at various positions along and away from the plate are given in Figs. 29 to 33 in Appendix D. Representative fluctuations above the plate are also shown.

The fluctuating signal from the thermocouple was passed through the Sanborn recorder where it was amplified. This amplified signal was recorded on FM mode on the HP tape recorder at a speed of 3-3/4 in./sec. The speed of the strip-chart was kept at 1 mm/sec. for all runs. The input level on the HP was adjusted so that the full scale on the Sanborn corresponded to full scale on the HP. The output level on the HP was adjusted to the maximum possible level; the signal from it then fell in the  $\pm 5$  V peak-to-peak range. In this way, maximum amplification of

the input signal was achieved without the necessity of additional amplifiers. Before each set of recordings the output voltage from the HP corresponding to the maximum and minimum positions on the strip-chart were recorded; these varied a little but most of the time were around +3 and -3V, thereby falling in the  $\pm 5V$  range required for the analog-to-digital converter.

The signal was recorded on the tape and strip-chart recorders simultaneously to facilitate documentation. Attenuation was set so that the signal covered as wide a range as possible on the strip chart. The tape-recorder counter was set to zero at a mark near the starting end of the tape. The counter reading at the beginning and end of each record, zero suppression, attenuation, y-position of the probe, etc., were all noted on the strip chart. Records were taken for about 2-6 minutes. Recording was possible on only one channel of the tape recorder due to a malfunctioning channel-selector switch.

#### DIGITIZATION

After a set of records for one power level was taken, the analog tape was digitized using a Nova-1200 minicomputer system. The detailed digitizing procedure has been documented in a "User's Guide" [109]. Sampling frequencies of 5-200 Hz could be selected by typing in an octal number corresponding to the frequency desired on the teletype. The runs at lower power levels with water were digitized as a rate of 10 samples/sec. and at 20 samples/sec. for the higher power levels. A sampling rate of 150 samples/sec. was used for all runs in mercury. Data were digitized at 7-bit accuracy and the (7+1)-bit data words were recorded on a PEC incremental tape recorder. The tape from this unit was IBM 370 compatible

so that it could be used directly as a data file for the computer program or for punching out data cards. Data cards were obtained initially but this practice was discontinued for reasons of cost.

A note on sampling frequency seems to be in order here. A high sampling rate, apart from increasing the processing cost, would yield correlated and highly redundant data. On the other hand, a low sampling rate leads to confusion between the low and high frequency components. The highest frequency which can be defined by sampling at a rate of  $1/h$  samples/sec. is  $1/2h$  Hz. Frequencies in the original data above this frequency of  $1/2h$  Hz, commonly known as the Nyquist frequency, will be folded back into  $0-1/2h$  Hz range. This problem is called aliasing. The sampling rates chosen in this work were based on reasons given before.

In the early part of this work, digitization was done by hand because of non-availability of an Analog-to-Digital facility. Apart from being laborious, this practice yielded inaccurate results because the maximum Nyquist frequency possible was only 0.5 Hz.

## STATISTICAL ANALYSIS

The basic theory used in this section is given in Chapter III and references mentioned therein. The major quantities calculated were the temperature power spectra, autocorrelation functions, intensity distributions, and integral time scales. A novel feature of the spectral analysis was the use of the fast Fourier transform (FFT).

Water. Normalized Power spectra of test and a few of the reported runs were computed using the modified form of a computer program--BMD02T [12], which calculated the power spectrum by the classical method of computing the discrete Fourier transform (DFT) of the autocorrelation

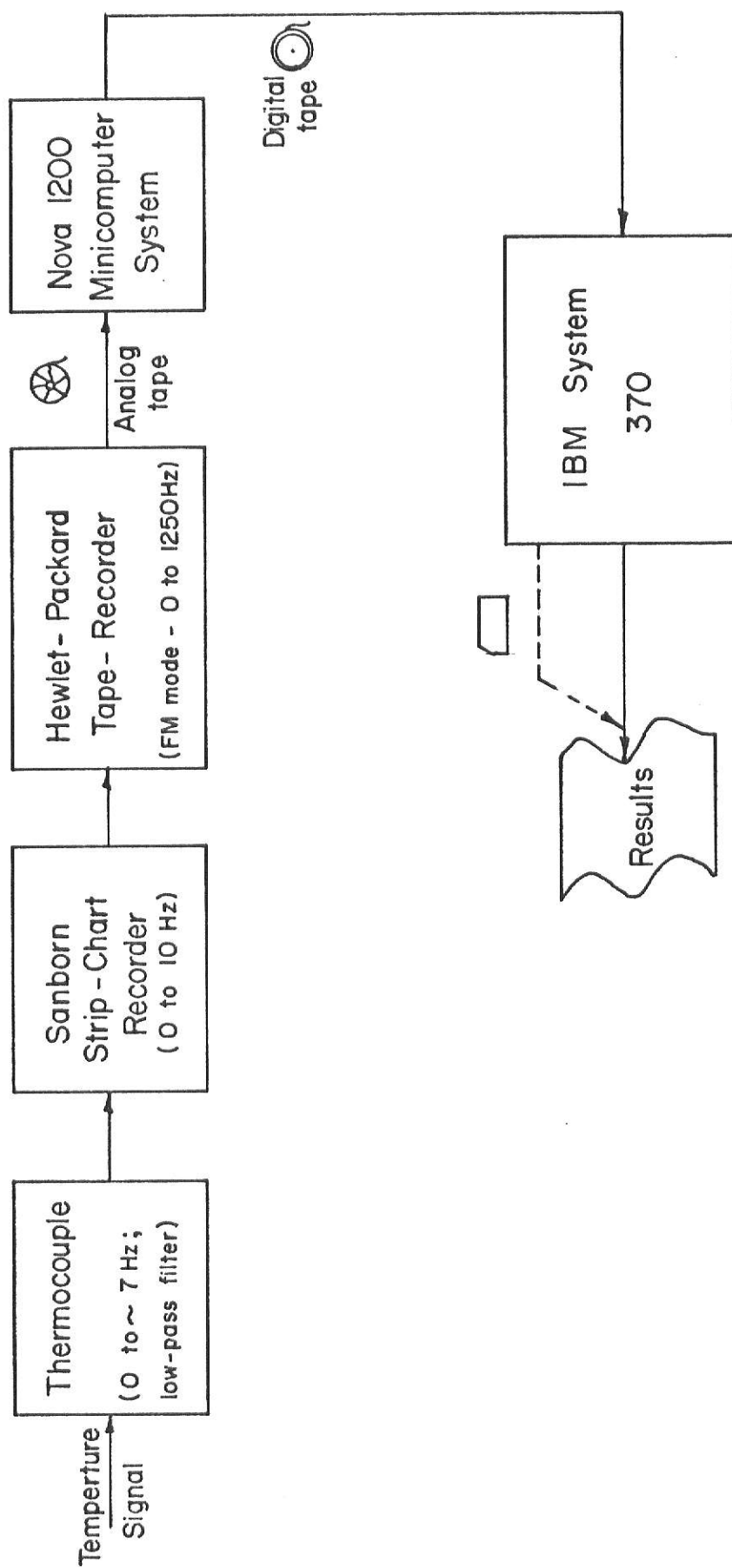


Fig. 9 Block Diagram for Data Acquisition and Processing.

function. Generally, 1000 samples and 100 lags were taken. All reported results analyzed with this method were examined up to a maximum frequency of 5 Hz. For most runs, however, the DFT's were calculated by the FFT method.

A brief discussion on the FFT method has already been given in Chapter III. The analysis scheme used here was given by Radar [80]. The autocorrelation was obtained by taking the inverse transform of the forward Fourier transform. The cosine transform of this autocorrelation was taken and a scaling factor incorporated to give results exactly similar to those got by the earlier method. A comparison of the results obtained from the two techniques is given in Fig. 10. Normalization in this and the previous case was done by the variance of the data. FFT's were calculated using the decimation in frequency method which requires less computations than the decimation in time method. Spectral smoothing was done by passing the raw spectral estimate through a 'Hamming' window. Analysis up to 10 Hz using  $2^{10}$  points and  $2^7$  lags were normally performed. However, any integer-power-of-two number of points could be, and were, used occasionally.

A check on the validity of the calculations were performed by finding the area under the normalized power spectrum. It should equal variance. Excellent agreement was found with errors up to 0.5% only.

The power spectra obtained at different stations in water are shown in Figs. 11 to 14. Some points in all spectral density plots have been omitted for clarity. A few autocorrelation plots have also been included (Fig. 15). A computer program for computing these and other quantities is given in Appendix F. The mean was extracted from the data before



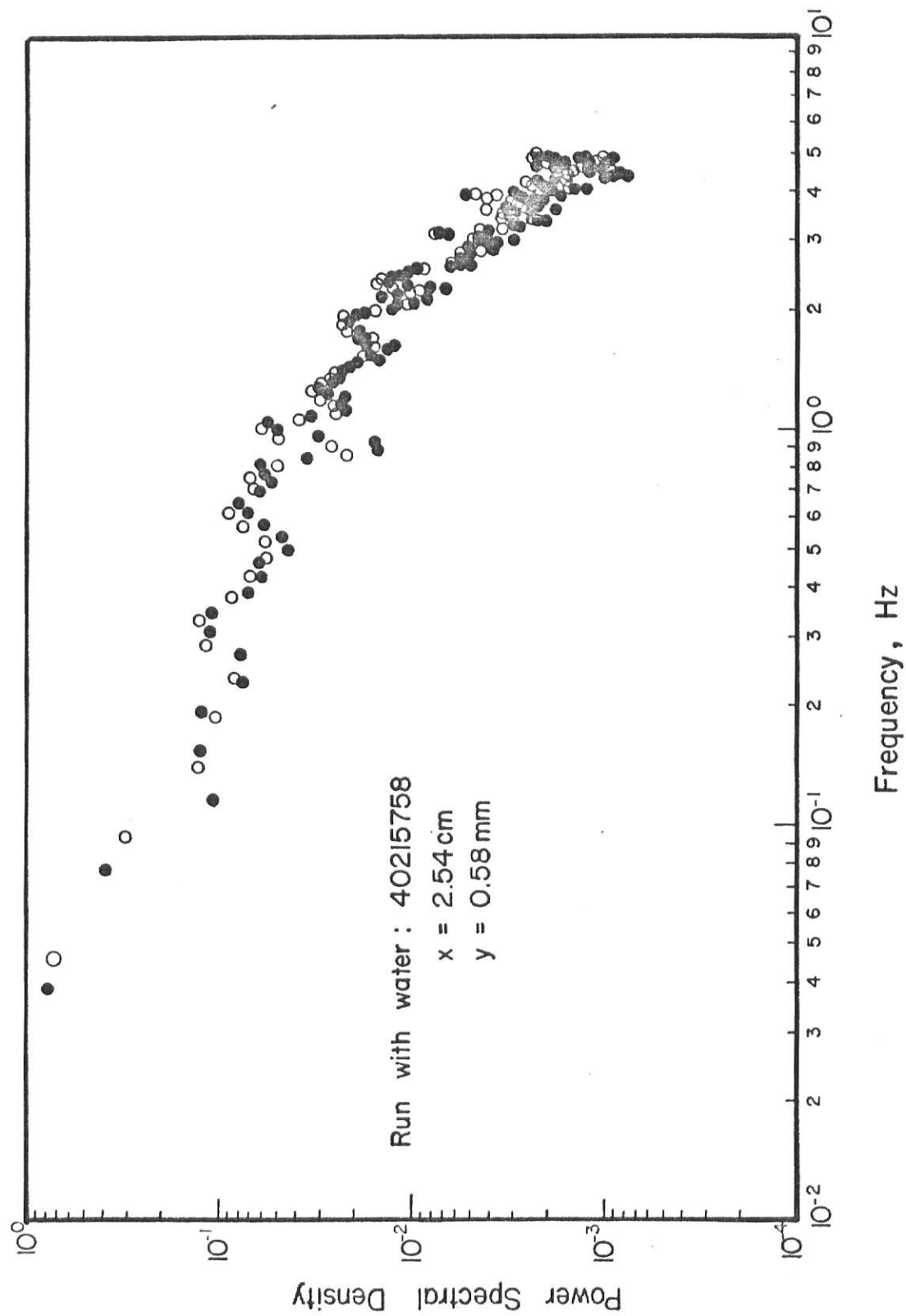


Figure 10 . Power Spectrum as Calculated by FFT (●) and Through Auto-correlation (○) .

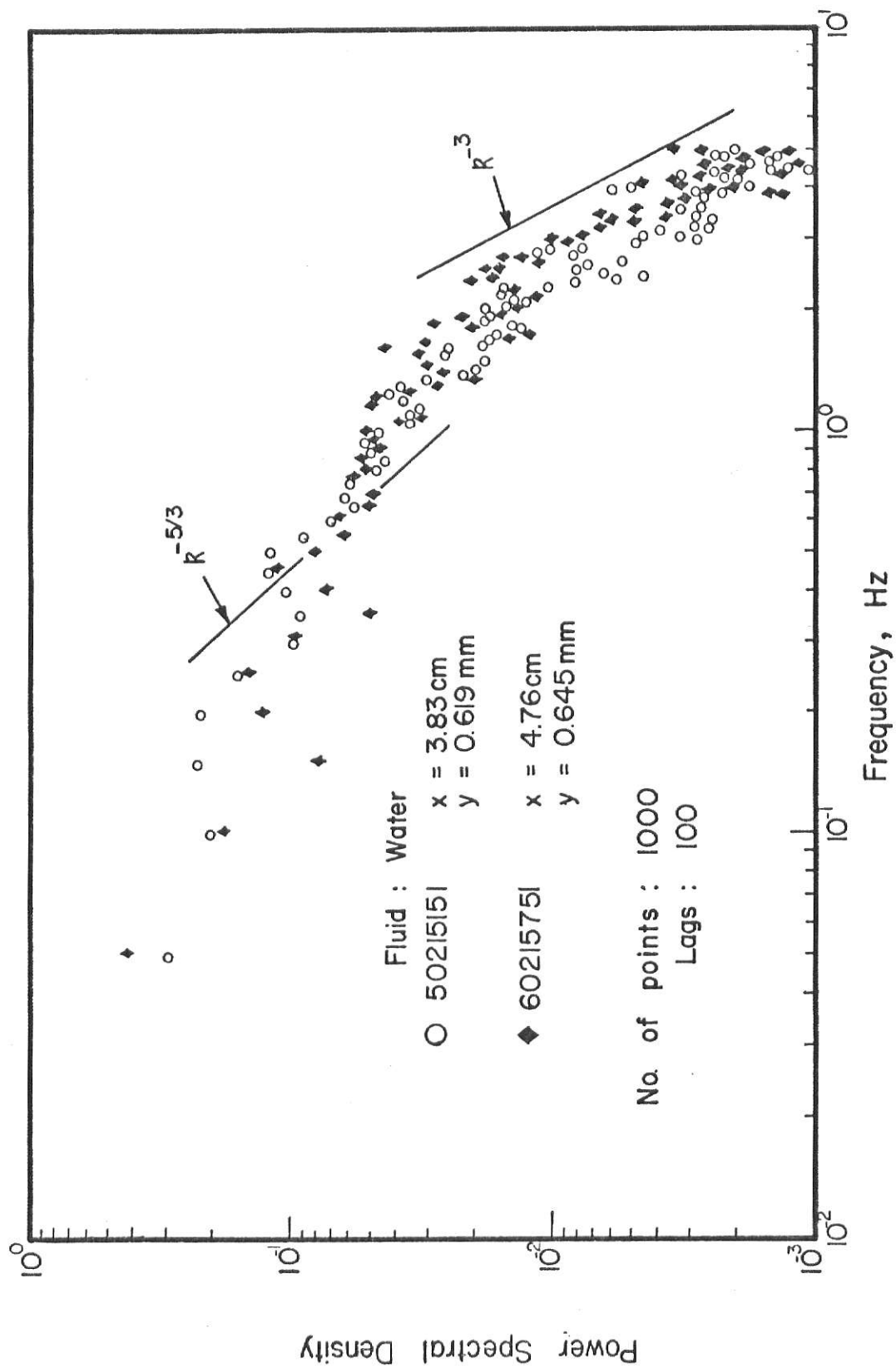


Fig.11 Variation of Temperature Power Spectra in the Vertical Direction.  
 (Power  $\approx 830\text{w}$ )

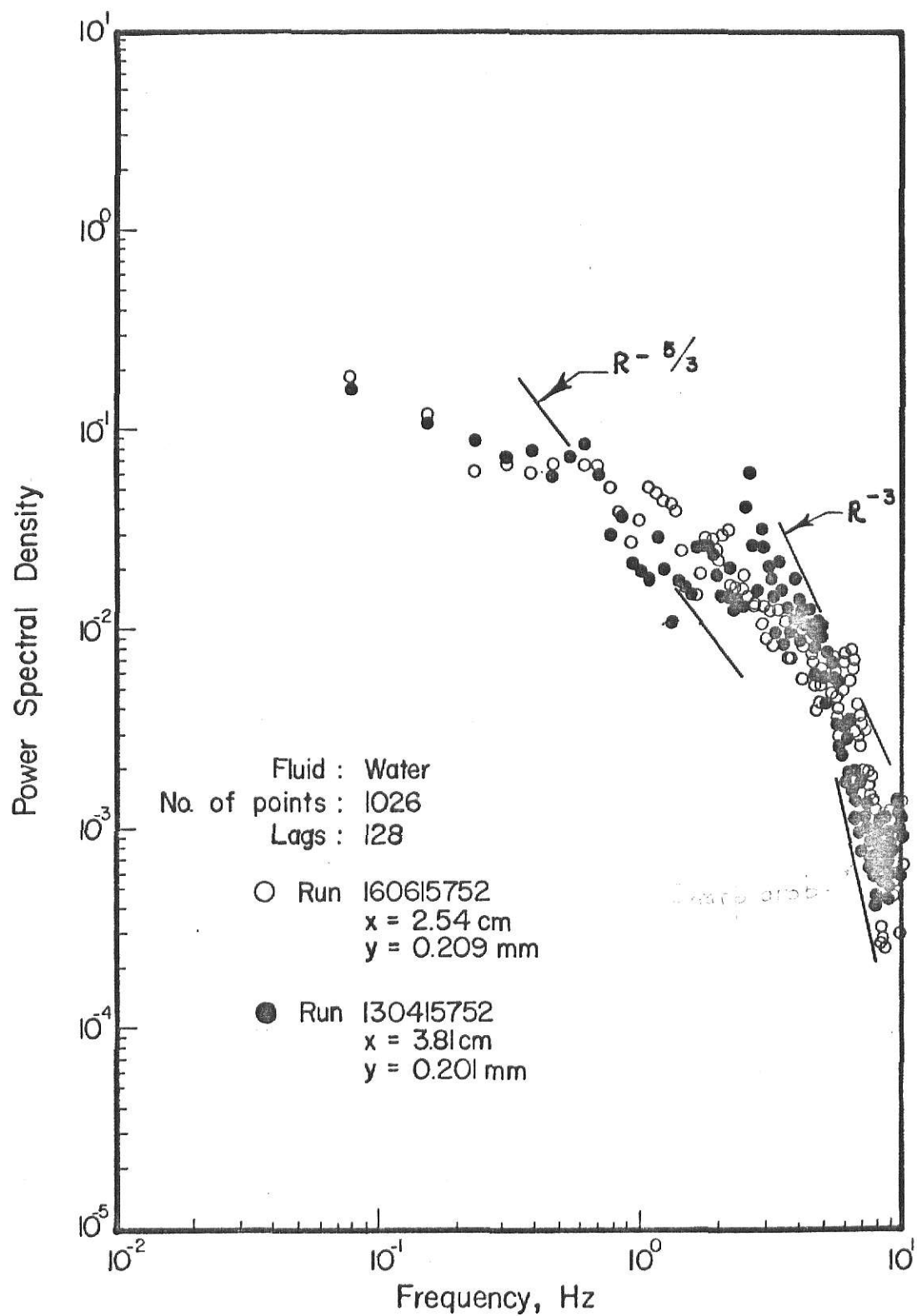


Fig.12 Variation of Temperature Power Spectra in the Vertical Direction. (near boiling conditions at the plate; Power  $\approx 1188$  W)

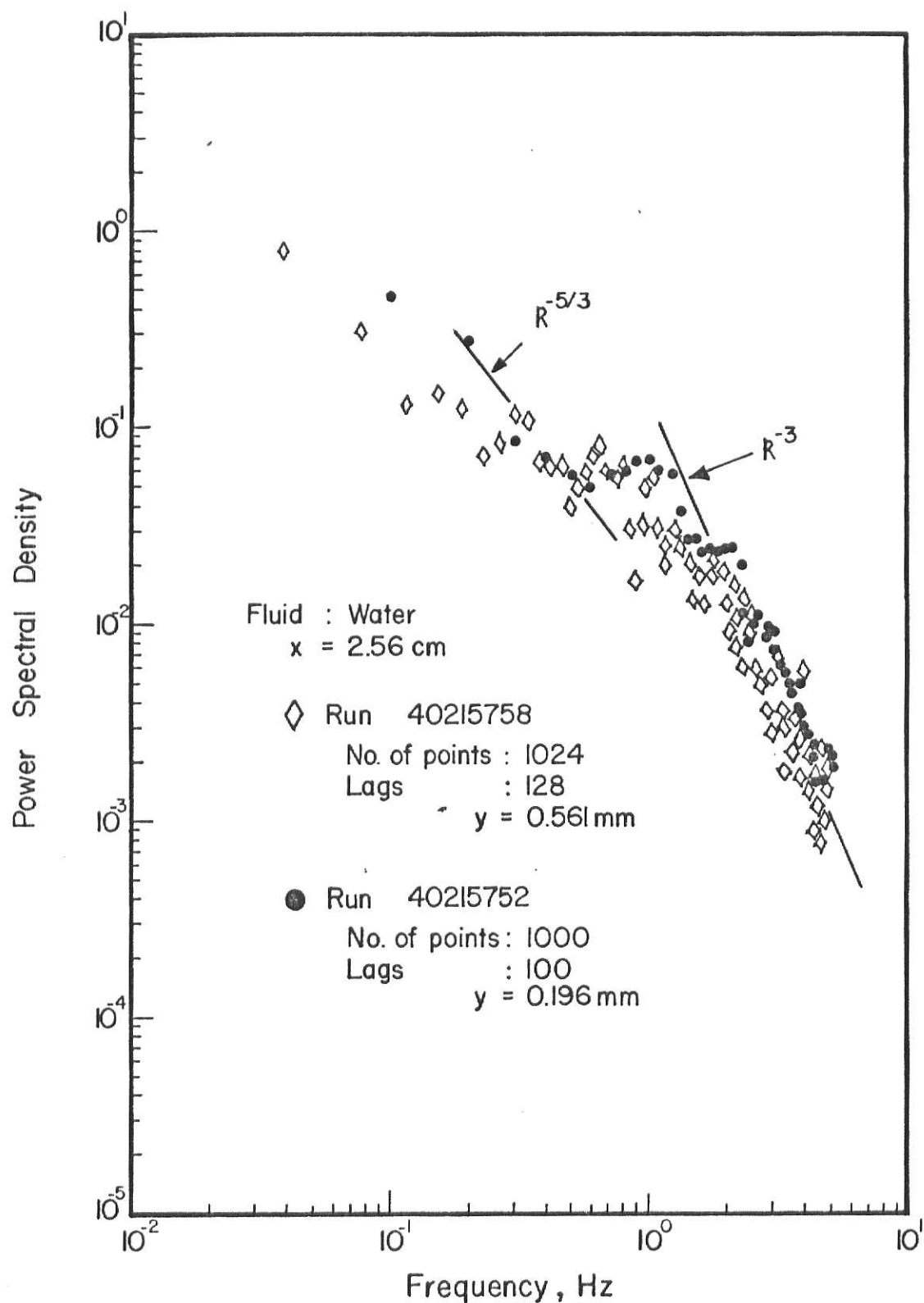


Fig.13 Variation of Temperature Power Spectra in the Horizontal Direction (Power  $\approx 830$ W)

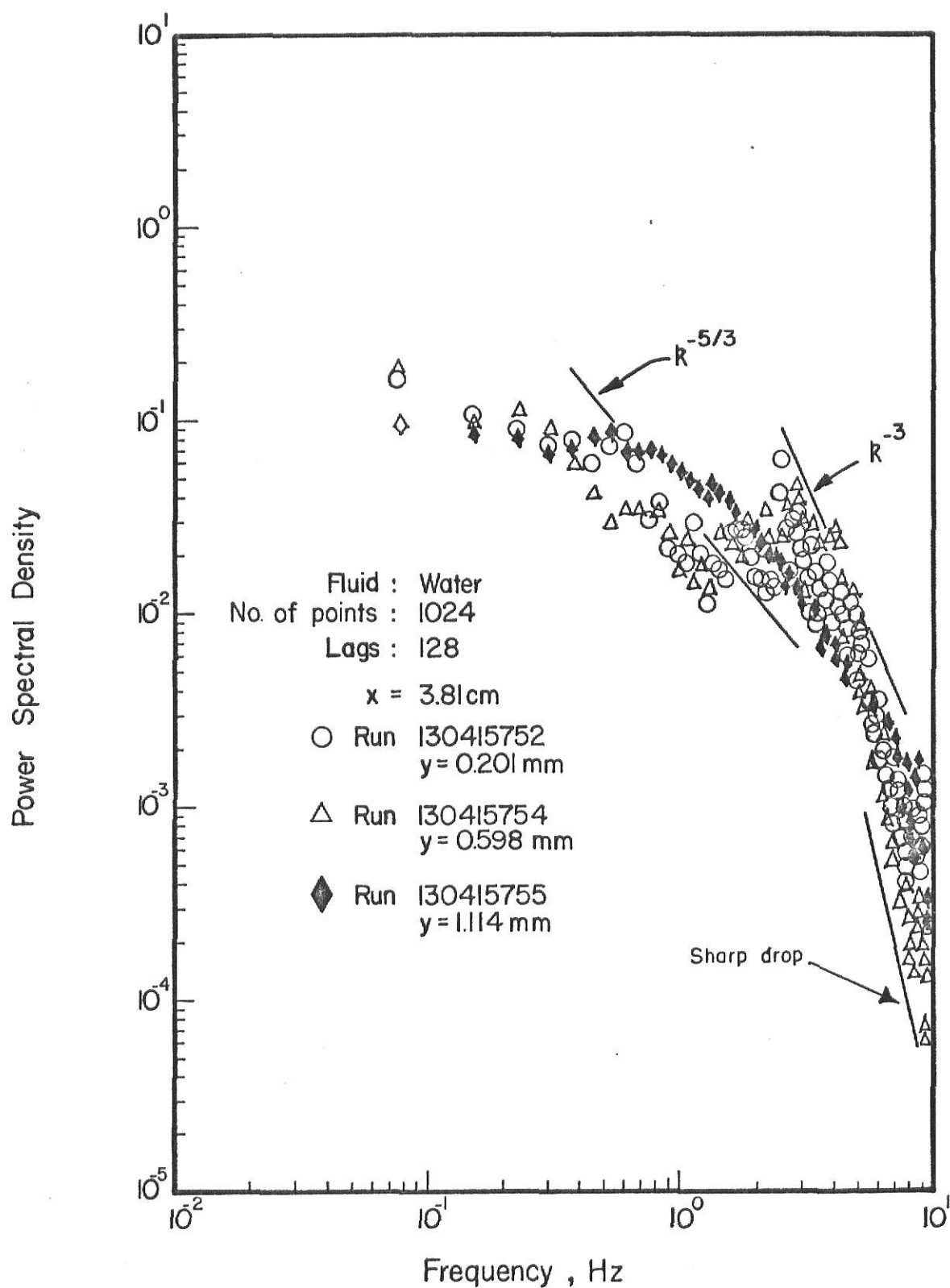


Fig.14 Variation of Temperature Power Spectra in the Horizontal Direction (near-boiling conditions at the plate; Power  $\approx 1188$  w)

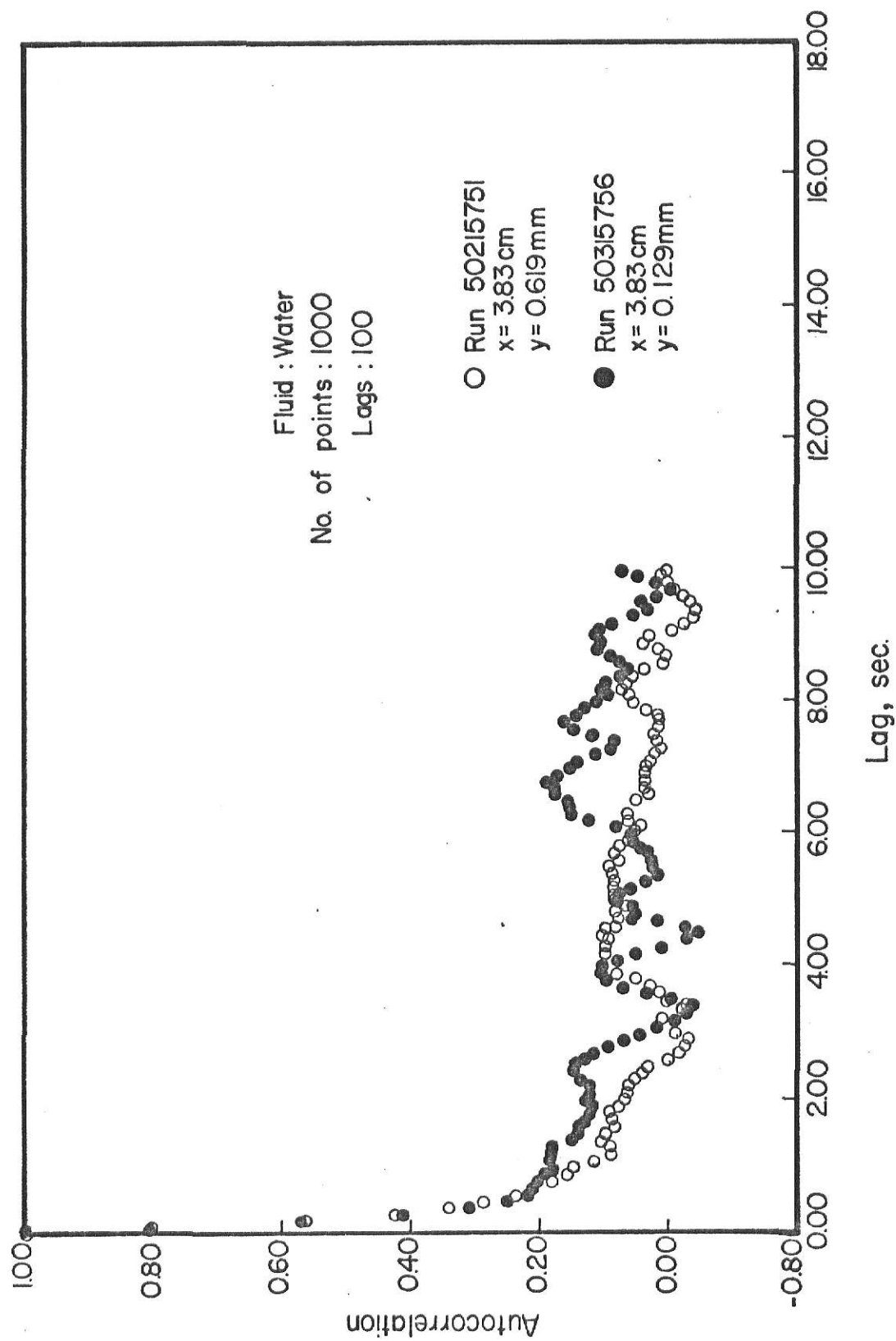


Fig.15 Autocorrelation of Turbulent Temperature Fluctuations.

performing calculations. The program also calculated the variance and the integral time scale of turbulent temperature fluctuations. Graphs of intensity distributions at different stations are given in Fig. 16. Integral time scale distributions are given in Fig. 17.

Mercury. The computation of power spectra for mercury presented some problems as, contrary to water data, the signal-to-noise ratio was low. Trial runs by low frequency digitization (10 and 20 samples/sec.) revealed significant aliasing (Fig. 18) and the suspicions that electrical noise was causing it were confirmed when a set of data was analyzed up to 100 Hz. It revealed two sharp peaks as shown in Fig. 26 (Appendix C). Continuation of the analysis by the same method meant that analysis would have to be performed up to at least 75 Hz though only up to about 10 Hz was necessary due to limitations imposed by the frequency response of the thermocouple. Data were next digitized at 200 samples/sec. The number of points per set had to be increased to at least 6144 and the lags to 256 in order that a representative section of the data be analyzed. It was found that the autocorrelation never dropped to zero, showing high correlation in the data, and that negative power was present at some frequencies although most literature on this topic takes the view that negative power is impossible. Increasing the number of samples or lags meant that the processing cost, even with FFT, would go up considerably.

In view of all these problems, this approach had to be abandoned and a pruned FFT, in conjunction with an approximate method to calculate the spectra given by Welch [49], was used. A total of 8192 points with 1024 points in each segment and 15 overlapping segments were used in each run. The cost of each run was reduced considerably as only 64 spectral points were calculated in each case (pruning). Spectral smoothing was done with

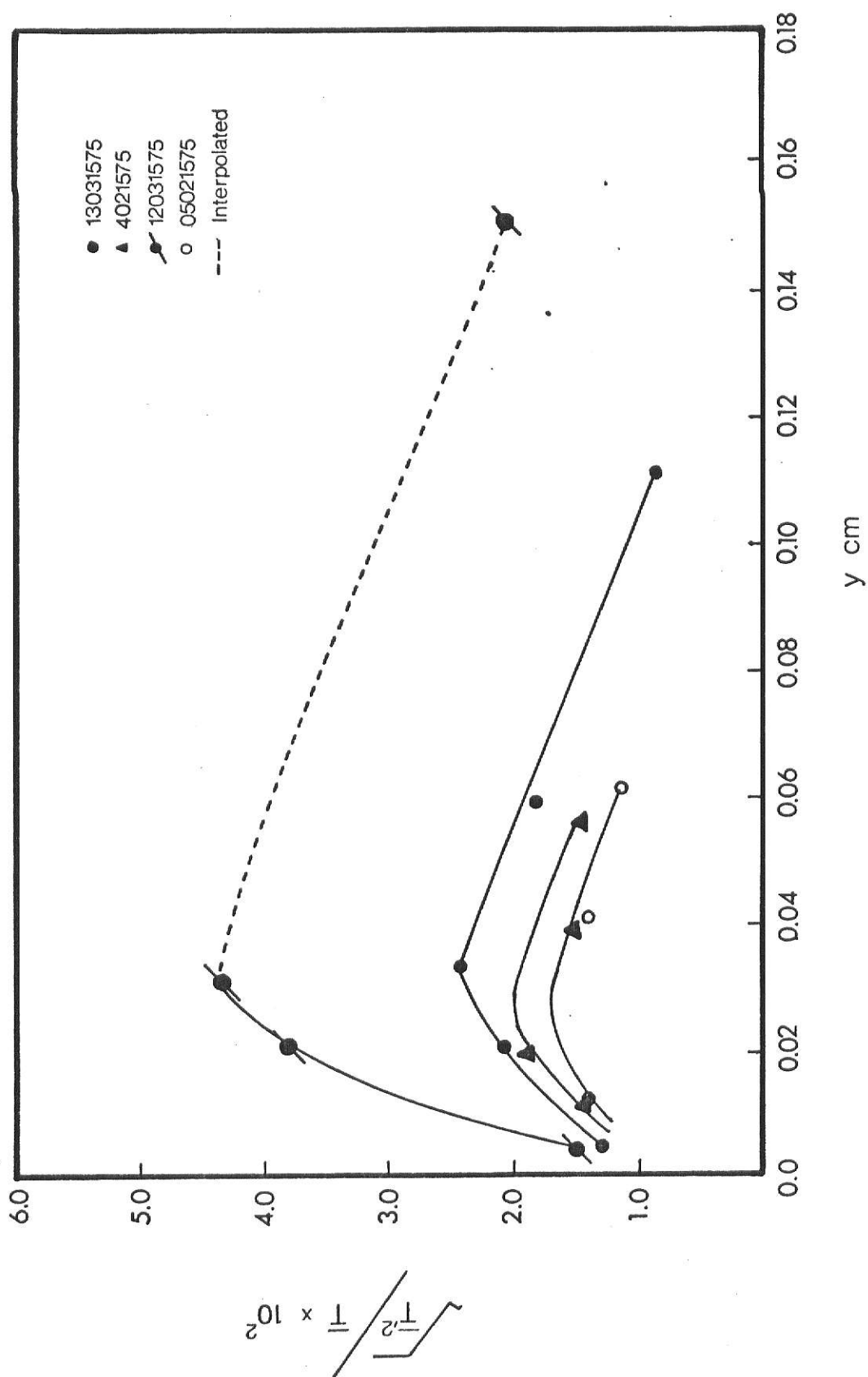


Fig.16 Variation of Intensity in Water



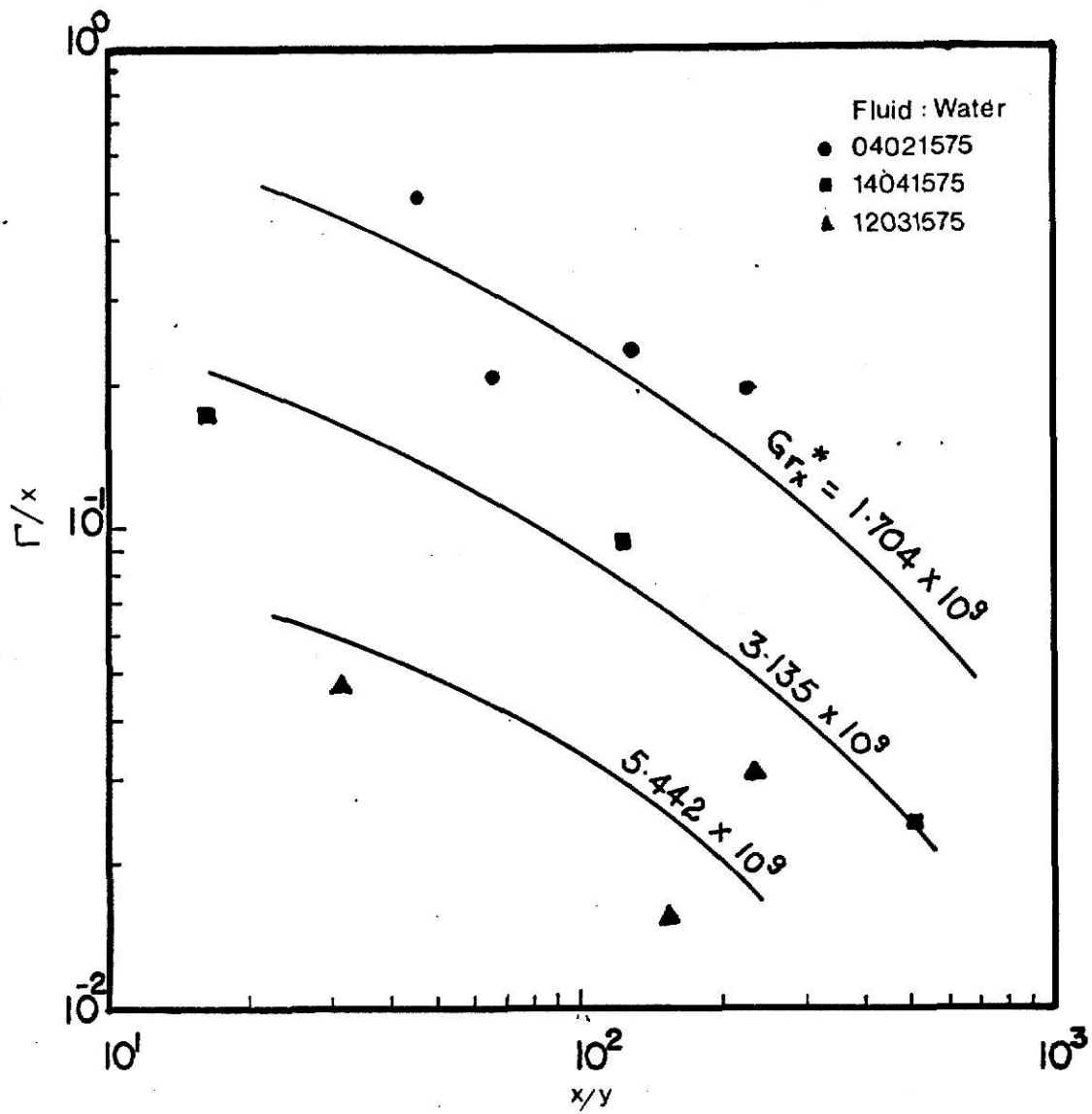


Fig 17 Variation of Integral Time Scale,  $\Gamma$

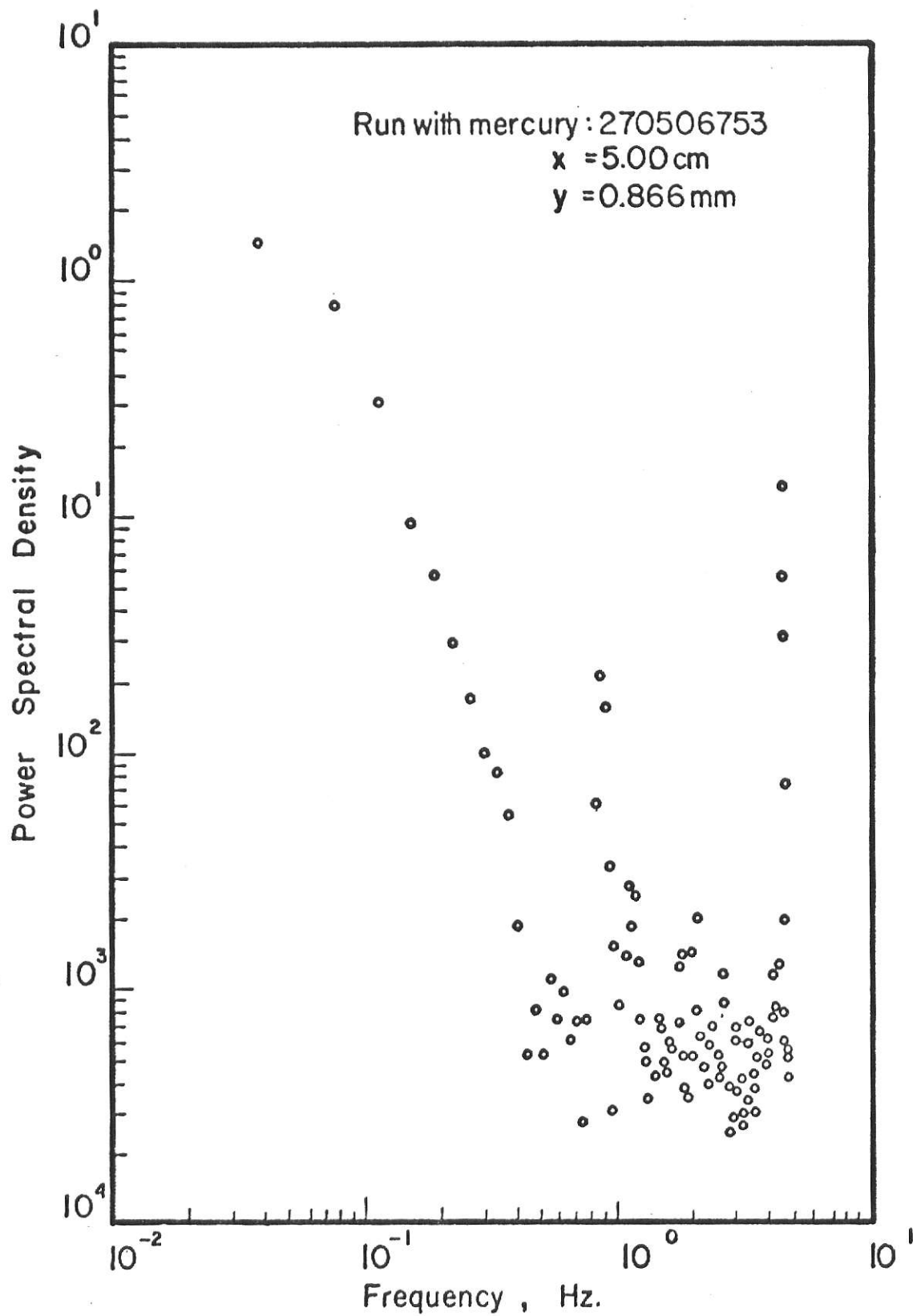


Fig.18 Power Spectrum Showing the Severe Aliasing Problem in Mercury.

a 'Hanning' window and normalization was done as before. All calculations were performed on the data with its mean extracted. The validity of the computations was checked as before, and though the method used was approximate, errors were only about 8%.

The power spectra, and intensity distributions calculated by using the computer program given in Appendix F, are presented and compared in Figs. 19 to 24.

#### HEAT TRANSFER RELATION

Figure 25 presents the local Nusselt numbers, for heat transfer in water and mercury, plotted against Rayleigh numbers. A fit of the data gave the following relation:

$$\text{Nu}_x = 6.32 (\text{Gr}_x^* \text{Pr})^{0.31} \quad (18)$$

This can be compared with Sparrow and Gregg's [94] solution (put in a dimensionless form using Rayleigh number) which predicted

$$\text{Nu}_x = 2.94 (\text{Gr}_x^* \text{Pr})^{0.2} \quad (19)$$

The agreement between theory and data is not very good. Generally speaking, discrepancies between theoretical works and experimental data are not uncommon as discussed in Chapter II.

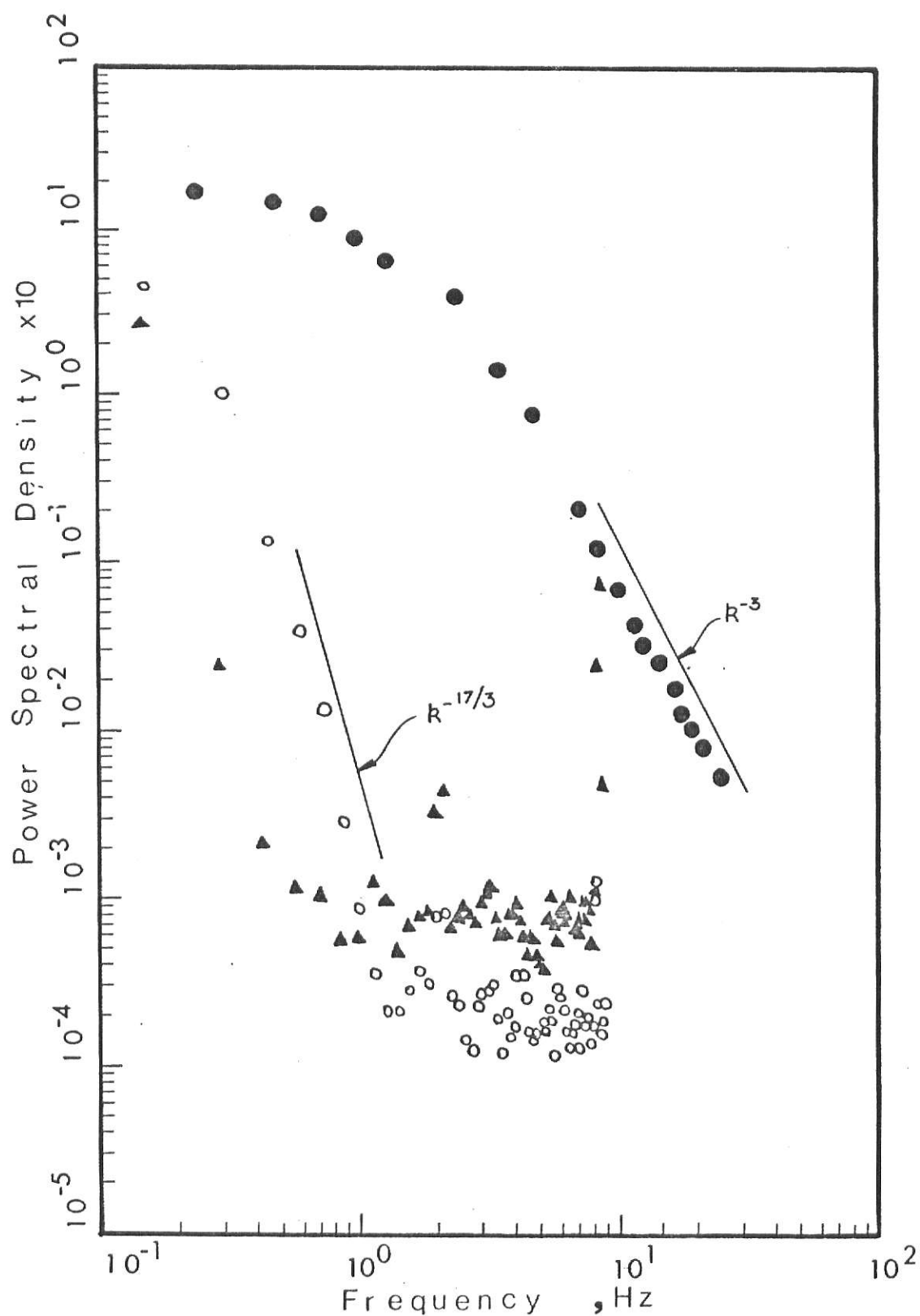


Fig.19 Variation of Power Spectra in the Vertical Direction in Mercury at  $y = 7.19$  mm (Power  $\approx 315$ W).

● Papailiou and Lykoudis (1974),  $x = 100$  mm,  $y = 0.25$  mm,  $P = 1300$  W.

○ Run 460519754,  $x = 49.2$  mm.

△ Run 460519753,  $x = 3.2$  mm.

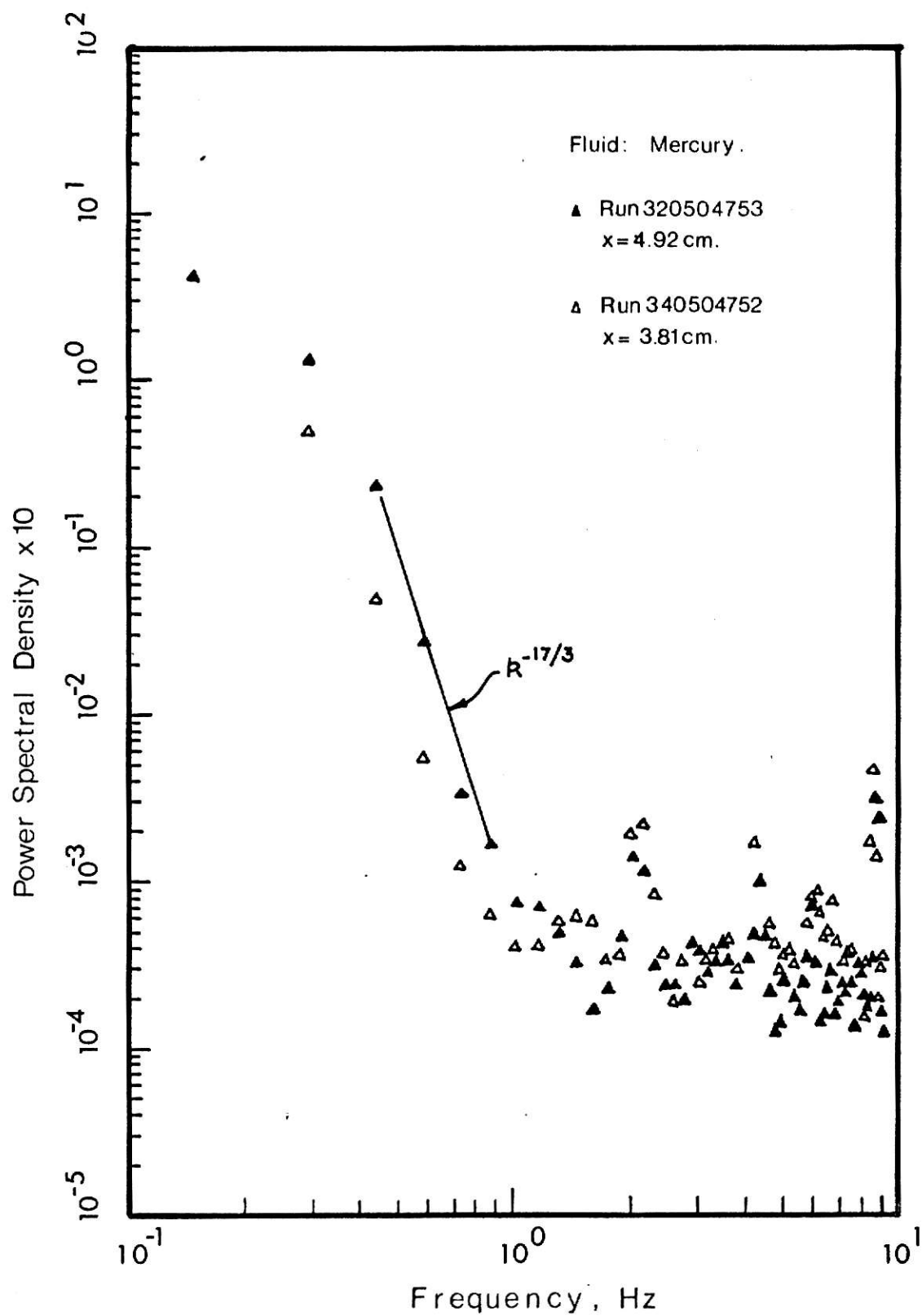


Fig. 20 Variation of Power Spectra in the Vertical Direction  
at  $y=0.84\text{mm}$  (Power=175 W).

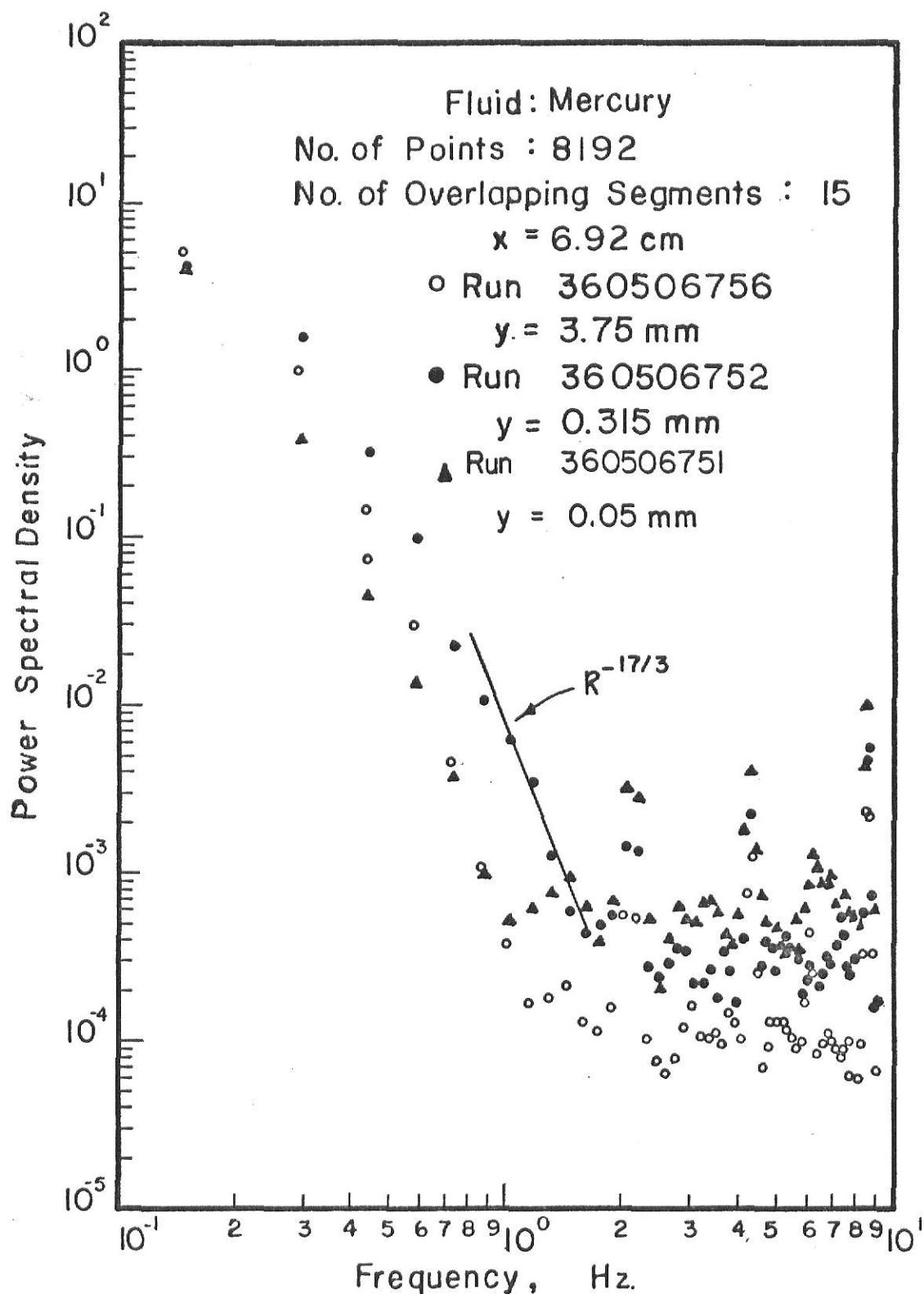


Fig.21 Variation of Power Spectra in the Horizontal Direction.(Power $\approx$ 335w)

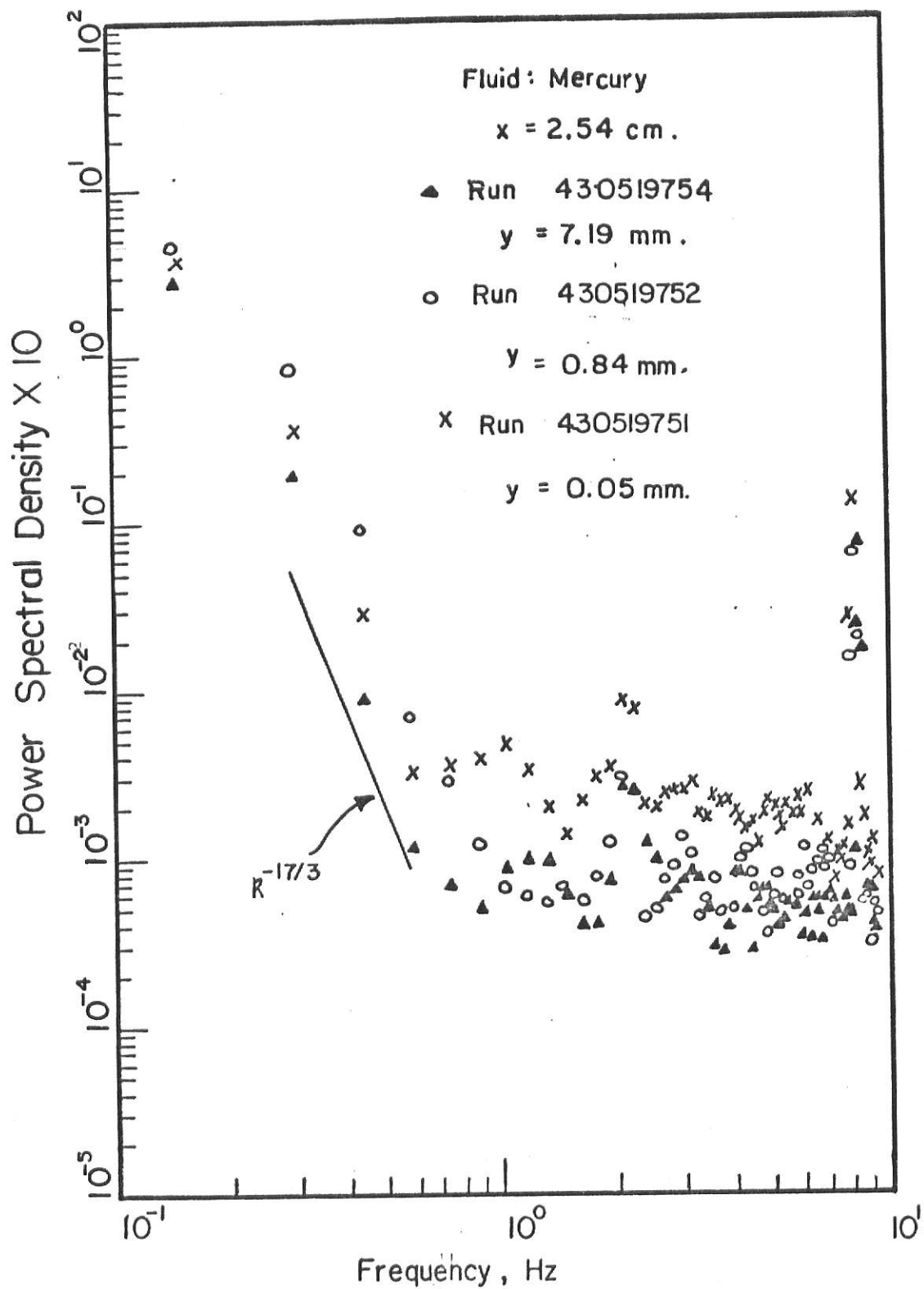


Fig.22 Variation of Power Spectra in the Horizontal Direction(Power  $\approx 168 \text{ w}$ )

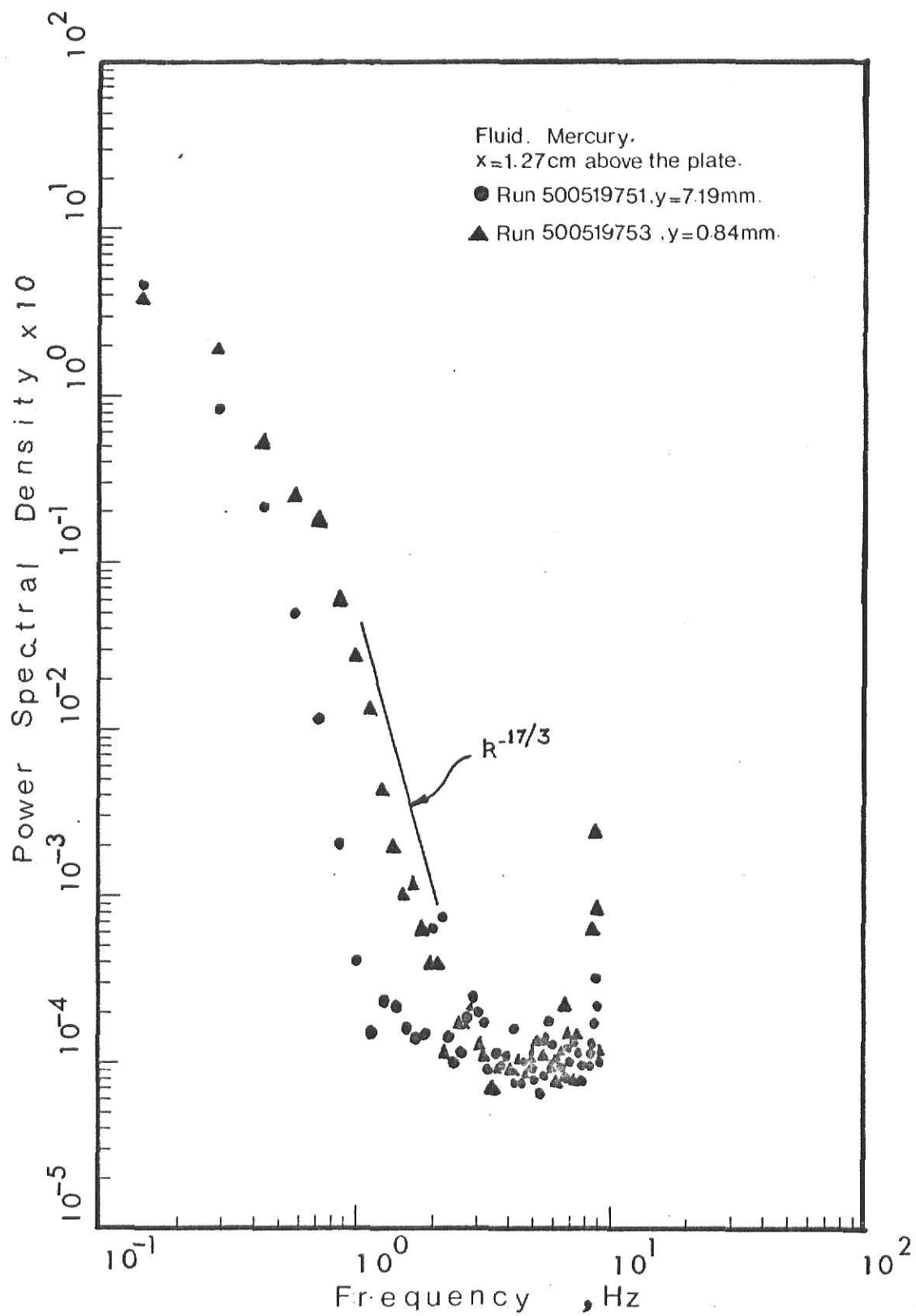


Fig. 23 Power Spectra above the plate (Power  $\approx 330$  W).



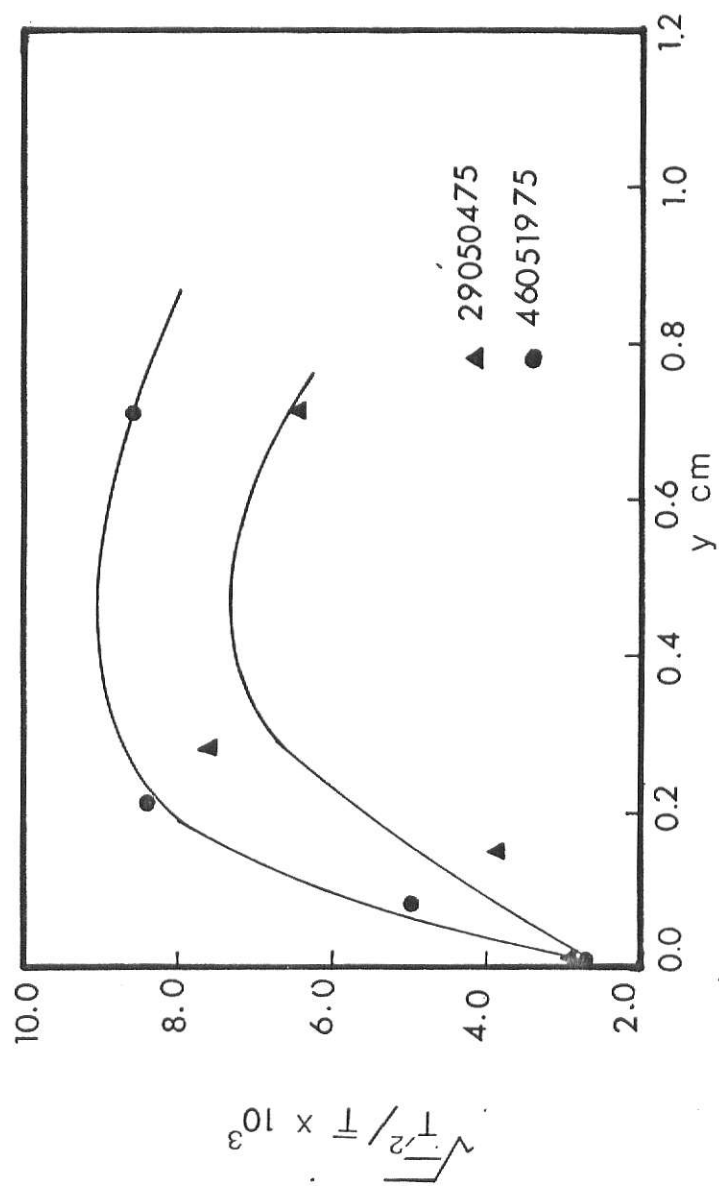


Fig.24 Variation of Intensity in Mercury

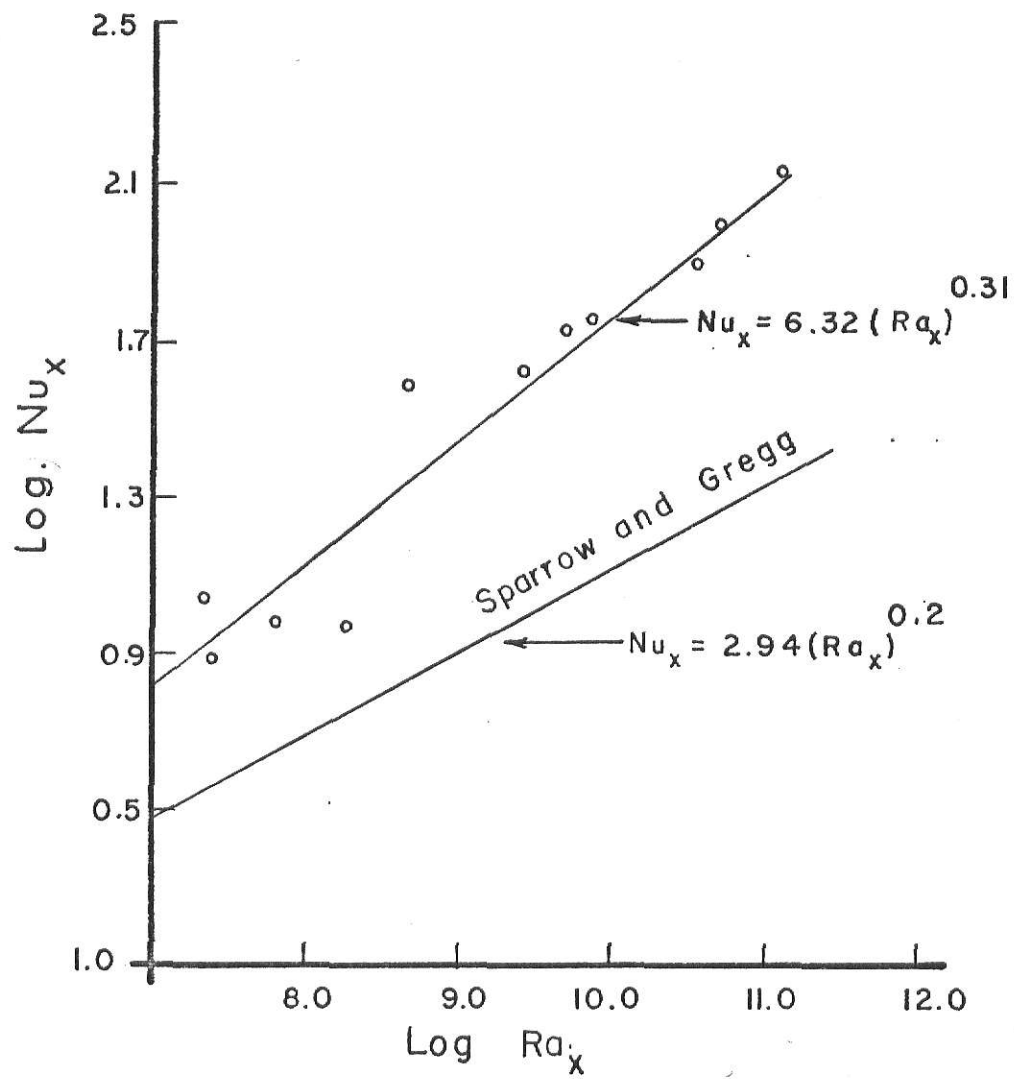


Fig. 25. Nusselt Number vs.  
Rayleigh Number.

## CHAPTER VI

## DISCUSSION OF RESULTS

## TEMPERATURE PROFILES

The experimental temperature profiles for water and mercury represented in dimensionless form using Sparrow and Gregg's [94] similarity parameter are presented in Figures 7 and 8.

From Figure 7 it is clear that the data for water show similarity at moderately high flux levels, but similarity is destroyed when temperatures at the plate approach boiling. This can be expected because of an expected change in the heat-transfer mechanism at very high power levels. The temperature distribution obeys the one-seventh power law showing the existence of a fully developed boundary layer. The scatter in data is attributed to random experimental errors.

The data for mercury for all measured power levels obeys similarity. Near-boiling conditions were not attained in mercury. The profiles for both water (Prandtl number about 3.5 for the runs) and mercury (Prandtl number about 0.025) appear to fall lower than Sparrow and Gregg's similarity solution. A comparison of the profiles shows that the thermal boundary layer for mercury was much thicker than that for water. As natural convection is temperature induced, similar behavior in the velocity boundary layer may be expected.

Based on the heat-transfer data a heat-transfer relationship was derived. Agreement between Sparrow and Gregg's [94] solution and the data was not very good.

## TEMPERATURE FLUCTUATIONS, INTENSITY DISTRIBUTIONS, AND INTERMITTENCY

The temperature intensity measurements for both fluids are given in

Figures 22 and 23. All the plots pass through a maximum with intensities falling rapidly very near the plate. A lack of data prevented an exact determination of the point of occurrence of the maxima. An examination of the intensity plots shows, however, that the maxima occurred at about the same distance from the plate in both the fluids. This indicates the existence of a fully developed boundary layer along most portions of the plate. The observation of fluctuations very close to the leading edge (Appendix D, Figures 29 and 31) support the view that the development of the natural convection boundary layer is very rapid with the laminar zone existing for only very short distance from the leading edge.

An examination of the temperature fluctuations (Appendix D) reveals that the variations were of low frequency indicating the existence of large scale convective motions in the fluid--a conclusion which will be shown to be true in the next section after an examination of the temperature spectra. It was also observed that the order of magnitude of the temperature drop across the boundary layer for both the fluids was of the same order as the maximum amplitude of the fluctuations. The maximum observed fluctuation was about  $22^{\circ}\text{C}$  for water and  $4^{\circ}\text{C}$  for mercury. However, the root-mean-square values of the fluctuations were at least an order-of-magnitude smaller than the temperature drop across the boundary layer ( $1^{\circ}\text{C}$  to  $4^{\circ}\text{C}$  for water and  $0.01^{\circ}\text{C}$  to  $0.5^{\circ}\text{C}$  for mercury). Thus, the conclusion reached by Lock and Trotter [63] that the structure of free convection boundary layer is different from that of a forced convection layer does not seem to be justified. In the present work, the intensities were found to be an order-of-magnitude less than the temperature drop across the boundary layer.

An examination of the fluctuations and intensities in the horizontal direction shows the presence of turbulent fluctuations very near the plate indicating the existence of a turbulent inner region. The outer part

of the boundary layer is characterized by a decrease in intensity (but the fall is gradual to levels far above zero) and by the presence of small scale fluctuations indicating a turbulent outer region. The observed decrease in intensities toward the wall region indicates an approach to a laminar sublayer. Large scale convective motions were observed with the probe touching the wall (i.e., sensing temperatures at  $y = 0.002''$ ) and also in the region above the plate (Figure 33, Appendix D). The existence of such motions very near the plate indicates that the laminar region of the turbulent boundary layer extends only up to distances very close to the plate. Similar fluctuations were observed by Lock and Trotter [63]. Another possibility is that the surface is renewed periodically by the eddies giving an impetus to a further examination of the wall region in natural convection flows by the surface renewal-penetration-type models. This model has been applied to natural convection [10], but more work needs to be done before anything definite can be said.

The integral time scale for water presented in Figure 24 seems to show inverse dependence on  $Gr_x^*$  and  $x/y$ . This can be expected because an increase in  $Gr_x^*$  or  $x/y$  increases the dissipation processes giving rise to smaller scales of turbulence. Although 'intermittency' was not computed, an examination of the temperature fluctuations reveals that it would be about unity close to the plate and approach zero toward the bulk of the fluid. A similar observation was made by Lock and Trotter.

#### TEMPERATURE SPECTRA

The temperature spectra for water and mercury (Figures 11 to 21) were examined in the light of various theoretical predictions (Chapter III) concerning the slopes in different segments of the spectra. The 'convection subrange' predicted by Batchelor [4, 5] for both the fluids either was

not present at all, or it was present but very indistinct. An examination of the results given by Papailiou and Lykoudis [75] seems to suggest that a  $k^{-5/3}$  region ( $k$  being the wave number) would not have been detected by those authors without a previous bias. A similar statement could be made about the present results. The results therefore indicate that significant anisotropy persists in and near the wall region and even toward the upper edge of the plate. Kolmogoroff's postulate of local isotropy cannot, therefore, be assumed in the range of conditions used in the present work. This can be expected because Kolmogoroff's postulate is strictly valid only at very high Reynolds (or Grashof) numbers. The Grashof numbers reached in the present work were only moderately high. The limitation imposed by the plate height did not allow data to be taken beyond 1-15/16" from the leading edge (except for fluctuations monitored above the plate). This explains the general absence of the convection subrange as the flow cannot be expected to be isotropic until a significant distance away from the leading edge.

According to Batchelor, a  $k^{-1}$  region would normally be expected to follow the convection subrange in the case of water. Inflection-type regions were observed next to the convection subrange, but the scatter in the plots prevented the determination of the slope. Small peaks were consistently observed in this region. These are probably due to aliasing. Similar, but sharper peaks, were observed for mercury and it was shown that these, too, were due to aliasing. The peaks in water are not as sharp as those in mercury because of the high signal-to-noise ratio in the data for water.

Beyond the region of slope -1, a 'dissipation subrange' characterized by a sharp drop as predicted by Batchelor was observed for water. The

slope in this region was about -3; theoretical slope in this region could not be estimated for comparison with the observed slope because of non-availability of velocity fluctuations. With near-boiling conditions at the plate, the high frequency end of the spectra dropped to a slope of about -6. Theoretical works predicting the slope of the spectra under such conditions are not available to the best of our knowledge.

In the case of mercury, the dissipation subrange had a slope which agreed well with Batchelor's prediction ( $k^{-17/3}$ ) rather than a  $k^{-3}$  behavior predicted by Gibson [38, 39] and observed by Papailiou and Lykoudis [75]. It is interesting to note that a region of approximately constant power is attained following the dissipation subrange in the mercury spectra. This cut-off occurs at a frequency of about 2 Hz; beyond this frequency the kinetic energy of the eddies is converted into heat and eddies acquire a constant power level. This kind of behavior is expected in any turbulent flow. The low value of this cut-off frequency indicates that turbulence in mercury was restricted to scales smaller than those for water. This fact is corroborated by a casual comparison of the fluctuations in water and mercury. A theoretical determination of the cut-off frequency would require a knowledge of the velocity fluctuations which were not available.

The power spectra for water do not seem to vary significantly in either the horizontal or vertical direction (Figures 11 to 14). In the spectra for mercury, however, the dissipation subrange shifts toward higher frequencies with increasing distance from the leading edge (Figures 17 and 18). This can be expected because of an intensification of the dissipation processes (and thus an increase in the small-scale eddies) with increasing distance along the plate. A comparison of the estimated

spectra with that obtained by Papailiou and Lykoudis shows that the present data lie at least an order-of-magnitude lower than their data. This can be expected because the data were taken by those authors at a minimum distance of 100 mm from the leading edge, whereas the plate was only 50.8 mm high in the present work.

In the horizontal direction, the dissipation subrange of the spectra for mercury (Figures 19 and 20) moves toward higher frequencies with decreasing distance toward the plate; the data very close to the plate (i.e., with the probe touching the plate), however, show a reversal in trend. Instead of moving toward higher frequencies, the spectra shift toward lower frequencies. As the formation of large scale eddies from small scale eddies is a physical impossibility, this indicates an increase in the eddy generation processes very near the wall. The spectra taken with probe touching the wall ( $y = 0.05$  mm) is observed to fall to a constant power level, however, and this implies that the eddy-dissipation processes in this region are not insignificant. The measured spectra, thus, seem to indicate that both eddy generation and decay take place in a region close to the wall (in addition to other probable locations in the system). As turbulence is generated at instability points, this implies that such points in the present system are located at the wall. Yang and Nee [118] determined theoretically that the inner layer is dominated by turbulent generation and decay. This conclusion seems very probable in the light of the present observations.

Our experiences with power spectral density estimation under a variety of difficult situations have led us to believe that the most important factors in its estimation are the digitizing frequency, the number of samples taken, and the number of lags or number of overlapping segments.



The frequency response of each instrument through which the signal passes must be checked first; these must be sufficiently high to include all the frequencies present in the system in order to include all the subranges present in the spectra. The signal-to-noise ratio becomes critical in cases where signal power is low. Finally, it is recommended that the first few runs be analyzed to sufficiently high frequencies to detect noise and signal power regions and to test the stationarity of the data.

#### AUTOCORRELATION AND PERIODICITY

Autocorrelation functions were calculated for all the data in water with a view of getting the periodicity of the eddies present. This information may be useful in the surface-renewal theory to predict heat and momentum transfer coefficients. Only two of the many plots calculated are presented in Figure 15. An examination of the results indicated that due to the absence of definite trends in the autocorrelation function, determination of single-valued periodicities in the records was impossible. Some of the results, however, did show some periodicity (Figure 15) but the number of such records was limited. During the course of this work, digital processing techniques were examined in detail and it is felt that the following techniques need to be examined further in order to establish the best technique to determine the periodicity of the eddies:

a. Digital Filtering: Due to the very slow nature of the fluctuations the use of conventional filters having broad passbands is not possible. Development of digital filtering techniques with narrow and variable passbands is recent. The most important harmonic present can be determined by examining the areas under various filtered bands.

b. Integral Time Scale: This quantity was suggested by Taylor to be

representative of the average size of eddies. However, a constant or variable multiplying factor may have to be incorporated into it before reasonable periodicity estimates can be determined from it. Integral time scales were determined in this study and are given in Figure 24. However, care must be taken not to overemphasize the temperature field, as eddy size and scale are characteristics of the velocity field.

c. Weighted Power Spectrum: As the power spectrum represents the contribution to power by various frequencies present in the system, it should be possible to determine an average frequency by evaluating a weighted estimate of the power spectrum. A multiplying factor may have to be used as in case (b) before.

## ERRORS

Three major types of errors were involved in this study: (i) random experimental errors, (ii) non-random experimental errors, and (iii) analytical errors. The errors in analysis were kept at a minimum by automating analytical schemes wherever possible. All such errors were estimated and have been reported at appropriate places. Random experimental errors were held responsible for some of the scatter in the quantities calculated. These errors are unavoidable and their magnitude was not estimated. Non-random experimental errors were avoided either analytically or experimentally as far as possible and are briefly discussed below.

Very near the plate the presence of the probe distorts the velocity and temperature fields due to an acceleration of the flow between the probe and the wall. This causes an increase in the heat transfer rates or a lowering of the reported temperature. This error was minimized by selecting a very thin probe (0.004" thick at end) and by inserting it in the vertical

direction parallel to the flow so that the field distortion effects were not felt at the point of measurement. The error due to electrical noise has been discussed before and analytical methods were used for its removal. Other errors such as the conduction error due to the stainless steel sheath surrounding the thermocouple, error due induced magnetic field at the leading edge and measurement errors were insignificant and have been discussed by Julian [52] with regard to their effect in the present system.

## CHAPTER VII

## CONCLUSIONS AND RECOMMENDATIONS FOR FURTHER STUDY

It is perhaps clear that a definite determination of the structure of turbulent free convection would require additional data on the velocity field. The measured temperature fluctuations, intensities, and power spectra, however, permit plausible qualitative conclusions to be drawn about the flow, its structure, and the processes taking place in it.

The turbulent free convection boundary layer seems to be similar in structure to a forced convection layer. It is made up of three regions: (a) a laminar sublayer, (b) a turbulent wall-influenced inner layer, and (c) a turbulent outer layer. This conclusion is in agreement with a few of the earlier works [76, 55, 118], but disagrees with Lock and Trotter's [63] conclusion. The measured data seems to indicate that the laminar region extends only up to distances very close to the plate, and that the development of the boundary layer is very rapid.

The measured temperature spectra for water and mercury seem to support the model proposed by Batchelor [4, 5] rather than that given by Gibson [38, 39] and experimentally verified for mercury by Papailiou and Lykoudis [75]. In both water and mercury, the 'convection subrange' characterized by a  $k^{-5/3}$  ( $k$  being the wave number) behavior was either not present at all, or it was present but very indistinct. The flow was thus significantly anisotropic and Kolmogoroff's postulate of local isotropy could not be assumed in the range of conditions used in the present work ( $10^8 \leq Gr_x^* \leq 10^{10}$  for mercury, and  $10^8 \leq Gr_x^* \leq 10^{11}$  for water). In the case of water, inflection-type regions were observed next to the convection subrange. The scatter in the data prevented the determination of the slope in this region but it seemed to agree well with Batchelor's prediction

( $k^{-1}$ ). In both the fluids a 'dissipation subrange' was present at the high frequency end of the spectra. Excellent agreement with Batchelor's prediction ( $k^{-17/3}$ ) was observed for mercury spectra.

For water, this region was characterized by a slope of -3 which again seems to agree well with the model given by Batchelor. With near-boiling conditions at the plate the high frequency end of the spectra in water dropped to a slope of about -6. It was observed that turbulence in mercury was restricted to small scale eddies (below  $\sim 2$  Hz); a region of constant 'power' was attained beyond this frequency.

It was observed that the spectra for water do not vary significantly in either the horizontal or vertical direction. The mercury spectra shift to higher frequencies with increasing distance from the leading edge. Similar behavior was observed with decreasing distance toward the wall. Very close to the wall, however, the spectra shift toward lower frequencies indicating an increase in the eddy-generation processes. Instability points (where turbulence is generated) in the flow may, therefore, be expected to be located at the wall. Integral time scales were measured for water and these seemed to show inverse dependence on  $Gr_x^*$  and  $x/y$ .

The temperature profiles, for both water and mercury, were found to be similar for moderately high heat flux and Grashof numbers. Similarity was destroyed, however, when temperatures at the plate approached boiling. The measured data fell lower than Sparrow and Gregg's [94] similarity solution. The boundary layer for mercury was found to be much thicker than that for water.

As mentioned earlier, additional velocity data are required to place the conclusions reached in this study on a firm footing. The measurement of velocity fluctuations presents serious experimental difficulties due to the limitations on the use of hot film anemometry when large temperature fluctuations exist in the flow (as in turbulent free convection). Such

measurement would thus have run parallel to the development in anemometry.

It is felt that data at Grashof numbers higher than that taken in the present work would be a contribution to the present state of knowledge on the subject. On the present apparatus this could be achieved by increasing either the power supplied to the plate or increasing the height of the plate. The use of the former option would invariably lead to serious experimental problems like those encountered in the present work in the case of mercury. Modification in the existing apparatus would therefore be recommended to incorporate a plate higher than the present one.

The options available in the analysis of data were examined in detail during the course of this work. It is believed that the analysis procedures are about the best possible under the present circumstances and technology. No work is therefore recommended in this direction at the present time.

Phenomenological studies using the conclusions of this study would, it is felt, be improvements on such existing studies and are therefore recommended. An examination of natural convection flows by the surface-renewal theory has been suggested earlier. Such a study could usefully use the results of the present study.

There has been an increased importance of natural convection in applications such as solar energy collectors, nuclear reactors, and studies concerning fluid flow in the earth's interior, atmosphere, and oceans. Fundamental and applied research on natural convection with a view to use it in such applications would be of social and technological importance. In most applications, however, free and forced convection occur together and it is felt that this problem should be given particular attention.

## REFERENCES AND BIBLIOGRAPHY

1. Ahmed, N., and K. R. Rao, "Orthogonal Transforms for Digital Processing," Springer-Verlag, Berlin (in press).
2. Antonia, R. A., and C. W. Van Atta, "On the Correlation Between Temperature and Velocity Dissipation Fields in a Heated Turbulent Jet," *J. Fluid Mechanics*, 67, 2, p. 273 (1975).
3. Babco, R. P., "A Closed-Form Solution for Laminar Free Convection on a Vertical Plate With Prescribed, Nonuniform, Wall Heat Flux," *J. Aerospace Sci.*, 26, 12, pp. 846-47 (1959).
4. Batchelor, G. K., "Small-Scale Variations of Convected Quantities Like Temperature in Turbulent Fluid," Part I, *J. Fluid Mechanics*, 5, p. 113 (1959).
5. Batchelor, G. K., I. D. Howells, and A. A. Townsend, "Small-Scale Variation of Convected Quantities Like Temperature in Turbulent Fluid," Part II, *J. Fluid, Mechanics*, 5, p. 134 (1959).
6. Batchelor, G. K., "The Theory of Homogeneous Turbulence," Cambridge University Press (1953).
7. Baley, F. J., "An Analysis of Turbulent Free Convection Boundary Layer on a Flat Plate," *Proceeding of the Institution of Mechanical Engineers*, 169, 20, p. 361 (1955).
8. Bendat, J. S., and A. G. Piersol, "Random Data: Analysis and Measurement Procedures," Wiley-Interscience (1971).
9. Berkovsky, B. M., and V. K. Polevikov, "Heat Transfer at High-Rate Free Convection," in "Heat Transfer 1974," Fifth International Heat Transfer Conference, Tokyo (1974).
10. Blackman, R. B., and J. W. Tukey, "The Measurement of Power Spectra," Dover (1958).
11. Bird, R. B., W. E. Stewart, and E. N. Lightfoot, "Transport Phenomena," John Wiley (1960).
12. BMD02T Computer Program for "Autocovariance and Power Spectral Analysis," Health Sciences Computing Facility, University of California, Los Angeles.
13. Bolgiano, R., "Turbulence Spectra in a Stably Stratified Atmosphere," *J. Geophysical Research*, 64, pp. 226-29 (1959).
14. Bolgiano, R., "Structure of Turbulence in Stratified Media," *J. Geophysical Research*, 67, 8, p. 3015 (1962).
15. Bradshaw, P., "An Introduction to Turbulence and Its Measurement," Pergamon Press, Oxford (1971).

16. Chang, B. H., "An Experimental Investigation of Natural Convection in Mercury at Low Grashof Numbers," M.S. thesis, Kansas State University (1970).
17. Chang, K. C., R. G. Akins, L. Burris, and S. G. Bankoff, "Free Convection of a Low Prandtl Number Fluid in Contact With a Uniformly Heated Vertical Plate," Argonne National Laboratory, ANL-6835 (1964).
18. Cheesewright, R., "Turbulent Natural Convection from a Vertical Plane Surface," J. Heat Transfer, Trans. ASME, 90C, p. 1 (1968).
19. Coles, D. E., and E. A. Hirst (Eds.), "Proceedings: Compt. of Turbulent Boundary Layers--1968 AFOSR-1FP-Stanford Conference, 2, Thermosciences Division, Stanford University (1969).
20. Corrsin, S., "Heat Transfer in Isotropic Turbulence," J. Applied Physics, 23, pp. 113-18 (1952).
21. Corrsin, S., "On the Spectrum of Isotropic Temperature Fluctuations in an Isotropic Turbulence," J. Applied Physics, 22, 4, p. 469 (1951).
22. Corrsin, S., "Turbulent Flow," American Scientist, 49, p. 300 (1961).
23. Corrsin, S., "Further Generalization of Onsager's Cascade Model for Turbulent Spectra," Physics Fluids, 7, p. 1156 (1964).
24. Eckert, E. R. G., and T. W. Jackson, "Analysis of Turbulent Free Convection Boundary Layer on Flat Plate," NACA Report 1015, 37 (1951).
25. Eckert, E. R. G., and E. Soehngen, "Interferometric Studies on the Stability and Transition to Turbulence of a Free Convection Boundary Layer," Inst. Mech. Eng. and ASME, Proc. General Disc. on Heat Trans., 321, London (1951).
26. Ede, A. J., "Advances in Free Convection," in Harnett, J. P., and T. F. Irvine (Eds.), "Advances in Heat Transfer," 4, Academic Press, New York (1967).
27. Eichhorn, R., "Measurement of Low Speed Gas Flows by Particle Trajectories: A New Determination of Free Convection Velocity Profiles," Int. J. Heat Mass Transfer, 5, p. 915 (1962).
28. Eigenson, L. S., "Les Lois Gouvernant La Transmission de La Aux Gaz Biotomiques Par Les Parois Des Cylindres Verticaux Dans Le Cas de Convection Naturelle," Compt. Rend. Acad. Sci. URSS, 26, p. 440 (1960).
29. Fiedler, H., and M. R. Head, "Intermittancy Measurements in Turbulent Boundary Layers," J. Fluid Mechanics, 25, p. 719 (1966).
30. Finston, M., "Free Convection Past a Vertical Plate," ZAMP, 7, pp. 527-29 (1956).
31. Fishenden, M., and O. A. Saunders, "An Introduction to Heat Transfer," Oxford University Press, London (1950).



32. Fujii, T., "Experimental Studies of Free Convection Heat Transfer," Bulletin, Japan Soc. Mech. Engrs., 2, 8, p. 555 (1959).
33. Fujii, T., "An Analysis of Turbulent Free Convection Heat Transfer from a Vertical Surface," Bulletin, Japan Soc. Mech. Engrs., JSME, 2, 8, pp. 559-63 (1959).
34. Friedlander, S. K., and L. Topper (Eds.), "Turbulence--Classic Papers on Statistical Theory," Interscience, New York (1961).
35. Gebhart, B., "Effects of Viscous Dissipation in Natural Convection," J. Fluid Mech., 14, pp. 225-32 (1962).
36. Gebhart, B., "Heat Transfer," McGraw-Hill, New York, pp. 251-73 (1961).
37. Gebhart, B., R. P. Dring, and C. E. Polymeropoulos, "Natural Convection from Vertical Surface, the Convection Transient Regime," J. Heat Transfer, Trans. ASME, C89, 1, pp. 53-59 (1967).
38. Gibson, C. H., "Fine Structure of Scalar Fields Mixed by Turbulence, I. Zero-Gradient Points and Minimal Gradient Surfaces," Physics Fluids, 11, 11, p. 2305 (1968).
39. Gibson, C. H., "Fine Structure of Scalar Fields Mixed by Turbulence, II. Spectral Theory," Physics Fluids, 11, 11, p. 2316 (1968).
40. Gibson, C. H., and Schwarz, "The Universal Equilibrium Spectra of Turbulent Velocity and Scalar Fields," J. Fluid Mechanics, 16, p. 365 (1963).
41. Godaux, F., and B. Gebhart, "An Experimental Study of the Transition of Natural Convection Flow Adjacent to a Vertical Surface," Int. J. Heat Mass Transfer, 17, p. 93 (1974).
42. Gold, B., and C. M. Charles, "Data Processing of Signals," McGraw-Hill (1969).
43. Grant, H. L., B. A. Hughes, W. M. Vogel, and A. Moilliet, "The Spectrum of Temperature Fluctuations in Turbulent Flow," J. Fluid Mechanics, 34, 3, pp. 423-42 (1968).
44. Griffiths, E., and A. H. Davis, "The Transmission of Heat by Radiation and Convection," Food Investigation Board, S.R. 9, DSIR H. M. Stationary Office, London (1931).
45. Hermann, R., "Waermeuebergangs bei Frier Konvektion I," Z. Physik., 33, 425 (1932); Z. Agnew. Math. Mech., 13, p. 433 (1933).
46. Hieber, C. A., "Natural Convection Around a Semi-Infinite Vertical Plate: Higher Order Effects," Int. J. Heat Mass Transfer, 17, p. 785 (1974).
47. Hinze, J. O., "Turbulence--An Introduction to Its Mechanism and Theory," McGraw-Hill (1959).

48. Humphreys, W. W., and J. R. Welty, "Private Communication," Oregon State University (1975).
49. "Special Issue on Fast Fourier Transforms," IEEE Trans. Audio Electroacoustics, AU-15:2 (1967).
50. Jofre, R. J., and R. F. Barron, "Free Convection Heat Transfer to a Rough Plate," Paper No. 67-WA/HT-38, ASME (1967).
51. Jones, B. G., "Recent Developments in Turbulence Measuring and Analyzing Techniques," in B. T. Chao (Ed.), "Advanced Heat Transfer," University of Illinois Press, Urbana (1969).
52. Julian, D. V., "An Experimental Study of Natural Convection Heat Transfer from a Uniformly Heated Vertical Plate Immersed in Mercury," Ph.D. dissertation, Kansas State University (1967).
53. Kao, A. Y., and S. Corrsin, "Experiments on Inertial Intermittency and Fine-Structure Distribution Functions in Fully Turbulent Fluid," J. Fluid Mechanics, 50, p. 285 (1971).
54. Kato, H., et al., "On the Turbulent Heat Transfer by Free Convection from a Vertical Plate," Int. J. Heat Mass Transfer, 11, p. 1117 (1968).
55. Kirdyashkin, A. G., et al., "Turbulent Free Convection and Stability at Heat Transfer Flat Surfaces," in "Heat Transfer 1974," Fifth Int. Heat Transfer Conf., Tokyo (1974).
56. Kistler, A. L., et al., "Preliminary Measurements of Turbulence and Temperature Fluctuations Behind a Heated Grid," NACA Res. Mem. No. RM54D19 (1954).
57. Klyachko, L. S., "Relations for the Critical State Describing Transition from Laminar to Turbulent Flow in Free Convection," Int. J. Heat Mass Transfer, 5, pp. 763-64 (1962).
58. Kolmogoroff, A. N., "The Local Structure of Turbulence in Incompressible Viscous Fluid for Very Large Reynolds Numbers," Dokl. Akad. Nauk. SSSR, 30, p. 301 (1941).
59. Kolmogoroff, A. N., "A Refinement of Previous Hypothesis Concerning the Local Structure of Turbulence in a Viscous Incompressible Fluid at High Reynolds Number," J. Fluid Mechanics, 13, p. 82 (1962).
60. Kovasznay, L. S. S., et al., "Large-Scale Motion in the Intermittent Region of a Turbulent Boundary Layer," J. Fluid Mechanics, 41, p. 283 (1970).
61. Larson, J. R., and R. J. Schoenhols, "Turbulent Free Convection in Near-Critical Water," J. Heat Transfer, Trans. ASME, C88, pp. 407-14 (1966).

62. Le Fevre, E. J., "Laminar Free Convection from a Vertical Plane Surface," Proc. 9th Intern. Congr. Appl. Mech., Brussels, 4, p. 168 (1956).
63. Lock, G. S., and F. J. Trotter, "Observations on the Structure of a Turbulent Free Convection Boundary Layer," Int. J. Heat Mass Transfer, 11, pp. 1225-32 (1968).
64. Lorenz, L., "Ueber das leitungsvermogen der metalle fur Wärme und Electricitat," Wiedemanns Annalen, 13, p. 582 (1881).
65. Lumley, J. L., "The Spectrum of Nearly Inertial Turbulence in a Stably Stratified Fluid," J. Atmospheric Sciences, 21, p. 99 (1964).
66. Lumley, J. L., and H. A. Panofsky, "The Structure of Atmospheric Turbulence," Interscience (1964).
67. Mason, H. B., and R. A. Seban, "Numerical Predictions for Turbulent Free Convection from Vertical Surfaces," Int. J. Heat Mass Transfer, 17, pp. 1329-36 (1974).
68. Mollendorf, J. C., and B. Gebhart, "An Experimental Study of Vigorous Transient Natural Convection," Paper No. 70-HT-2, ASME (1970).
69. Nye, J. O., and R. S. Brodkey, "The Scalar Spectrum in the Viscous-Convective Subrange," J. Fluid Mechanics, 29, 1, pp. 153-63 (1967).
70. Nee, V. W., and L. S. G. Kovaszney, "A Simple Phenomenological Theory of Turbulent Shear Flows," Physics Fluids (1969).
71. Obukhoff, A. M., "The Structure of the Temperature Field in Turbulent Flow," Izv. Akad. Nauk, SSSR, Ser. Geofiz, 13, 58 (1949).
72. Ostrach, S., "An Analysis of Laminar Free Convection Flow and Heat Transfer About a Flat Plate Parallel to the Direction of the Generating Body Force," NACA, Report 1111, pp. 63-79 (1953).
73. Ostrach, S., in "High Speed Aerodynamics and Jet Propulsion," Vol. IV, "Theory of Laminar Flows" (F. K. Moore, ed.), Section F., Princeton University Press, New Jersey (1964).
74. Otnes, R. K., and L. Enochson, "Digital Time Series Analysis," Wiley-Interscience (1972).
75. Papailiou, D. D., "Magneto-Fluid Mechanics Turbulent Free Convection," Ph.D. dissertation, Purdue University (1971).
76. Papailiou, D. D., and P. S. Lykoudis, "Turbulent Free Convection Flow," Int. J. Heat Mass Transfer, 17, p. 161 (1974).
77. Pirovano, A., S. Viannay, and M. Jannot, "Convection Naturelle en Regime Turbulent Le Long Dune Plaque Plane Verticale," Fourth Int. Heat Transfer Conference, Paris, Paper No. 1.8, 4, Elsevier, Amsterdam (1970).

78. Pohlhausen, E., "Der Wärmeaustausch zwischen festen Körpern und Flüssigkeiten mit kleiner Reibung und kleiner Wärmeleitung," ZAMM, 1, p. 115 (1921).
79. Prandtl, L., "Über Flüssigkeitsbewegung bei sehr kleiner Reibung," Proceedings of the Third Intern. Math. Kongr., Heidelberg (1904), also translated in NACA TM-452 (1928).
80. Rader, C. S., "An Improved Algorithm for High Speed Autocorrelation With Application to Spectral Estimation," IEEE, Trans. Audio Electroacoustics, AU-18, 2, p. 439 (1970).
81. Rajgopal, R., "Adaptation of Surface Renewal and Penetration Type Models to Turbulent Momentum and Heat Transfer for Newtonian and Non-Newtonian Fluids," Ph.D. dissertation, University of Akron (1974).
82. Ramakrishniah, M. A., "A Study of FFT Pruning and Its Applications," Master's Report, Kansas State University (1974).
83. Rust, J. H., and A. Sesonske, "Turbulent Temperature Fluctuations in Mercury and Ethylene Glycol in Pipe Flow," J. Heat Mass Transfer, 9, pp. 215-27 (1966).
84. Saunders, O. A., "Natural Convection in Liquids," Proc. Roy. Society (London), A172, pp. 55-71 (1939).
85. Saxton, J. A. (Ed.), "Proceedings of Colloquium on Spectra of Meteorological Variables," Radio Science, 4, p. 1099 (1969).
86. Schechter, R. S., and H. S. Isbin, "Natural-Convection Heat Transfer in Regions of Maximum Fluid Density, A.I.Ch.E. Journal, 4, pp. 81-89 (1958).
87. Scherberg, M. G., "Natural Convection Near and Above Thermal Leading Edges on Vertical Walls," Int. J. Heat Mass Transfer, 5, pp. 1001-10 (1962).
88. Schlichting, H., "Boundary Layer Theory," Pergamon, Oxford (1968).
89. Schmidt, E., and W. Beckmann, "Das Temperatur und Geschwindigkeitsfeld vor einer Wärme Abgebenden Senkrechten Platte bei Naturlicher Konvektion," Tech. Mech. Thermodynamik, Bd. 1, 10, p. 341 (1930), continued Bd. 1, 11, p. 391 (1930).
90. Shur, G. N., "Eksperimental'nyye issledovaniya energeticheskogo spectra atmosferynoy turbulentnost," Trudy, 43, 79-90 (Trans. as AID Report T-63-55 Aerospace Info, Div., Lib. Cong.).
91. Siegel, R., "Analysis of Laminar and Turbulent Free Convection from a Smooth Vertical Plate With Uniform Heat Dissipation Per Unit Surface Area," G. E. Report R54GL89 (1954).
92. Sparrow, E. M., "Free Convection With Variable Properties and Variable Wall Temperatures," Ph.D. thesis, Harvard University (1956).

93. Sparrow, E. M., "Laminar Free Convection on a Vertical Plate With Prescribed Nonuniform Wall Heat Flux or Prescribed Nonuniform Wall Temperature," NACA TN 3508 (1955).
94. Sparrow, E. M., and J. L. Gregg, "Laminar Free Convection from a Vertical Plate With Uniform Surface Heat Flux," Trans. ASME, 78, pp. 435-40 (1956).
95. Sparrow, E. M., and J. L. Gregg, "The Variable Fluid-Property Problem in Free Convection," Trans. ASME, 80, pp. 879-86 (1958).
96. Sparrow, E. M., and J. L. Gregg, "Similar Solutions for Free Convection from a Nonisothermal Vertical Plate," Trans. ASME, 80, pp. 379-86 (1958).
97. Sparrow, E. M., F. K. Tsou, and E. F. Kurtz, Jr., "Stability of Laminar Free Convection Flow on a Vertical Plate," Physics Fluids, 8, 8, p. 1559 (1965).
98. Squire, H. B., in "Modern Developments in Fluid Dynamics," Oxford University Press, London (1938).
99. Sugawara, S., and I. Hichiyoshi, "Effects of Prandtl Number on Heat Transfer by Natural Convection--The Case Where Prandtl Number Is Comparatively Small," Proc. 3rd Japan National Congress for Applied Mechanics (1953).
100. Szewczyk, A. A., "Stability and Transition of the Free Convection Layer along a Vertical Flat Plate," Int. J. Heat Mass Transfer, 5, pp. 903-14 (1962).
101. Tani, I., "Low-Speed Flows Involving Bubble Separations," Progress in Aero. Sci., 5, p. 70 (1964).
102. Taylor, G. I., "Statistical Theory of Turbulence," Parts I-IV, Proc. Roy. Soc., A, 151, pp. 421-78 (1935).
103. Thomas, L. C., "The Applicability of the Renewal--Penetration Model to Transport Processes Associated with Axial Flow and Flow Past Submerged Bodies," Ph.D. dissertation, Kansas State University (1968).
104. Thomas, L. C., and M. L. Wood, "A Surface Renewal Based Analysis of Fully Turbulent Free Convection," Private communication, Department of Mech. Engr., University of Akron, Ohio (1974).
105. Townsend, A. A., "The Diffusion of Heat Spots in Isotropic Turbulence," Proc. Roy. Soc., 209, p. 418 (1951).
106. Tribus, M., "Discussion on Similar Solutions for Free Convection from a Nonisothermal Vertical Plate," Trans. ASME, 80, p. 1180 (1958).
107. Tritton, D. J., "Turbulent Free Convection Above a Heated Plate Inclined at a Small Angle to the Horizontal," J. Fluid Mechanics, 16, p. 417 (1963).

108. Veda, H., and J. O. Hinze, "Fine Structure Turbulence in the Wall Region of a Turbulent Boundary Layer," J. of Fluid Mechanics, 67, Part 1, p. 125 (1975).
109. User's Guide, "Analog to Digital Conversion Using NOVA-1200 Mini-computer" (available with Dr. R. G. Akins, Chem. Engr. Dept., Kansas State University, Manhattan).
110. Van Atta, C. W., "Influence of Fluctuations in Local Dissipation Rates on Turbulent Scalar Characteristics in the Inertial Subrange," Physics Fluids, 14, p. 1803 (1971).
111. Van Atta, C. W., "Influence of Fluctuations in Dissipation Rates on Some Statistical Properties of Turbulent Scalar Fields," IZV. Atmos. Ocean. Phys., 7, (1974).
112. Vliet, G. C., and C. K. Liu, "An Experimental Study of Turbulent Natural Convection Boundary Layers," J. Heat Transfer, 94, p. 17 (1972).
113. Warneford, I. P., and D. F. Fussey, "Natural Convection from a Constant Heat Flux Inclined Flat Plate," in "Heat Transfer 1974," Fifth Int. Heat Transfer Conf., Tokyo (1974).
114. Warner, C. Y., and V. S. Arpaci, "An Experimental Investigation of Turbulent Natural Convection in Air at Low Pressure Along Vertical Heated Flat Plate," Int. J. Heat Mass Transfer, 11, pp. 397-406 (1968).
115. Yaglom, A. M., "On the Local Structure of the Temperature Field in Turbulent Flow" (Doklady), Academy of Sciences, USSR, 69, 6, p. 743 (1949).
116. Yaglom, A. M., "The Influence of Fluctuations in Energy Dissipation on the Shape of Turbulence Characteristics in the Inertial Interval, Sov. Phys. Dokl., 11, p. 26 (1966).
117. Yang, K. T., and E. W. Jerger, "First-Order Perturbations of Laminar Free Convection Boundary Layers on a Vertical Plate," J. Heat Transfer, Trans. ASME, C86, 1, pp. 107-115 (1964).
118. Yank, K. T., and V. W. Nee, "Structure of Turbulent Free Convection Boundary Layers Along a Vertical Plate," T. N. No Themis-UND-69-1, University of Notre Dame, Indiana (1969).
119. Yu, S. C., M.S. thesis (in progress), Kansas State University (1975).

## APPENDIX A

## GLOSSARY

This list contains some of the words used in turbulence and not defined in the text; the definitions given are to be used only as an aid to understanding and are not exact.

Attenuator. Any network, usually of resistances only, whose output voltage or current is a fixed or adjustable fraction of the input voltage or current. Attenuation is defined as for amplification but is less than unity (but is usually expressed as a number greater than one).

Diffusivity. The ratio of a flux, or transport rate, to the mean gradient of the quantity being transported. If the transport is molecular, the diffusivity is a property of the fluid; if turbulent, the diffusivity obeys no simple laws and is generally different for transport in different directions. Diffusivity based on transport by mean velocity only has no significance.

Eddy. This is a designedly vague term: it is used to describe a typical motion in turbulent flow, usually covering a range of wavelengths of less than, say, 10 to 1, so that we can talk of large and small eddies in the same volume of fluid.

Ensemble. A set of samples of a random process. An ensemble average is an average over repeats of an experiment: we would have to use ensemble averages when studying, say, the turbulent boundary layer on a rapidly oscillating body. Ensemble averages are often used in mathematical discussions but the ergodic hypothesis says, roughly speaking, that ensemble



averages and time averages are equivalent if the process is statistically stationary.

Ergodic. See Ensemble.

Flux. A 'flow' of some quantity other than mass.

Gaussian. A Gaussian or 'normal' process is one with the probability distribution

$$P(X) = \frac{1}{\sqrt{2\pi\overline{X'^2}}} \exp \left( -\frac{1}{2} \frac{X'^2}{\overline{X'^2}} \right)$$

where  $\overline{X'^2}$  is the variance. The central limit theorem ensures that most random molecular phenomena are Gaussian. Turbulence is significantly non-Gaussian, consisting of a large number of loosely related processes (eddies).

Homogeneous. Statistically independent of position in space, e.g., independent of  $x$ . Not necessarily isotropic.

Intermittency. Fraction of time over which the flow at a given point is turbulent.

Isotropic. Statistically independent of direction, e.g.,  $\overline{u'^2} = \overline{v'^2} = \overline{w'^2}$ . In practice isotropic turbulence must also be homogeneous.

Local isotropy. Isotropy of the small scale eddies.

Process. Any sequence of events (usually restricted to a sequence that has to be described by statistical quantities) including continuous sequences like  $X(t)$ .



Random. Not simply (e.g., periodically) dependent on the independent variables, but not necessarily discontinuous.

Scale. A typical value of a dimension (usually velocity or length): for instance, the length scale of the largest eddies in a pipe flow is the pipe radius or diameter.

Signal. Any voltage or current applied to a circuit.

Spectral Window. A function of frequency expressing the contribution of the spectral density at each frequency to the average value of an estimate of (smoothed) spectral density.

Stationarity. The state of being stationary.

Stationary. Statistically independent of time (or of one or more space coordinates), e.g.,

$$\lim_{\theta \rightarrow \infty} \frac{1}{\theta} \int_{t_0}^{t_0+\theta} X^2(t) dt$$

independent of  $t_0$ .

Statistical. Relating to probabilities or average properties, e.g.,  $\overline{X'^2}$ , rather than randomly fluctuating properties, e.g.,  $X(t)$ .

Stochastic. (Greek stochos, guess) Relating to random processes.

Structure. The dimensionless properties of a turbulence field, e.g., correlation shapes as opposed to absolute values like integral scales or intensities.

## APPENDIX B

## NOMENCLATURE

The following notation is used throughout the thesis. If a symbol is used to represent more than one quantity, the first time it occurs for each quantity is given in parenthesis. A subscript, etc., used with a symbol has the usual meaning which the subscript represents.

d	Diameter
F(f), F(k)	Power spectral density with reference to frequency F(f), or wave number, F(k). The latter is the more commonly used form in theoretical works.
f(y)	Function of y
g	Acceleration due to gravity
h	Film heat transfer coefficient
i	$\sqrt{-1}$
k	Thermal conductivity (p. xviii), Wave number magnitude (p. 20), Real number (p. 24)
$L_c$	Obukhoff-Corrsin length scale
$L_K$	Kolmogoroff length scale
m	Real number
N	Number of samples
P	Pressure
Q( $\tau$ )	Autocovariance
R( $\tau$ )	Autocorrelation
T	Temperature
t	Time
U	Mean velocity
u, v, w	Velocity in the x, y, z directions
W	$e^{-i(2\pi/N)}$

$X(t), X(m)$	Continuous (2) or discrete (14) random signal
$x, y, z$	Cartesian coordinate axes; in free convection it is customary to use $x$ as the vertical and $y$ as the horizontal direction.

### Suffixes

Numeral 1, 2, etc.	Point or value number
$i, j, k$	Directions $x, y, z$
$i, j, k, l$	Dummy parameter
$L$	Length of plate
$\max, \min$	Maximum, minimum
$R$	Reference quantity
$w$	At the wall
$x, y, z$	Cartesian coordinate axes
$\infty$	Bulk (temperature)

### Superscripts

-	Mean or average (2), vector (9)
'	Fluctuating quantity
*	Modified (e.g., modified Grashof number, $Gr_x^*$ )

### Dimensionless numbers

$Gr_x^*$	Modified Grashof number based on $x$ , $\frac{g \beta q x^4}{k v^2}$
$Gr_L^*$	Modified Grashof number based on $L$
$Nu_x$	Local Nusselt number, $\frac{h_x x}{k}$

Pr	Prandtl number, $\frac{\nu}{\alpha}$ or $\frac{C_p \mu}{k}$
Ra <sub>x</sub>	Rayleigh number, Gr <sub>x</sub> Pr
R <sub>f</sub>	Flux Richardson number, $\frac{g}{T_g} \frac{w' \bar{T}}{\overline{u'_i u'_j} \overline{U_{ij}}}$ (T <sub>g</sub> is temperature gradient)

### Greek letters

ε	Rate of viscous dissipation of turbulent kinetic energy per unit volume
α	Thermal diffusivity
θ	Sample length or time
∇	Divergence ( $\partial/\partial x + \partial/\partial y + \partial/\partial z$ )
Γ	Integral time scale
γ	Root mean square rate of strain
μ	Viscosity
ρ	Density
η	Similarity variable, $\frac{y}{x} \left[ \frac{Gr_x^*}{5} \right]^{1/5}$
ν	Kinematic viscosity or momentum diffusivity, $\mu/\rho$
τ	Time lag
π	Constant = 3.1416
χ	Mean local rate of strain parameter

## APPENDIX C

### NOISE ANALYSIS

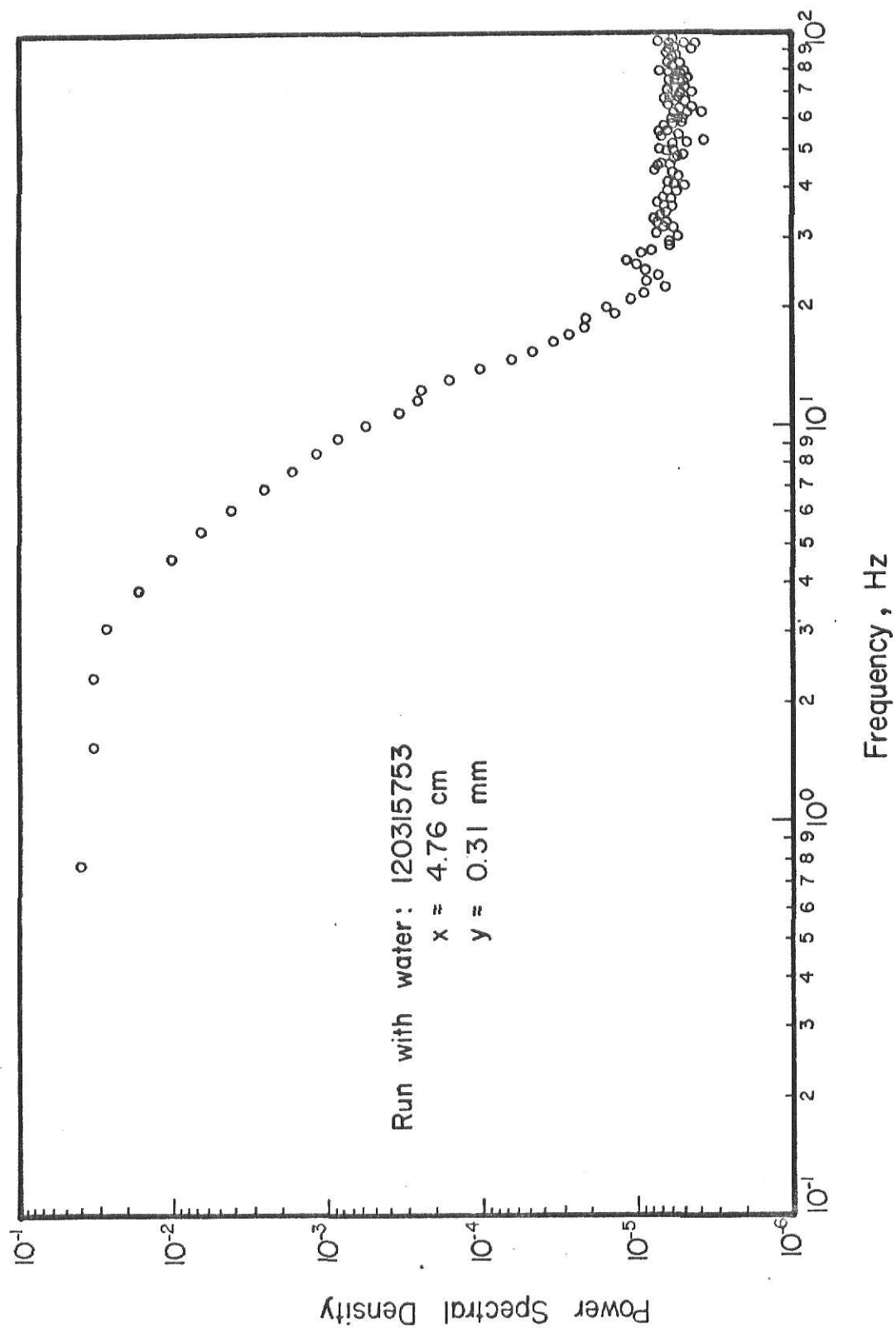


Figure 2.6 Power Spectrum of Signal-plus-Noise showing Negligible Noise (60Hz)-to-Signal Level.

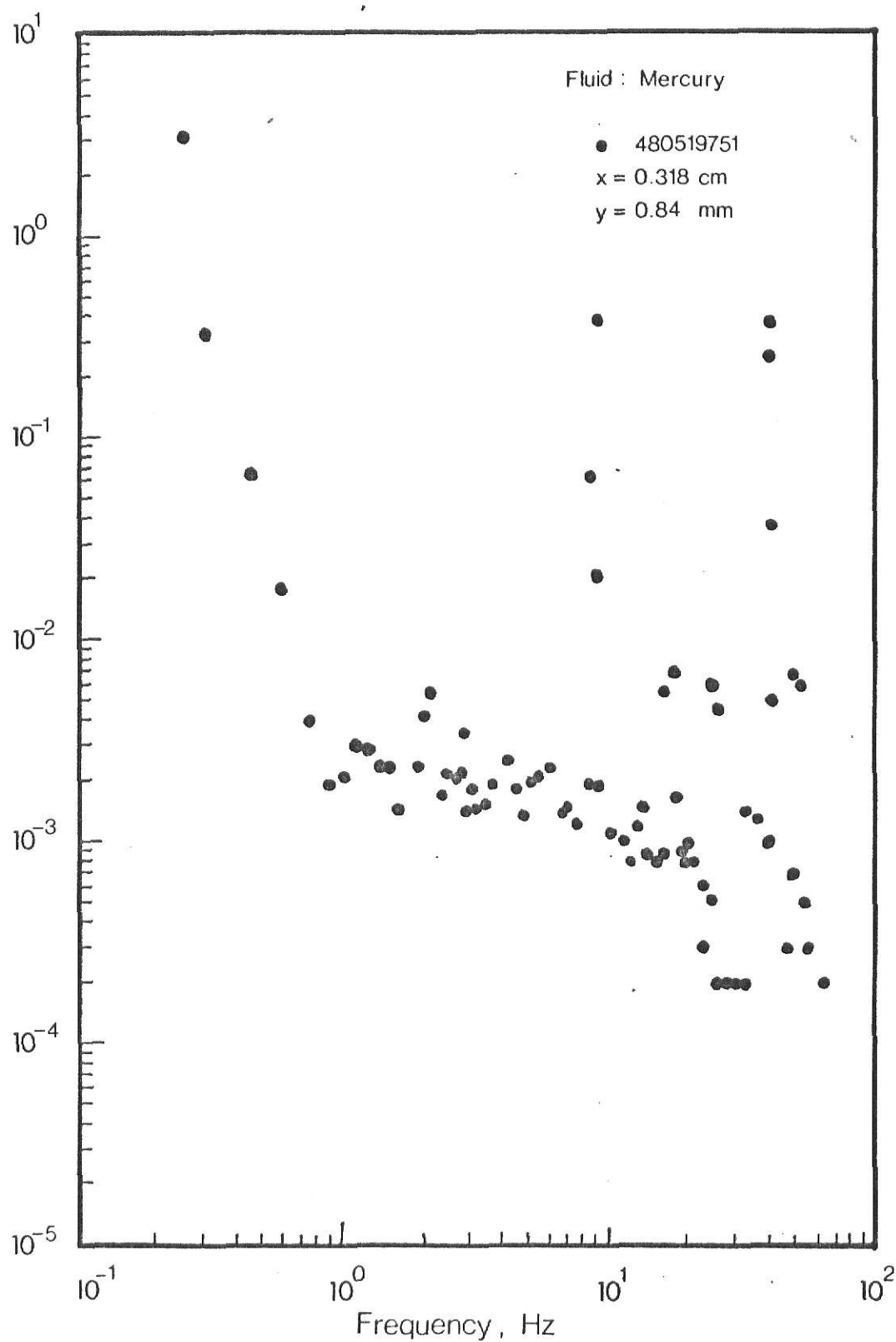
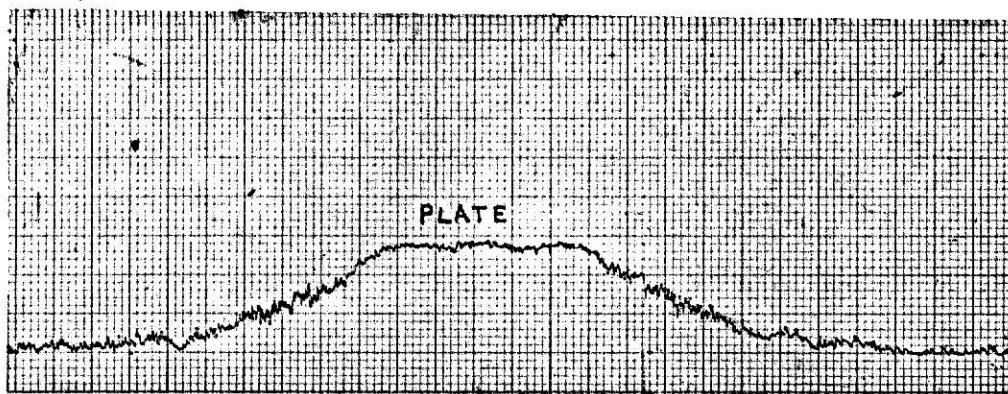


Fig 27 Power Spectrum of Signal-plus-Noise Showing Significant Noise Level in Mercury (Power  $\approx 330$  W)

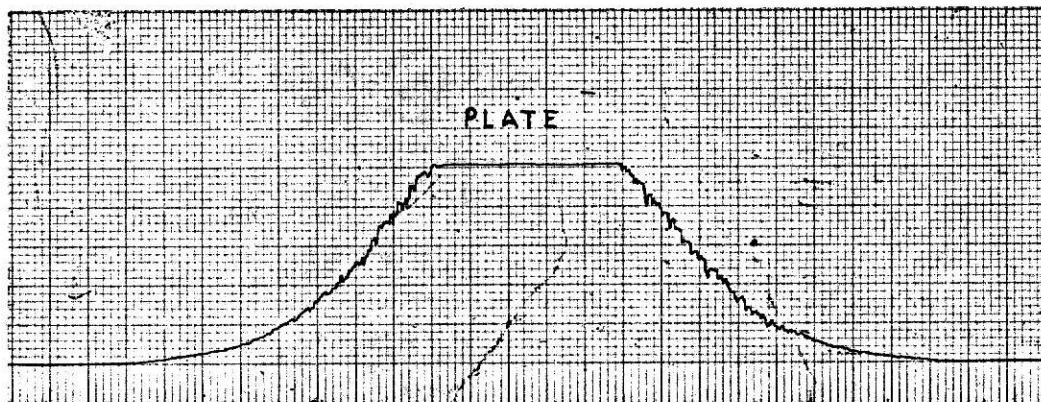
## APPENDIX D

### REPRESENTATIVE RUNS



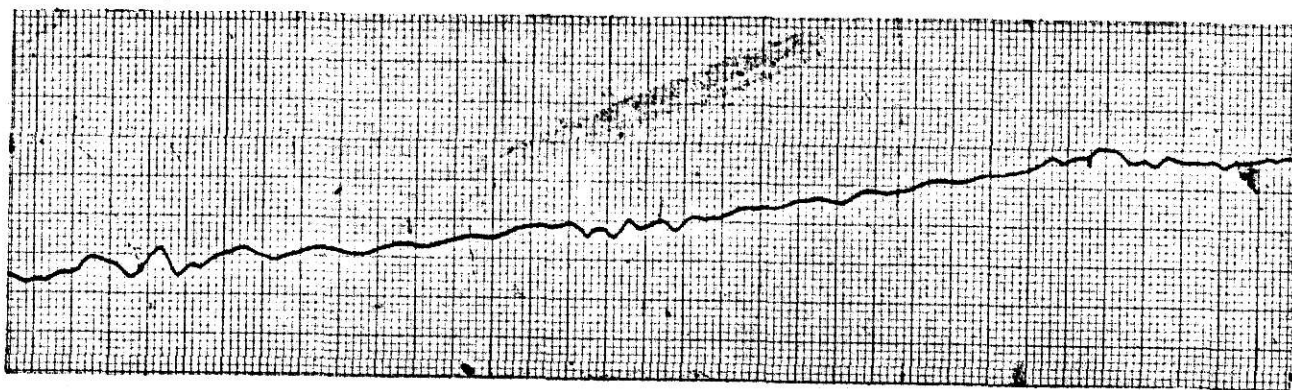


Run: 12031575  
 $Gr_x^* = 5.44 \times 10^{10}$   
 Power = 1186 W  
 $x = 4.76$  cm.  
 Attenuation = 100  
 Chart Speed = 1 mm/sec.

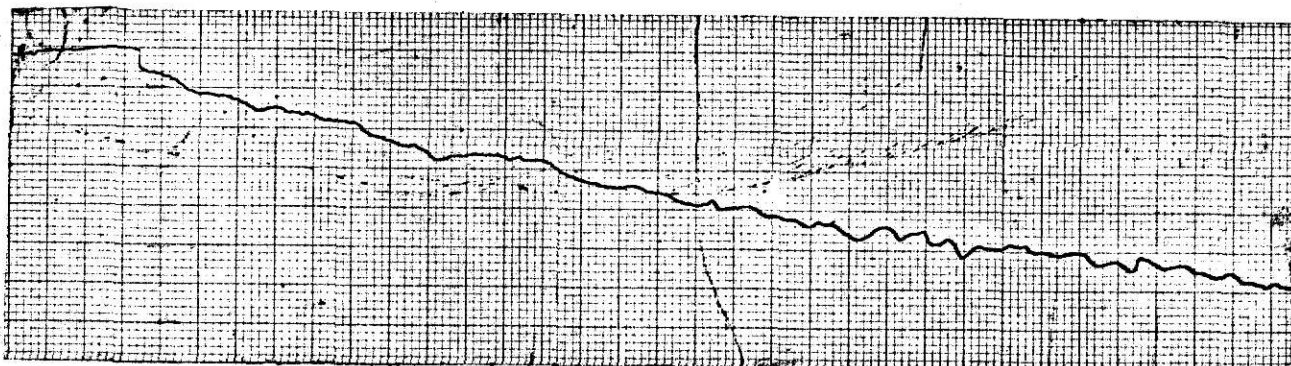


Run: 4021575  
 $Gr_x^* = 1.7037 \times 10^9$   
 Power = 823.2 W  
 $x = 2.54$  cm.  
 Attenuation = 50  
 Chart Speed = 1 mm/sec.

Fig. 28. Temperature Profiles for Water

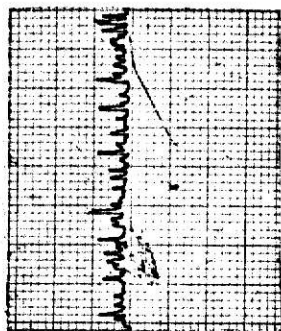


Run: 29050675  
 $Gr_x^* = 8.11 \times 10^8$   
 Power = 103 W  
 $x = 4.76$  cm  
 Attenuation = 5  
 Chart Speed = 1 mm/sec.

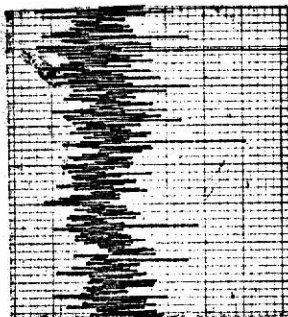


Run: 46051975  
 $Gr_x^* = 2.97 \times 10^9$   
 Power = 313.6 W  
 $x = 4.92$  cm  
 Attenuation = 10  
 Chart Speed = 1 mm/sec.

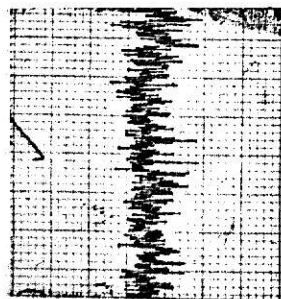
Fig. 29. Temperature Profiles for Mercury



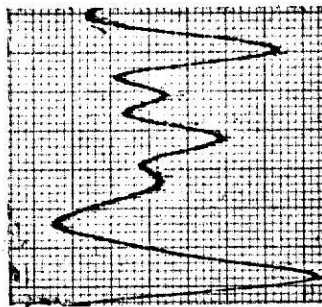
Run: 12031575  
 x = 4.763 cm.  
 y = 1.54 mm.  
 Attenuation = 20



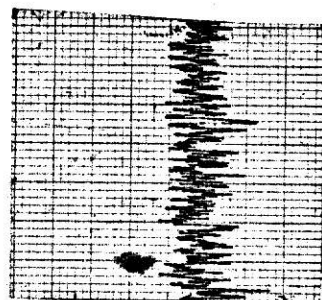
Run: 12031575  
 x = 4.763 cm.  
 y = 0.204 mm.  
 Attenuation = 20



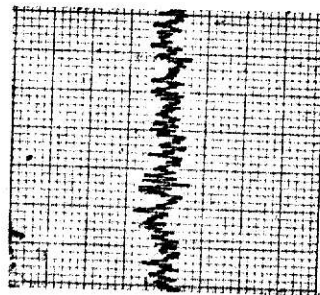
Run: 12041575  
 x = 4.763 cm.  
 y = 0.05 mm.  
 Attenuation = 20



Run: 18031575  
 x = 0.159 cm.  
 y = 2.04 mm.  
 Attenuation = 1



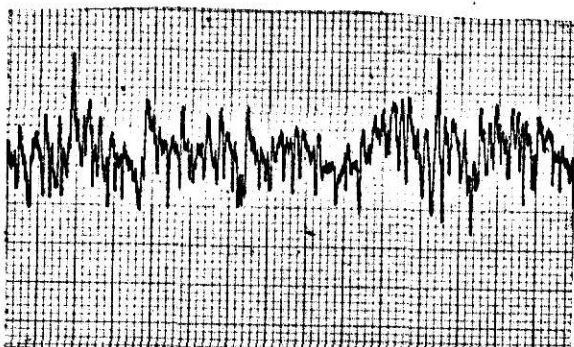
Run: 18031575  
 x = 0.159 cm.  
 y = 0.214 mm.  
 Attenuation = 10



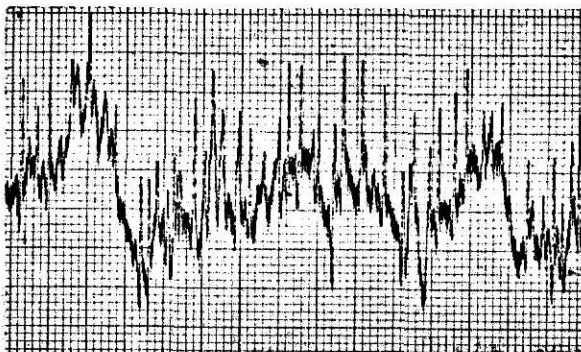
Run: 18031575  
 x = 0.159 cm.  
 y = 0.05 mm.  
 Attenuation = 10

Fig. 30. Temperature Fluctuations in the Horizontal Direction in Water

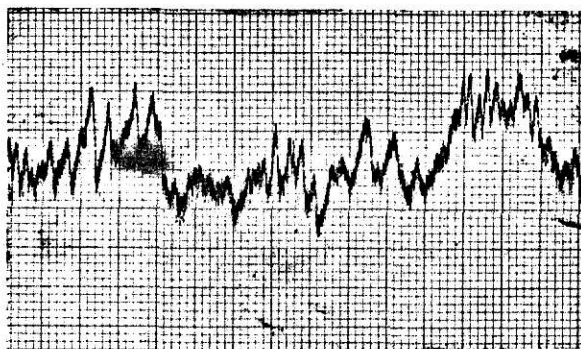
(Power = 1186 W;  $10^5 < Gr_x^* < 10^{11}$ )



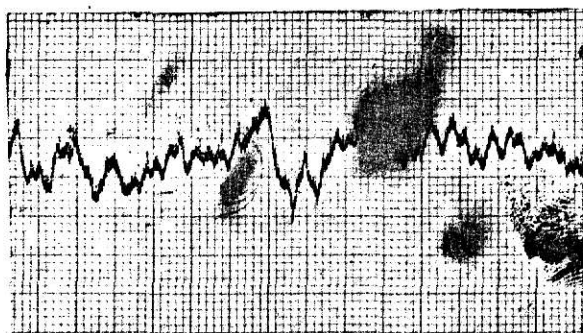
Run: 07022775  
 x = 4.76 cm.  
 Attenuation = 5



Run: 08022775  
 x = 3.81 cm.  
 Attenuation = 2



Run: 09022775  
 x = 2.54 cm.  
 Attenuation = 2



Run: 11022775  
 x = 1.27 cm.  
 Attenuation = 2

Fig. 31. Temperature Fluctuations in the Vertical Direction in Water  
 ( $y \approx 0.25$  mm; Power  $\approx 561.3$  W;  $10^9 \leq Gr_x^* \leq 10^{11}$ )

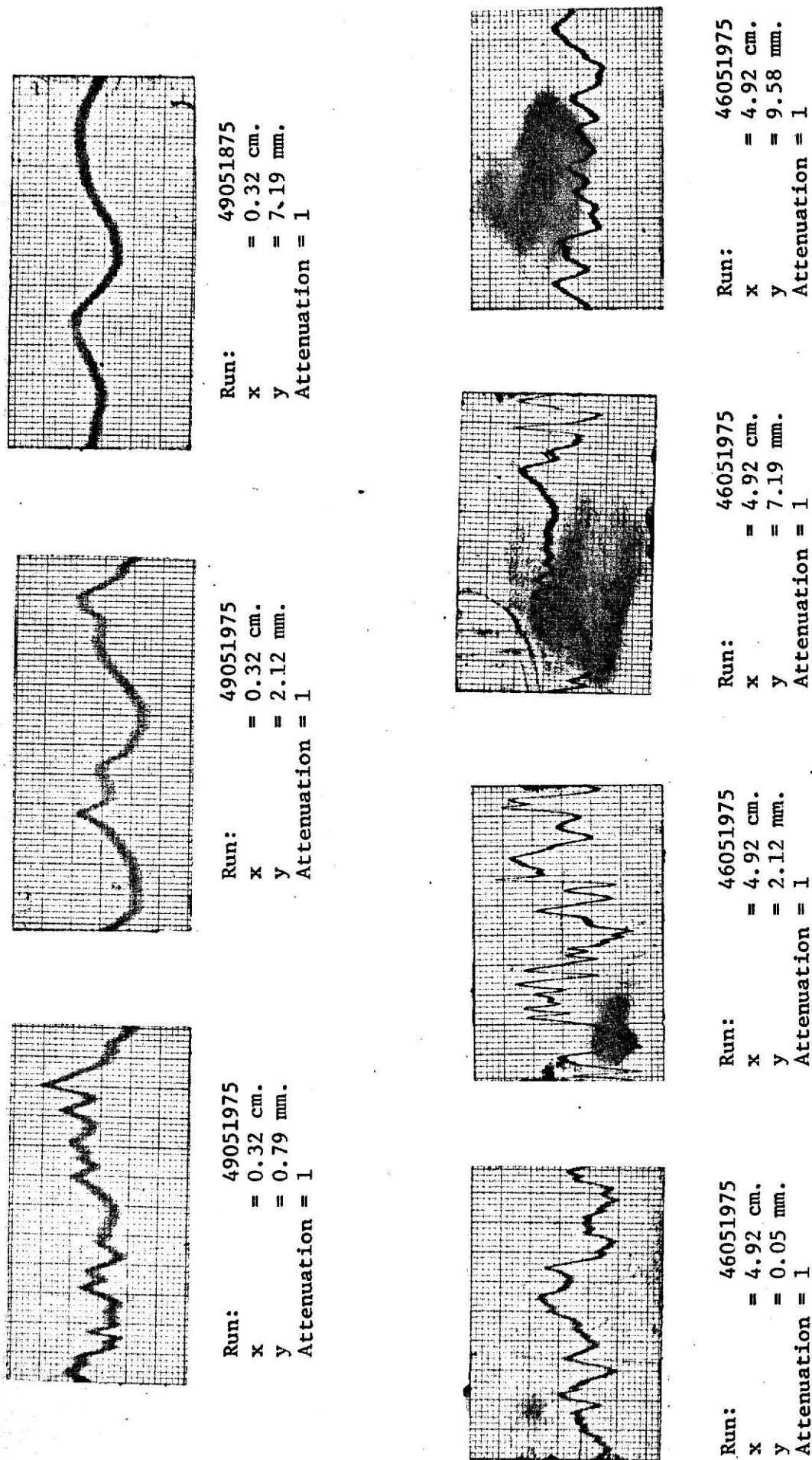
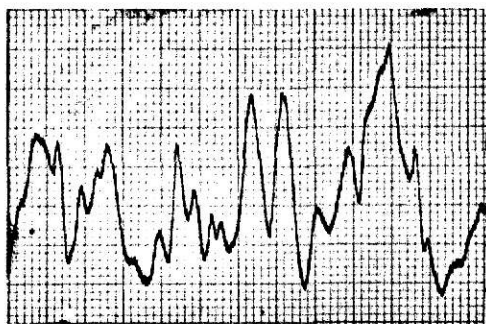
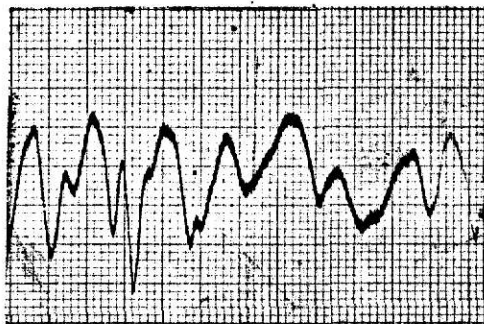


Fig. 32. Temperature Fluctuations in the Horizontal Direction in Mercury  
 ( $Gr_x^* = 5.38 \times 10^4$  for Run 49051975 and  $2.97 \times 10^9$  for Run 46051975)

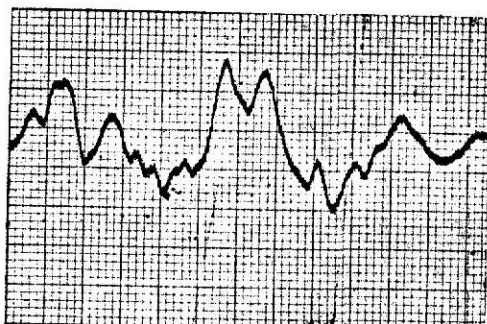




Run: 50051975  
 x = 1.27 cm above  
     the plate  
 y = 7.19 mm.  
 Attenuation = 1



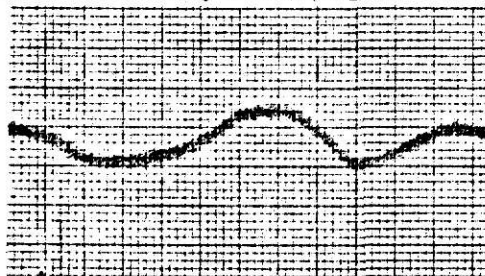
Run: 46051925  
 x = 4.92 cm.  
 y = 7.19 mm.  
 Attenuation = 1



Run: 47051975  
 x = 3.81 cm.  
 y = 7.19 mm.  
 Attenuation = 1

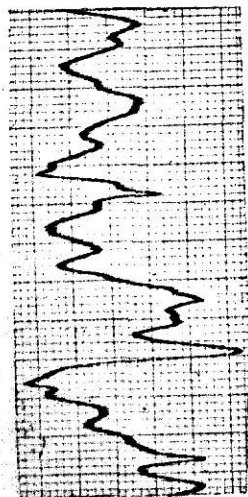


Run: 48051975  
 x = 2.54 cm.  
 y = 7.19 mm.  
 Attenuation = 1



Run: 49051975  
 x = 0.32 cm.  
 y = 7.19 mm.  
 Attenuation = 1

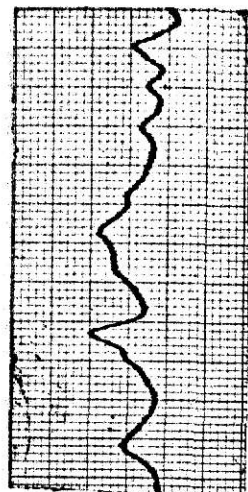
Fig. 33. Temperature Fluctuations in the Vertical Direction in Mercury  
 $(10^8 \leq Gr_x^* \leq 10^{10}$  except for Run 49051975 when  $Gr_x^* = 5.38 \times 10^4$ )



Run: 41051975  
 x = 1.27 cm. above the plate  
 y = 1.59 mm.  
 Attenuation = 1



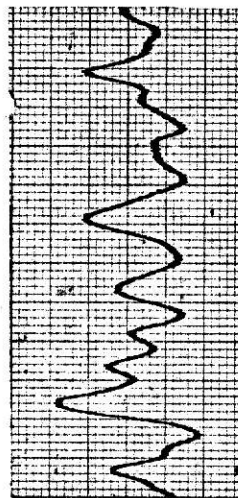
Run: 41051975  
 x = 1.27 cm. above the plate  
 y = 7.19 mm.  
 Attenuation = 1



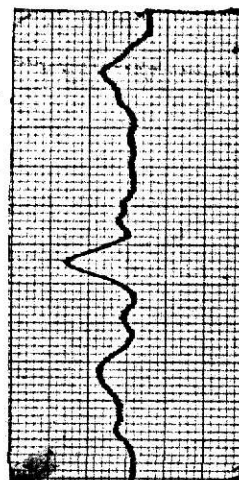
Run: 41051975  
 x = 1.27 cm. above the plate  
 y = 11.11 mm.  
 Attenuation = 1



Run: 41051975  
 x = 0.32 cm. above the plate  
 y = 0.05 mm.  
 Attenuation = 1



Run: 41051975  
 x = 0.32 cm. above the plate  
 y = 7.19 mm.  
 Attenuation = 1

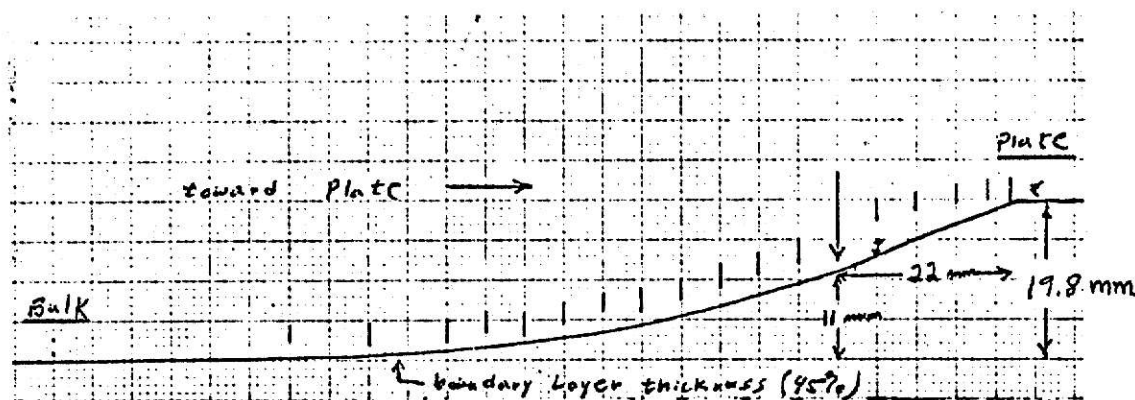


Run: 41051975  
 x = 0.32 cm. above the plate  
 y = 11.11 mm.  
 Attenuation = 1

Fig. 34. Temperature Fluctuations above the Plate in Mercury  
 (Power = 107.9 W at the plate)

## APPENDIX E

## SAMPLE CALCULATIONS \*



Run 140 with Water      May 28, 1967

Time from startup: 8 hours

Height of plate: 2 inches

Thickness of plate: .004 inch

Distance from leading edge:  $1\frac{1}{2}$  inch = 3.81 cm

Ambient temperature:  $34.0^{\circ}\text{C}$

Voltage: .665 volts

Current:  $1.34 \times 30 = 40.2$  amps

Zero suppression:  $2 \times .670 = 1.34$  mv

Chart speed: 1 mm/second

Attenuation: 5

Sensitivity: .002 mv/mm

\* All figures and Tables used in this refer to, and are given in Julian [ 52 ].



Temperature Of Plate

$$TW \text{ (mv)} = \# \text{ mm} \times \text{attenuation} \times \text{sensitivity} + \text{zero suppression}$$

$$1.538 = 19.8 \text{ mm} \times 5 \times 0.002 \text{ mv/mm} + 1.34 \text{ mv}$$

$$TW \text{ (}^{\circ}\text{C)} = 38.27^{\circ}\text{C} \quad (\text{Table 5})$$

Temperature At Infinity

$$TINF \text{ (mv)} = \text{zero suppression} = 1.34 \text{ mv}$$

$$TINF \text{ (}^{\circ}\text{C)} = 33.52^{\circ}\text{C} \quad (\text{Table 5})$$

Reference Temperature For Physical Properties

$$TR = TW - 0.3 \times (TW - TINF) \quad (\text{from Sparrow [92]})$$

$$TR = 38.27 - 0.3 (38.27 - 33.52) = 36.85^{\circ}\text{C}$$

Physical Properties Of Water

$$\text{Density: } 0.9934 \text{ gm/cm}^3 \quad (\text{Figure 40})$$

$$\text{Viscosity: } 6.966 \times 10^{-3} \text{ gm/cm sec} \quad (\text{Figure 42})$$

$$\text{Prandtl number: } 4.65 \quad (\text{Figure 39})$$

$$\text{Thermal conductivity: } 1.498 \times 10^{-3} \text{ cal/cm sec } ^{\circ}\text{C} \quad (\text{Figure 38})$$

$$\text{Coefficient of thermal expansion: } 3.593 \times 10^{-4} / ^{\circ}\text{C} \quad (\text{Figure 41})$$

Power Dissipated In Plate

$$\text{Total power dissipated in equipment} = V \times I$$

$$= 0.665 \times 40.2 = 26.73 \text{ watts}$$

$$\text{Total resistance (copper rods, contact, and plate)} = V/I = 0.0165 \Omega$$

$$\text{Resistance of plate} = \frac{\rho l}{A}$$

$\rho$  = resistivity  $\approx 73.15 \times 10^{-6} \Omega - \text{cm}$  at  $37^\circ\text{C}$  (Communication with Supplier)

$\ell$  = length of plate =  $4 \text{ in} \times 2.54 \text{ cm/in} = 10.16 \text{ cm}$

$A$  = cross sectional area =  $2 \times 0.004 \text{ (in)}^2 \times (2.54)^2 \text{ cm}^2/\text{in}^2 = 0.05161 \text{ cm}^2$

$$R_p = \frac{73.15 \times 10^{-6} (10.16)}{0.05161} = 0.0144 \Omega$$

$$\begin{aligned} \text{Actual power dissipated in plate} &= P_T \times \frac{R_p}{R_T} = 26.73 \times \frac{0.0144}{0.0165} \\ &= 23.34 \text{ watts (87.4\% of total)} \end{aligned}$$

### Heat Flux

$$\begin{aligned} \text{Heat flux} &= \frac{\text{Power}}{\text{Surface Area}} = \frac{23.34}{2 \times 2 \times 4 \text{ in}^2} = 1.459 \text{ watts/in}^2 \\ &= 1.459 \text{ watts/in}^2 \times \frac{492 \text{ BTU/hr ft}^2}{\text{watts/in}^2} = 717.8 \text{ BTU/hr ft}^2 \\ &= 1.459 \text{ watts/in}^2 \times \frac{0.0371 \text{ cal/sec cm}^2}{\text{watts/in}^2} = 0.05413 \text{ cal/sec cm}^2 \end{aligned}$$

Check by differentiating experimental curve (approximation only)

$$\begin{aligned} q &= -k \frac{\partial T}{\partial x} = -k \frac{(20.5 - 13.0) \text{ mm}}{-20 \text{ mm}} \times \frac{(\text{must convert mm to } ^\circ\text{C})}{(2.6458 \times 10^{-3} \text{ cm/mm})^{**}} \\ &= (1.5 \times 10^{-3}) \left( \frac{1.8^\circ\text{C}}{5.3 \times 10^{-2}} \right) \\ q &\approx 0.051 \text{ cal/sec cm}^2 \end{aligned}$$

### Modified Grashoff Number

$$\begin{aligned} \text{Based on } x \quad Gr_x^* &= \frac{g \beta q x^4 \rho}{k \mu^2} \\ Gr_x^* &= \frac{(980) (3.593 \times 10^{-4}) (0.05413) (3.81)^4 (0.9934)^2}{(1.498 \times 10^{-3}) (6.966 \times 10^{-3})^2} \end{aligned}$$

\*\*

This conversion factor is discussed later.

$$= \left[ \frac{\text{cm}}{\text{sec}^2} \mid \frac{1}{^\circ\text{C}} \mid \frac{\text{cal}}{\text{cm}^2 \text{sec}} \mid \frac{\text{gm}^2}{\text{cm}^6} \mid \frac{\text{cm sec } ^\circ\text{C}}{\text{cal}} \mid \frac{\text{cm}^2 \text{ sec}^2}{\text{gm}^2} \right]$$

$$\text{Gr}_x^* = 5.451 \times 10^7$$

$$\text{Based on L: } \text{Gr}_L^* = \frac{g\beta q L^4 \rho^2}{k\mu^2} = 1.724 \times 10^8$$

### Nusselt Number

$$\text{Nu}_x = \frac{h_x x}{k} \quad \text{and } q = h (T_W - T_\infty)$$

$$\text{Nu}_x = \frac{qx}{k (T_W - T_\infty)} = \frac{(5.413 \times 10^{-2}) (3.81)}{(1.498 \times 10^{-3}) (38.27 - 33.52)}$$

$$\left[ \frac{\text{cal}}{\text{sec cm}^2} \mid \text{cm} \mid \frac{\text{cm sec } ^\circ\text{C}}{\text{cal}} \mid \frac{1}{^\circ\text{C}} \right]$$

$$\text{Nu}_x = 28.95$$

### Dimensionless Temperature At Sample Location From Plate

$$T = 11 \text{ mm} \times 5.0 \times 0.002 \text{ mv/mm} + 1.34 \text{ mv} = 36.17^\circ\text{C}$$

$$\frac{T - T_\infty}{T_W - T_\infty} = \frac{36.17 - 33.52}{38.27 - 33.52} = 0.558$$

### Dimensionless Distance At Sample Location From Plate

Motor: 2 rev/min

Pitch of screw: 1/32" per turn

Speed of chart: 1 mm/sec

Factor:

$$\frac{2 \text{ rev}}{\text{min}} \times \frac{1 \text{ min}}{60 \text{ sec}} \times \frac{1 \text{ in}}{32 \text{ rev}} \times \frac{2.54 \text{ cm}}{\text{in}} \times \frac{\text{sec}}{1 \text{ mm}} = 2.6458 \times 10^{-3} \text{ cm/mm}$$

$$y = \text{distance from plate} = 2.6458 \times 10^{-3} \text{ cm/mm} \times 22 \text{ mm} = 0.0582 \text{ cm}$$

$$\eta = \text{dimensionless distance} = \frac{y}{x} \left[ \frac{\text{Gr}_X^*}{5} \right]^{1/5}$$

$$\eta = \frac{0.0582}{3.81} \left[ \frac{5.451 \times 10^7}{5} \right]^{1/5} = 0.390$$

## APPENDIX F

### COMPUTER PROGRAMS





# Computer Program for Calculating Power Spectrum in Water

[illegible]





## Computer Program for Calculating Power Spectrum in Mercury

```

C THIS PROGRAM CALCULATES POWER SPECTRUM BY FAST FOURIER TRANSFORM (FFT)
C IT IS ESPECIALLY USEFUL FOR TURBULENT ANALYSIS WHEN SIGNAL-TO-NOISE
C RATIO IS SMALL & SIGNAL IS NOT HIGHLY FLUCTUATING (FOR FG, MERCURY)
C WHERE 60 HZ NOISE IS TO BE CUT OFF
C INPUT CARDS ARE
C CARD # 1 -- PUNCH NO. OF RECORDS IN COL. 1 TO 3
C CARD # 2 -- PUNCH -- COL. 1 TO 10 -- RUN NO., COL. 11 TO 20 -- NO. OF DATA
C POINTS ATTENUATION -- COL. 21 TO 30; SPEED -- COL. 30 TO 40;
C ZERO SUPP. -- COL. 41 TO 50; DIS. 'X' -- COL. 51 TO 60; DIS. 'Y' -- COL. 61 TO
C 70; SENSITIVITY -- COL. 71 TO 80
C CARD # 31 SAMPLING INTERVAL -- COL. 1 TO 8; 'I' IN COL. 9 -- 10 IF DATA
C ON TAPE IS TO BE PUNCHED ON CARDS, 'O' OTHERWISE; 'J' IN COL. 19 -- 20 IF
C DATA IS READ FROM CARDS, 'O' OTHERWISE
C
C DIMENSION X(8000),W(1024),P(512),F(512)
C DIMENSION ITRF(8000)
C COMPLEX X(1024),COMPLX
C COMPLEX MULT(512)
C REAL INT
C REAL ITS
C
C NBI # OF OVER-LAPPING SEGMENTS
C NI # OF POINTS IN A SEGMENT
C LOG2NI LOG OF NI TO THE BASE OF 2
C NBI # OF POINTS, Y/TAU
C NBI # OF POINTS OVERLAPPED
C
C LILEG OF AF TO THE PAGE 2
C NS=512
C N=1024
C N2=N/2
C CALL MPPOWER(MULT,N2)
C LOG2N=LOG
C CALL PLOTS(ITRF,8000)
C CALL PLOT(0,0,-11,0,3)
C CALL PLOT(0,0,-9,0,3)
C READ 5,NR
C 5 FORMAT (I3)
C DO 500 IR=1,NR
C L=0
C NF=64
C CALL DATA(XR,NR,CT)
C TT=NR*CT
C XBAR=C
C
C COMPUTATION OF MEAN AND VARIANCE OF DATA AND MEAN REMOVAL
C
C DO 6 I=1,NA
C XBAR=XBAR+XX(I)
C 6 CONTINUE
C XBAR=XBAR/FLNAT(NNI)
C PWR=0.
C DO 8 I=1,NA
C XX(I)=XX(I)-XBAR
C PWR=PWR+XX(I)*XX(I)
C 8 CONTINUE
C VAR=PWR/FLNAT(NNI)
C VAR=(NN/NA-1)*(N/NS)*I
C NF=0.
C
C TWOPI=2.*3.141593
C DO 10 I=1,N
C ARG=TWOPI*FLNAT(I-1)/FLNAT(N)
C W(I)=0.5*(1.-COS(ARG))
C WE=WE+W(I)*W(I)
C 10 CONTINUE
C PRINT 12,NA,N,NF
C 12 FORMAT('TOTAL NUMBER OF POINTS =',I5,X,'NUMBER OF POINTS IN A SE
C GMENT =',I4,/,/,', 'NUMBER OF OVER-LAPPING SEGMENTS =',I3,/,/,', 'NF
C ,PGY IN THE HANNING WINDOW =',F3,/)
C PRINT 13,PWR,VAR
C 13 FORMAT('0',I0X,'MEAN =',F3,15X,'VARIANCE =',F10,4,/)
C INT=1/VAR*(.5)/XBAR
C PRINT 14,INT
C 14 FORMAT('0',I0X,'SIGNAL INTENSITY',F10,4)
C
C OVERLAPPE FFT METHOD (HANNING WELCH) TO COMPUTE POWER SPECTRUM
C ONLY NF=64 POINTS ARE CALCULATED (PRUNING)
C SPECTRUM SMOOTHING WITH HANNING WINDOW
C
C DO 15 I=1,NF
C P(I)=0.
C 15 CONTINUE
C DO 16 IR=1,NR
C N=1+11*NS
C DO 20 I=1,N
C X=X(I+K)
C XW=X(I+K)
C X(I)=COMPLX(XW,0.)
C 20 CONTINUE
C
C TAKE FFT TO OBTAIN TWO-SIDED POWER SPECTRUM
C
C CALL FFTPIX,LOG2N,L,N,NF,MULT)
C
C CONVERT TO ONE-SIDED POWER SPECTRUM
C
C DO 30 I=1,NF
C AMP=ABS(X(I))
C IF (I.EQ.1) GO TO 25
C P(I)=P(I)+2.*AMP*AMP
C GO TO 30
C 25 P(I)=P(I)+AMP*AMP
C 30 CONTINUE
C 50 CONTINUE
C PWR=0.
C FO=1./TT
C DO 100 I=1,NF
C P(I)=P(I)/FLNAT(NR)*WE*FO*INT(I)
C
C NORMALIZATION WITH VARIANCE
C MULTIPLICATION BY 10. FOR CONVENIENCE IN PLOTTING
C
C PWR=PWR*P(I)
C P(I)=P(I)*10./VAR
C F(I)=FO*INT(I)-1)*FO
C 100 CONTINUE
C PRINT 81,(F(X),X=1,NF)
C PRINT 82,(P(X),X=1,NF)
C 81 FORMAT('0',/,/, ' FREQUENCY POINTS 1',/,/, ' (10F5.4)')

```



## ACKNOWLEDGMENT

I would like to express my sincere gratitude to my major professor, Dr. R. C. Akins, for his guidance, advise, and direction throughout the course of this study. I would also like to thank Drs. L. T. Fan, D. R. Hummels, and J. C. Matthews for reading the thesis, making useful suggestions, and serving on my advisory committee. Mr. T. Natarajan's help and suggestions in digitizing and analyzing the data are gratefully acknowledged.

The secretarial staff of the Chemical Engineering Department, especially Mrs. Karen Carrel, deserves a special mention for doing an excellent job of typing the manuscripts. I appreciate the understanding of the faculty and my colleagues in the Chemical Engineering Department. This work would not have been possible without the help and support of my numerous friends and the love and encouragement of my family.

The use of the Nova-1200 minicomputer system and the Hewlett-Packard tape recorder by the Electrical and Mechanical Engineering Departments, respectively, is gratefully acknowledged. Partial financial assistance for this study was provided by the Engineering Experiment Station Project #25-60 and National Science Foundation Grant #GK-35777.

AN EXPERIMENTAL STUDY OF TURBULENT NATURAL  
CONVECTION IN WATER AND MERCURY

by

ASHOK JAIN

B. Tech., Indian Institute of Technology (Bombay), 1973

---

AN ABSTRACT OF A MASTER'S THESIS

submitted in partial fulfillment of the  
requirements for the degree

MASTER OF SCIENCE

Department of Chemical Engineering

KANSAS STATE UNIVERSITY  
Manhattan, Kansas

1975

## ABSTRACT

An experimental investigation of turbulent natural convection from a uniformly heated 4 x 2 x 0.004 in. vertical flat plate immersed in water and mercury was carried out. The main objective of the study was the determination of the structure of turbulent natural convection boundary layer flow and the processes taking place in it.

Temperature profiles and fluctuations at different stations along the plate were measured with a copper-constantan thermocouple sheathed in a 0.008-inch diameter stainless-steel tube. Data were taken in the range  $10^8 \leq Gr_x^* \leq 10^{10}$  for mercury, and  $10^8 \leq Gr_x^* \leq 10^{11}$  for water. The results for temperature profiles were presented on dimensionless plots. Temperature fluctuations were used to obtain 'power' spectra, intensity distributions, integral time scales, and autocorrelations. A novel feature of the analysis was the use of the fast Fourier Transform. The power spectra for both the fluids showed a general absence of the 'convection subrange' characterized by  $k^{-5/3}$  ( $k$  being the wave number) behavior. In the case of water, the spectra seemed to follow a  $k^{-1}$  dependence next to the convection subrange. In both the fluids a 'dissipation subrange,' characterized by  $k^{-17/3}$  dependence in mercury and an exponential ( $k^{-3}$ ) drop in water, was observed. With near-boiling conditions at the plate in water, the high frequency end of the spectra dropped sharply. In mercury, a region of constant power was attained beyond 2 Hz approximately. The spectra for water seemed to vary insignificantly in either the vertical or horizontal direction. The mercury spectra shift to higher frequencies with increasing distance from the leading edge or decreasing distance toward the wall. Very near the wall the spectra

seemed to shift toward lower frequencies. The intensity distributions in both the fluids pass through a maxima with the intensities falling very near and far away from the plate. The integral time scale for water seemed to show inverse dependence on Grashof numbers and dimensionless distance.

Based on the analysis it was found that free convection boundary layer was similar in structure to a forced convection layer. The data indicate that the laminar region of the boundary layer extends only up to distances very close to the plate. Turbulence in natural convection seems to be restricted to small scale eddies. The flow was found to be significantly anisotropic. The data indicate that instability points (where turbulence is generated) are located at or very near the plate. The dimensionless temperature profiles were similar except when near-boiling conditions were approached at the plate (as in the case of water).